

博士論文

論文題目 Surface modification of cellulose nanofibrils
toward new bio-based polymer nanocomposites

(セルロースナノフィブリル表面改質による
新規バイオ系高分子ナノ複合体の調製)

氏名 藤澤 秀次

Table of Contents

Chapter 1

General Introduction

1.1	Cellulose	1
1.1.1	Brief introduction	
1.1.2	Structure and morphology of cellulose microfibrils	
1.2	Nanocelluloses	3
1.2.1	Cellulose nanowhiskers	
1.2.2	Microfibrillated celluloses	
1.2.3	TEMPO-oxidized cellulose nanofibrils	
1.3	Cellulose/polymer nanocomposite	6
1.3.1	Polymer nanocomposite	
1.3.2	Cellulose/polymer nanocomposite	
1.3.3	Challenges for cellulose/polymer nanocomposite: Problem statement	
1.4	Surface modification of cellulose nanofibrils	8
1.4.1	Surface modification of cellulose nanofibrils	
1.4.2	Selective surface modification of TOCNs	
1.5	Research objectives	8
1.6	References	9

Chapter 2

Selective Surface Modification of Cellulose Nanofibrils through TEMPO-Mediated Oxidation

2.1	Abstract	16
2.2	Introduction	16
2.3	Materials and methods	18
2.3.1	Materials	
2.3.2	Preparation of TOCNs	
2.3.3	Formation of <i>N</i> -acylureas	
2.3.4	Amine-salt formation with alkyl amines	

2.3.5	Amine-salt formation with PEG amines	
2.3.6	Analyses	
2.4	Results and discussion	21
2.4.1	Formation of <i>N</i> -acylureas	
2.4.1.1	Chemical structures of reaction products of TOCN-COOH with DIC in DMF	
2.4.1.2	The effect of reaction time on the formation of <i>N</i> -acylurea groups	
2.4.1.3	Reaction of TOCN-COOH with DCC in DMF	
2.4.1.4	Characteristics of TOCN- <i>N</i> -acylureas	
2.4.1.5	Hydrophobicity of the TOCN- <i>N</i> -acylureas	
2.4.2	Amine-salt formation with alkyl amines	
2.4.2.1	Chemical structures of alkylated TOCNs	
2.4.2.2	Nano-dispersibility of alkylated TOCNs in IPA	
2.4.2.3	Preparation of alkylated TOCN films	
2.4.3	Amine-salt formation with PEG amines	
2.4.3.1	Nano-dispersibility of PEG-TOCNs in non-polar organic solvents	
2.4.3.2	Chemical structure of PEG-TOCNs	
2.4.4	Dispersibility of surface-modified TOCNs in organic solvents	
2.5	Conclusions	40
2.6	References	41

Chapter 3

Preparation and Characterization of PEG-TOCN/PLLA Nanocomposites

3.1	Abstract	43
3.2	Introduction	43
3.3	Materials and methods	45
3.3.1	Materials	
3.3.2	Preparation of PEG-TOCN dispersions in chloroform	
3.3.3	Preparation of PEG-TOCN/PLLA nanocomposites	
3.3.4	Analyses	
3.4	Results and discussion	47
3.5	Conclusions	52
3.6	References	52

Chapter 4

Comparison of Mechanical Reinforcement Effects of Surface-Modified Cellulose Nanofibrils and Carbon Nanotubes in PLLA Composites

4.1	Abstract.....	54
4.2	Introduction.....	54
4.3	Materials and methods	55
4.3.1	Materials	
4.3.2	Preparation of PEG-TOCN and PEG-SWCNT dispersions in chloroform	
4.3.3	Preparation of PEG-TOCN/PLLA and PEG-SWCNT/PLLA composite films	
4.3.4	Analyses	
4.4	Results and discussion	57
4.4.1	PEG-TOCN and PEG-SWCNT dispersions in chloroform	
4.4.2	PEG-TOCN and PEG-SWCNT/PLLA composite films	
4.4.3	Model approach	
4.5	Conclusions.....	66
4.6	References.....	67

Chapter 5

The effect of PEG-TOCNs on the crystallization behavior and thermo-mechanical properties of PLLA

5.1	Abstract.....	70
5.2	Introduction.....	70
5.3	Materials and methods	72
5.3.1	Materials	
5.3.2	Preparation of PEG-TOCN/PLLA composite films	
5.3.3	Analyses	
5.4	Results and discussion	74
5.4.1	Non-isothermal crystallization behavior	
5.4.2	Isothermal crystallization behavior	
5.5	Conclusions.....	83
5.6	References.....	83

Chapter 6

Summary.....88

Appendix.....90

Publications.....94

Acknowledgement.....97

Chapter 1

General Introduction

1.1 Cellulose

1.1.1 Brief introduction

Cellulose, (1→4)- β -D-glucan, is the most abundant carbon resource on earth (Figure 1.1). It is produced by plants, trees, bacteria and some animals (tunicate) via the biosynthesis, and the total annual biomass production is as high as 1.5×10^{12} tons.¹ Because of the increasing demand for sustainable and environmentally friendly products, cellulose is a prime candidate for replacing oil-based feedstocks. Due to its favorable properties such as hydrophilicity, chemical stability, biodegradability, biocompatibility, and renewability, cellulose has been historically used in various material fields such as textile, and pulp and paper industries. Since cellulose molecule contains three hydroxyl groups in an anhydroglucose unit (position 2, 3 and 6 of the anhydroglucose unit, Figure 1.1), physical and chemical properties of celluloses can be tailored by substitution of the hydroxyl groups. Such cellulose derivatives have been produced on an industrial scale, and contributed to the development of high-tech materials such as flat panel components in liquid crystal displays, hollow fibers for artificial kidney dialysis, components of medicines, and food additives.

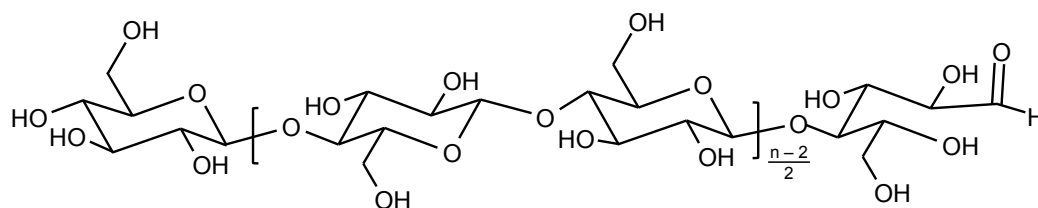


Figure 1.1. The chemical structure of cellulose (n: degree of polymerization).

1.1.2 Structure and morphology of cellulose microfibrils

Cellulose is organized into unique crystalline nanofibrils via the biosynthesis.² The nanofibrils are typically called cellulose microfibrils.³ The cellulose microfibrils are the smallest elements next to cellulose molecules,

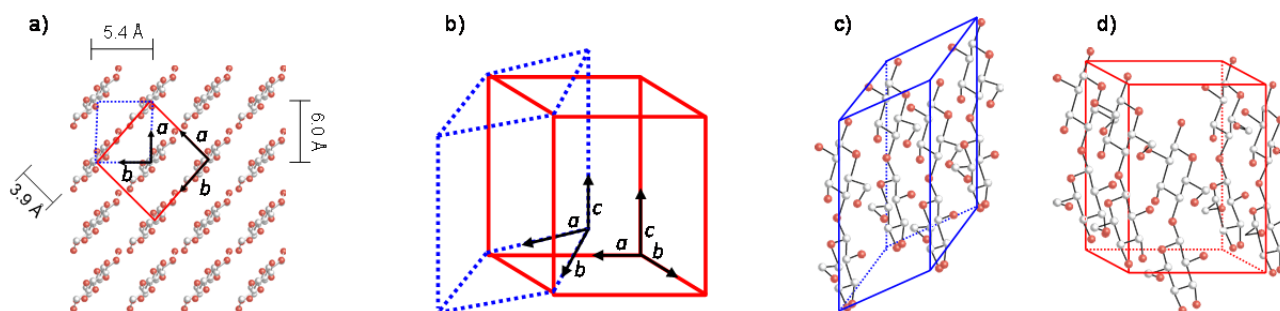


Figure 1.2. Schematic of the unit cells for cellulose I $_{\alpha}$ (triclinic, red line) and I $_{\beta}$ (monoclinic, blue line). (a) Crystal structure of cellulose I viewed orthogonal to the ab plane with the unit cells of cellulose I $_{\alpha}$ and I $_{\beta}$, (b) relative configuration of I $_{\alpha}$ with respect to I $_{\beta}$ unit cell, and the models of I $_{\alpha}$ (c) and I $_{\beta}$ (d) unit cells.

and composed of two different allomorphs (Figure 1.2), namely cellulose I $_{\alpha}$ (a triclinic and one-chain unit cell) and I $_{\beta}$ (a monoclinic two-chain unit cell),⁴⁻⁶ which are collectively called cellulose I. In the cellulose I crystals, cellulose chains are tightly packed with a parallel-up configuration, and the microfibrils exhibit high crystallinity. The aspect ratios of the microfibrils are as high as >300, with small widths of 2–20 nm, and these sizes depend on the source of cellulose origin. The microfibrils show excellent physical properties such as high crystal moduli (130–150 GPa),⁷⁻⁹ high strength (3–6 GPa),¹⁰ and a low coefficient of thermal expansion along the c -axis direction (6 ppm K⁻¹),¹¹ arising from their high crystallinity.

Higher plant celluloses form especially ultrafine cellulose microfibrils with ~3 nm in width consisting of approximately 30–40 cellulose chains (Figure 1.3), and the microfibrils play a significant role on the structural support of the plant bodies. Because of their mechanical reinforcing potential and nano-size, the plant cellulose microfibrils have been attracting attention as renewable building blocks in nanomaterials, and isolation of the microfibrils from the plant body is a critical challenge that must be met to successfully produce high-performance nanomaterials. However, it is difficult to isolate the microfibrils because they are firmly hooked up with one another by interfibrillar attractive forces such as hydrogen bondings. Therefore, extensive research has been reported on the production technique of nano-fibrillated celluloses, which is typically called nanocelluloses, based on both mechanical and chemical approaches.

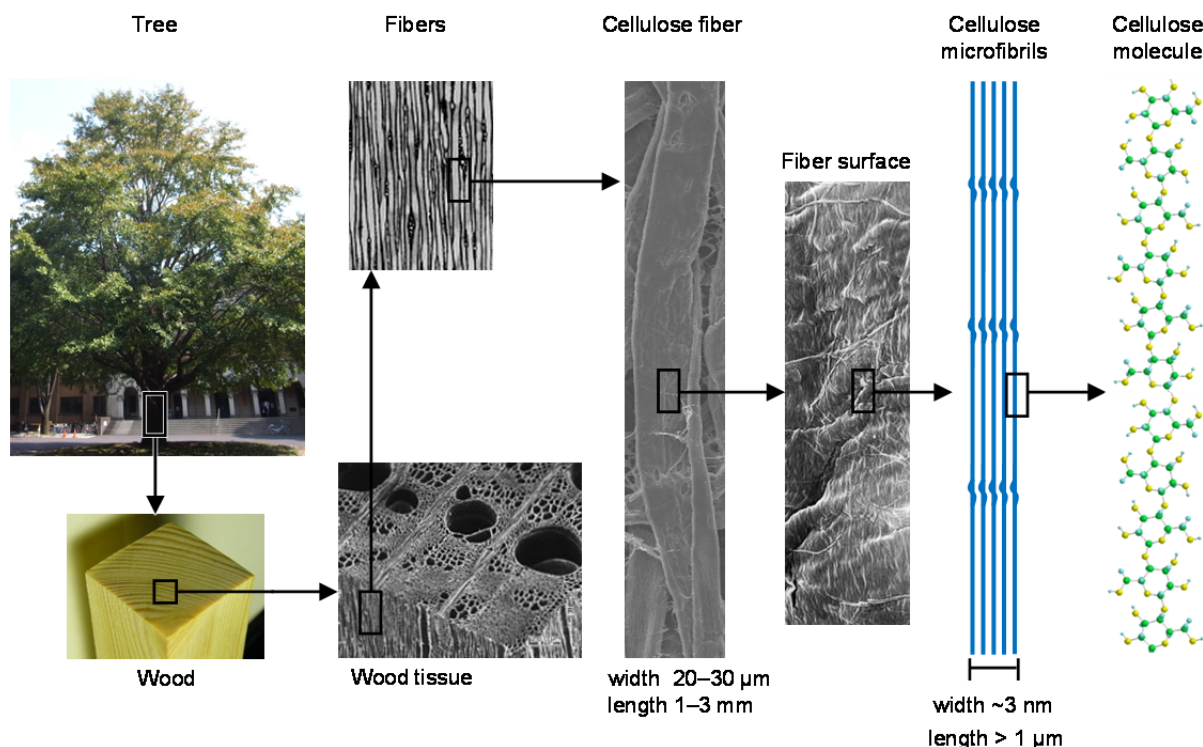


Figure 1.3. The hierarchical structure of wood celluloses.

1.2 Nanocelluloses

1.2.1 Cellulose nanowhiskers

Stable suspensions of rod-like crystalline cellulose nanoparticles can be prepared by submitting native cellulose to a harsh sulfuric acid hydrolysis often followed by ultrasonication. Such nanoparticles are typically called “cellulose nanowhiskers”. Cellulose nanowhiskers can be extracted generally from plants and the mantle of tunicates, and the shape and size are more or less fixed by the source of the cellulose. The sulfuric acid treatment provides sulfate ester groups on cellulose crystal surfaces, and the negatively-charged sulfate groups on the surface of the nanowhiskers make it possible for them to be stably suspended in aqueous media. Prolongation of the hydrolysis time induces not only an increase in surface charge but also decreases in both yield and length of the fibrils. Controlled sulfuric acid hydrolysis of wood cellulose yields suspensions of

highly crystalline nanowhiskers with ~5 nm in width and 100–300 nm in length,¹² with yields of 30–50 %. The preparation of cellulose nanowhiskers by the treatment of wood or cotton fibers with sulfuric acid was first reported by Rånby.¹³⁻¹⁴ In 1959, Marchessaut et al. discovered that the nanowhisiker suspensions display birefringence beyond a critical concentration.¹⁵ Revol et al. demonstrated in the early 1990s that cellulose nanowhiskers form a chiral nematic liquid-crystalline phase.¹⁶ Following this discovery, the optical and liquid-crystalline properties of cellulose suspensions were the focus of several studies.¹⁷⁻²²

1.2.2 *Microfibrillated celluloses*

Microfibrillated cellulose (MFC) can be prepared from wood cellulose by harsh aqueous mechanical treatment, such as a high pressure homogenizer treatment,²³⁻²⁴ a grinder treatment,²⁵⁻²⁶ a microfluidizer treatment,²⁷ and a pressure refiner treatment.²⁸ The homogenization process results in disintegration of the wood celluloses, and viscous MFC suspensions in water can be obtained. Since MFC is usually consists of bundles of cellulose microfibrils, the width and length of MFC are typically in the range of 20–40 nm and several micrometers, respectively. Enzymatic pretreatment can facilitate the nanofibrillation during the mechanical treatment, and MFCs with 5–30 nm²⁹⁻³⁰ in width are successfully prepared. By drying the MFC gels, stiff, strong, and tough MFC films can be prepared.³¹⁻³² Taking advantage of their fine web-like and highly fibrous network structure, flexible and deformable “sponge-like” aerogels can also be prepared by freeze-drying of aqueous MFC gels.³³

1.2.3 *TEMPO-oxidized cellulose nanofibrils*

Catalytic and selective oxidation of primary hydroxyl groups of carbohydrates using 2,2,6,6-tetramethylpiperidiny-1-oxyl (TEMPO) has opened up new possibilities of development of polysaccharide chemistry (Figure 1.4). Since the first report by de Nooy et al.,³⁴ this technique has been applied to various kinds of polysaccharides to obtain the corresponding polyuronic acids.³⁵⁻³⁹

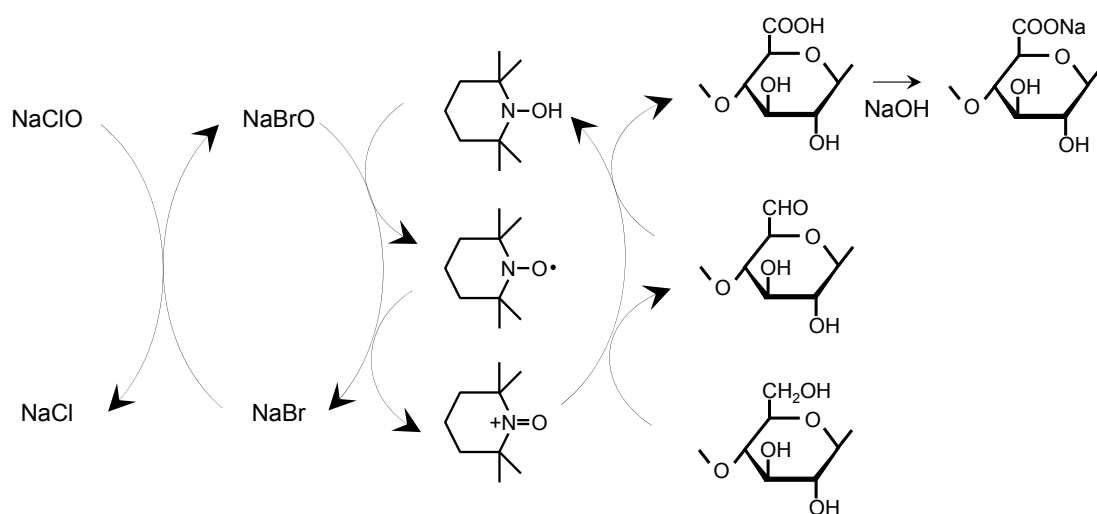


Figure 1.4. Regioselective oxidation of C6 primary hydroxyls of cellulose to C6 carboxylate groups by TEMPO/NaBr/NaClO oxidation in water at pH 10.

Recently, the TEMPO-mediated oxidation has been applied to native celluloses to obtain cellulose nanofibrils.⁴⁰⁻⁴³ The oxidation can selectively and efficiently convert the C6-primary hydroxyl groups exposed on crystalline cellulose microfibrils to C6-carboxylate groups.⁴⁴ The original crystal structure of cellulose I, the crystallinity indices and the crystal sizes were unchanged after the oxidation.^{41,44-45} The oxidized nanofibrils can be individualized at the microfibril level by gentle mechanical treatments in water, by repulsive forces such as osmotic pressure and/or electrostatic repulsion. When wood celluloses are used, the obtained TEMPO-oxidized wood celluloses are convertible to TEMPO-oxidized cellulose nanofibrils (TOCNs) of ~3 nm in width and >1 μm in length dispersed at the individual nanofibril level in water. Figure 1.5 shows characteristic images of cellulose nanowhiskers, MFC, and TOCNs, which were prepared from wood celluloses. TOCNs have obviously higher dispersibility and aspect ratios with a uniform width of ~3 nm, than the other nanocelluloses. Therefore, TOCNs are attractive building blocks for nanomaterial architecture. Transparent TOCN films can be prepared by casting the TOCN dispersions in water, and the films exhibit high gas barrier properties,⁴⁶⁻⁴⁷ low thermal expansion rates,⁴⁶ and high Young's modulus and strength.^{42, 46} The TOCN dispersions can also be converted to stiff hydrogels and tough aerogels.⁴⁸

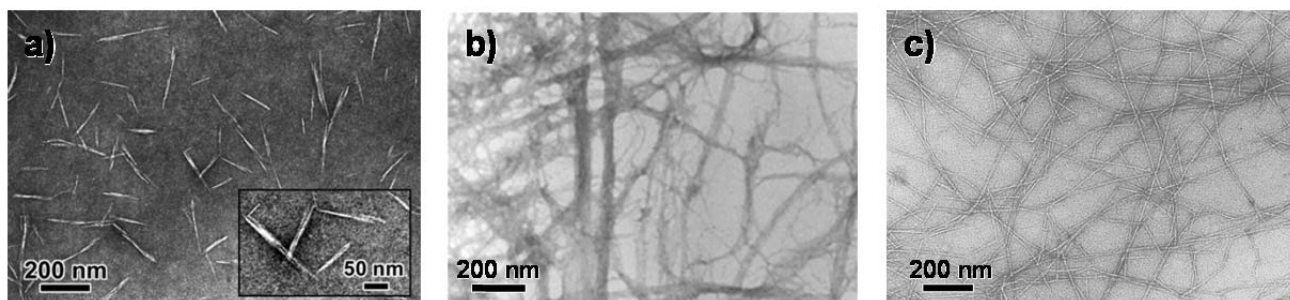


Figure 1.5. TEM images of nanocelluloses: (a) cellulose nanowhiskers,⁴⁹(b) MFC, and (c) TOCNs.⁴¹

1.3 Cellulose/polymer nanocomposite

1.3.1 Polymer nanocomposite

Polymers have been a part of life in the world because of their advantages such as ease of production, light weight, and often ductile nature. However, polymers have lower modulus and strength as compared to metals and ceramics. One way to improve their mechanical properties is to reinforce polymers with rigid fillers such as minerals, ceramics, or metals. Using this approach, mechanical properties of the polymers can be effectively improved with small additions of the fillers. Since the first reports in the late 1980s,⁵⁰⁻⁵¹ “polymer nanocomposite”, which is the polymer material reinforced with nanofillers, has attracted substantial academic and industrial interest. Recently, carbon nanotubes,⁵²⁻⁵⁴ graphene,⁵⁵⁻⁵⁷ and nanoclays,⁵⁸⁻⁶⁰ have often been used as nanofillers in polymers, and the mechanical properties of the polymers, such as strength, elastic modulus, and thermal deformation can be substantially improved with small amounts of the fillers. Therein, the rigid nanofillers serve as the load bearing and reinforcing part, and the stress is transferred at the interface between the nanofillers and polymer matrices. Since specific surface areas of the nanofillers are several orders of larger than those of microfillers, the nanocomposites often exhibit superior mechanical properties to traditional microcomposites with the small addition.

1.3.2 Cellulose/polymer nanocomposite

Cellulose nanofibrils hold great potential as a renewable alternative to the above-mentioned nanofillers. The cellulose nanofibrils have high elastic modulus and large specific surface areas, and therefore, contribute to the principal structural support of living plant bodies. Because of their reinforcing potential, the use of the cellulose nanofibrils as nanofiller has attracted considerable interest. In the mid-1990s,⁶¹⁻⁶² Favier et al. first reported the reinforcing potential of tunicin cellulose whiskers in poly(styrene-co-butyl acrylate) matrix, by casting a mixture of aqueous suspensions of the poly(styrene-co-butyl acrylate) latex and the nanowhiskers. They demonstrated that the storage modulus of the polymer can be significantly increased above the glass–rubber transition temperature by the addition of the nanowhiskers, which was well explained by the percolation model. Following these reports, a number of cellulose nanofibril/polymer nanocomposites have been reported so far.⁶³⁻⁶⁵ Most of these works have focused on improvement in elastic modulus and tensile strength of polymers. Besides these properties, coefficient of thermal expansion,⁶⁶⁻⁶⁷ thermal conductivity⁶⁸ optical properties,⁶⁹ and oxygen barrier property⁷⁰ of cellulose/polymer nanocomposites have been investigated for their wider applications such as electronic devices, packaging, and biomedical applications.

1.3.3 Challenges for cellulose/polymer nanocomposite: Problem statement

Although cellulose/polymer nanocomposites generally exhibit better thermal dimensional stability, elastic moduli, and tensile strengths than neat polymers, the cellulose nanofibrils inherently have two main issues as a nanofiller because of their polar and hydrophilic nature: (i) low dispersibility in polymer matrix and (ii) poor interfacial interaction with the matrix. Low dispersibility of the nanofibrils in polymer nanocomposites leads to mechanical properties far below theoretical predictions, and poor interactions between the nanofibrils and polymer matrices generally result in brittle behavior of the resultant nanocomposites. A possible solution for this is surface modification of the cellulose nanofibrils. Suitable surface modification can improve not only the dispersibility but also the nanofibrils/polymer interfacial interaction, which leads to effective stress transfer to the nanofibrils.

1.4 Surface modification of cellulose nanofibrils

1.4.1 Surface modification of cellulose nanofibrils

Various kinds of surface modification methods have been applied to cellulose nanofibrils so far. Covalent modification of the hydroxyl groups on the nanofibril surfaces is a simple and major technique for tailoring the surface properties, which is through acetylation,⁷¹⁻⁷³ esterification by “grafting onto”⁷⁴⁻⁷⁶ or “grafting from”⁷⁷⁻⁸⁴ method, etherification,⁸⁵⁻⁸⁶ urethanation,⁸⁷⁻⁸⁹ and silylation.⁹⁰⁻⁹² However, it is generally difficult to control the covalent reactions; the reactions could proceed into the crystallite core, which leads to losing the unique characteristics of crystalline cellulose nanofibrils. Physisorption of surfactant on cellulose whiskers enhance the dispersibility in nonpolar organic solvents,⁹³⁻⁹⁴ and using the dispersions, mechanically enhanced cellulose/polypropylene nanocomposite can be prepared.⁹⁵⁻⁹⁶

1.4.2 Selective surface modification of TOCNs

The chemical modification of hydroxyl groups on the crystalline cellulose surfaces has the problem that the reaction could proceed to the internal region of the cellulose. On the other hand, cellulose nanofibril surfaces can be selectively and densely modified by using carboxyl groups of TOCNs. On the surface of TOCNs, carboxyl groups densely exist,^{40, 43-44} and the carboxyl groups can be used as selective anchoring sites for further modification of the nanofibril surfaces.⁹⁷⁻¹⁰² The main advantage of this strategy is that cellulose nanofibril surfaces can be selectively modified without losing the unique reinforcing potential of the nanofibrils.

1.5 Research objectives

The first objective of this research was to selectively modify the TOCN surfaces to facilitate their dispersion in organic media. TOCN surfaces were selectively modified on covalent and non-covalent approaches, by using surface carboxyl groups as anchoring sites (Figure 1.6). The dispersibilities of the surface-modified TOCNs were evaluated in various organic solvents. The second objective was to develop

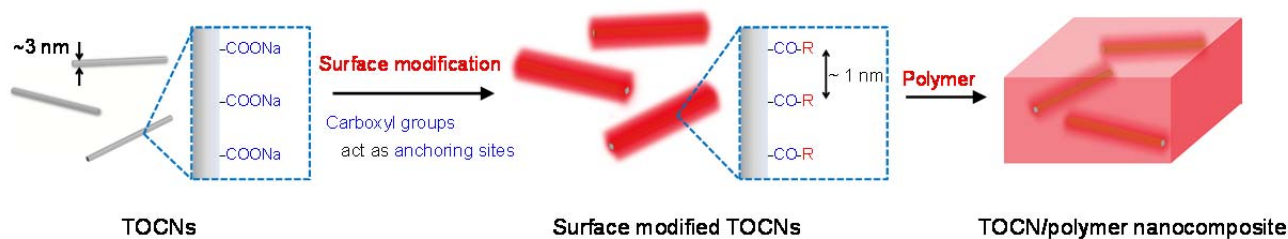


Figure 1.6. Schematic illustration of the process for the preparation of TOCN/polymer nanocomposites.

TOCN/poly(L-lactide) (PLLA) nanocomposites using the surface-modified TOCNs as nanofillers. The mechanical reinforcing properties of the surface-modified TOCNs were evaluated using theoretical models, and compared against those of surface-modified single-walled carbon nanotubes. Moreover, the effect of surface-modified TOCNs on crystallization kinetics of PLLA was evaluated.

1.6 References

1. D. Klemm, F. Kramer, S. Moritz, T. Lindstrom, M. Ankerfors, D. Gray and A. Dorris, "Nanocelluloses: A New Family of Nature-Based Materials." *Angew. Chem. Int. Edit.* 2011, **50**, 5438–5466.
2. I. M. Saxena and R. M. Brown, Jr., "Cellulose Biosynthesis: Current Views and Evolving Concepts." *Ann. Bot.* 2005, **96**, 9–21.
3. Y. Nishiyama, "Structure and Properties of the Cellulose Microfibril." *J. Wood. Sci.* 2009, **55**, 241–249.
4. R. H. Atalla and D. L. Vanderhart, "Native Cellulose: A Composite of Two Distinct Crystalline Forms." *Science* 1984, **223**, 283–285.
5. Y. Nishiyama, P. Langan and H. Chanzy, "Crystal Structure and Hydrogen-Bonding System in Cellulose $I\beta$ from Synchrotron X-Ray and Neutron Fiber Diffraction." *J. Am. Chem. Soc.* 2002, **124**, 9074–9082.
6. Y. Nishiyama, J. Sugiyama, H. Chanzy and P. Langan, "Crystal Structure and Hydrogen Bonding System in Cellulose $I\alpha$ from Synchrotron X-Ray and Neutron Fiber Diffraction." *J. Am. Chem. Soc.* 2003, **125**, 14300–14306.
7. I. Sakurada, Y. Nukushina and T. Ito, "Experimental Determination of the Elastic Modulus of Crystalline Regions in Oriented Polymers." *J. Polym. Sci.* 1962, **57**, 651–660.
8. A. Sturcova, G. R. Davies and S. J. Eichhorn, "Elastic Modulus and Stress-Transfer Properties of Tunicate Cellulose Whiskers." *Biomacromolecules* 2005, **6**, 1055–1061.

9. S. Iwamoto, W. Kai, A. Isogai and T. Iwata, "Elastic Modulus of Single Cellulose Microfibrils from Tunicate Measured by Atomic Force Microscopy." *Biomacromolecules* 2009, **10**, 2571–2576.
10. T. Saito, R. Kuramae, J. Wohlert, L. A. Berglund and A. Isogai, "An Ultrastrong Nanofibrillar Biomaterial: The Strength of Single Cellulose Nanofibrils Revealed via Sonication-Induced Fragmentation." *Biomacromolecules* 2013, **14**, 248–253.
11. R. Hori and M. Wada, "The Thermal Expansion of Wood Cellulose Crystals." *Cellulose* 2005, **12**, 479–484.
12. S. Beck-Candanedo, M. Roman and D. G. Gray, "Effect of Reaction Conditions on the Properties and Behavior of Wood Cellulose Nanocrystal Suspensions." *Biomacromolecules* 2005, **6**, 1048–1054.
13. B. G. Ranby, "Aqueous Colloidal Solutions of Cellulose Micelles." *Acta Chem. Scand.* 1949, **3**, 649–650.
14. B. G. Ranby, "Cellulose and Muscle - the Colloidal Properties of Cellulose Micelles." *Discuss Faraday Soc* 1951, 158–164.
15. R. H. Marchessault, F. F. Morehead and N. M. Walter, "Liquid Crystal Systems from Fibrillar Polysaccharides." *Nature* 1959, **184**, 632–633.
16. J. F. Revol, H. Bradford, J. Giasson, R. H. Marchessault and D. G. Gray, "Helicoidal Self-Ordering of Cellulose Microfibrils in Aqueous Suspension." *Int. J. Biol. Macromol.* 1992, **14**, 170–172.
17. X. M. Dong, T. Kimura, J. F. Revol and D. G. Gray, "Effects of Ionic Strength on the Isotropic-Chiral Nematic Phase Transition of Suspensions of Cellulose Crystallites." *Langmuir* 1996, **12**, 2076–2082.
18. J. Araki, M. Wada, S. Kuga and T. Okano, "Flow Properties of Microcrystalline Cellulose Suspension Prepared by Acid Treatment of Native Cellulose." *Colloid Surface A* 1998, **142**, 75–82.
19. J.-F. Revol, L. Godbout, X.-M. Dong, D. G. Gray, H. Chanzy and G. Maret, "Chiral Nematic Suspensions of Cellulose Crystallites; Phase Separation and Magnetic Field Orientation." *Liq. Cryst.* 1994, **16**, 127–134.
20. J. Araki, M. Wada, S. Kuga and T. Okano, "Birefringent Glassy Phase of a Cellulose Microcrystal Suspension." *Langmuir* 2000, **16**, 2413–2415.
21. D. G. Gray, "Chemical Characteristics of Cellulosic Liquid-Crystals." *Faraday Discuss.* 1985, **79**, 257–264.
22. K. E. Shpsovitz, H. Qi, W. Y. Hamad and M. J. MacLachlan, "Free-Standing Mesoporous Silica Films with Tunable Chiral Nematic Structures." *Nature* 2010, **468**, 422–425.
23. A. F. Turbak, F. W. Snyder and K. R. Sandberg, "Microfibrillated Cellulose, a New Cellulose Product-Properties, Uses, and Commercial Potential." *J. Appl. Polym. Sci.: Appl. Polym. Symp.* 1983, **37**, 815–827.
24. H. FW, C. RL, H. JK and S. KR, "Microfibrillated Cellulose: Morphology and Accessibility." *J. Appl. Polym. Sci.: Appl. Polym. Symp.* 1983, **37**, 797–813.
25. T. Taniguchi and K. Okamura, "New Films Produced from Microfibrillated Natural Fibres." *Polym. Int.* 1998, **47**, 291–294.
26. K. Abe, S. Iwamoto and H. Yano, "Obtaining Cellulose Nanofibers with a Uniform Width of 15 Nm

- from Wood.” *Biomacromolecules* 2007, **8**, 3276–3278.
27. T. Zimmermann, E. Pohler and T. Geiger, “Cellulose Fibrils for Polymer Reinforcement.” *Adv. Eng. Mater.* 2004, **6**, 754–761.
 28. A. Chakraborty, M. Sain and M. Kortschot, “Cellulose Microfibrils: A Novel Method of Preparation Using High Shear Refining and Cryocrushing.” *Holzforschung* 2005, **59**, 102–107.
 29. M. Pääkkö, M. Ankerfors, H. Kosonen, A. Nykanen, S. Ahola, M. Österberg, J. Ruokolainen, J. Laine, P. T. Larsson, O. Ikkala and T. Lindström, “Enzymatic Hydrolysis Combined with Mechanical Shearing and High-Pressure Homogenization for Nanoscale Cellulose Fibrils and Strong Gels.” *Biomacromolecules* 2007, **8**, 1934–1941.
 30. M. Henriksson, G. Henriksson, L. A. Berglund and T. Lindström, “An Environmentally Friendly Method for Enzyme-Assisted Preparation of Microfibrillated Cellulose (MFC) Nanofibers.” *Eur. Polym. J.* 2007, **43**, 3434–3441.
 31. M. Henriksson, L. A. Berglund, P. Isaksson, T. Lindstrom and T. Nishino, “Cellulose Nanopaper Structures of High Toughness.” *Biomacromolecules* 2008, **9**, 1579–1585.
 32. S. Iwamoto, K. Abe and H. Yano, “The Effect of Hemicelluloses on Wood Pulp Nanofibrillation and Nanofiber Network Characteristics.” *Biomacromolecules* 2008, **9**, 1022–1026.
 33. M. Pääkkö, J. Vapaavuori, R. Silvennoinen, H. Kosonen, M. Ankerfors, T. Lindström, L. A. Berglund and O. Ikkala, “Long and Entangled Native Cellulose I Nanofibers Allow Flexible Aerogels and Hierarchically Porous Templates for Functionalities.” *Soft Matter* 2008, **4**, 2492–2499.
 34. A. E. J. Denooy, A. C. Besemer and H. Vanbekkum, “Highly Selective Nitroxyl Radical-Mediated Oxidation of Primary Alcohol Groups in Water-Soluble Glucans.” *Carbohydr. Res.* 1995, **269**, 89–98.
 35. P. L. Bragd, H. van Bekkum and A. C. Besemer, “TEMPO-Mediated Oxidation of Polysaccharides: Survey of Methods and Applications.” *Top. Catal.* 2004, **27**, 49–66.
 36. P. S. Chang and J. F. Robyt, “Oxidation of Primary Alcohol Groups of Naturally Occurring Polysaccharides with 2,2,6,6-Tetramethyl-1-Piperidine Oxoammonium Ion.” *J. Carbohydr. Chem.* 1996, **15**, 819–830.
 37. A. Isogai and Y. Kato, “Preparation of Polyuronic Acid from Cellulose by TEMPO-Mediated Oxidation.” *Cellulose* 1998, **5**, 153–164.
 38. Y. Kato, J. Kaminaga, R. Matsuo and A. Isogai, “TEMPO-Mediated Oxidation of Chitin, Regenerated Chitin and -Acetylated Chitosan.” *Carbohydr. Polym.* 2004, **58**, 421–426.
 39. N. Tamura, M. Wada and A. Isogai, “TEMPO-Mediated Oxidation of (1 → 3)- β -D-Glucans.” *Carbohydr. Polym.* 2009, **77**, 300–305.
 40. T. Saito, Y. Nishiyama, J. L. Putaux, M. Vignon and A. Isogai, “Homogeneous Suspensions of Individualized Microfibrils from TEMPO-Catalyzed Oxidation of Native Cellulose.” *Biomacromolecules* 2006, **7**, 1687–1691.
 41. T. Saito, S. Kimura, Y. Nishiyama and A. Isogai, “Cellulose Nanofibers Prepared by TEMPO-Mediated Oxidation of Native Cellulose.” *Biomacromolecules* 2007, **8**, 2485–2491.
 42. T. Saito, M. Hirota, N. Tamura, S. Kimura, H. Fukuzumi, L. Heux and A. Isogai, “Individualization of

- Nano-Sized Plant Cellulose Fibrils by Direct Surface Carboxylation Using TEMPO Catalyst under Neutral Conditions.” *Biomacromolecules* 2009, **10**, 1992–1996.
43. A. Isogai, T. Saito and H. Fukuzumi, “TEMPO-Oxidized Cellulose Nanofibers.” *Nanoscale* 2011, **3**, 71–85.
 44. Y. Okita, T. Saito and A. Isogai, “Entire Surface Oxidation of Various Cellulose Microfibrils by TEMPO-Mediated Oxidation.” *Biomacromolecules* 2010, **11**, 1696–1700.
 45. T. Saito and A. Isogai, “TEMPO-Mediated Oxidation of Native Cellulose. The Effect of Oxidation Conditions on Chemical and Crystal Structures of the Water-Insoluble Fractions.” *Biomacromolecules* 2004, **5**, 1983–1989.
 46. H. Fukuzumi, T. Saito, T. Iwata, Y. Kumamoto and A. Isogai, “Transparent and High Gas Barrier Films of Cellulose Nanofibers Prepared by TEMPO-Mediated Oxidation.” *Biomacromolecules* 2009, **10**, 162–165.
 47. H. Fukuzumi, S. Fujisawa, T. Saito and A. Isogai, “Selective Permeation of Hydrogen Gas Using Cellulose Nanofibril Film.” *Biomacromolecules* 2013, **14**, 1705–1709.
 48. T. Saito, T. Uematsu, S. Kimura, T. Enomae and A. Isogai, “Self-Aligned Integration of Native Cellulose Nanofibrils Towards Producing Diverse Bulk Materials.” *Soft Matter* 2011, **7**, 8804–8809.
 49. S. Elazzouzi-Hafraoui, Y. Nishiyama, J. L. Putaux, L. Heux, F. Dubreuil and C. Rochas, “The Shape and Size Distribution of Crystalline Nanoparticles Prepared by Acid Hydrolysis of Native Cellulose.” *Biomacromolecules* 2008, **9**, 57–65.
 50. Y. Fukushima and S. Inagaki, “Synthesis of an Intercalated Compound of Montmorillonite and 6-Polyamide.” *J. Inclusion Phenom.* 1987, **5**, 473–482.
 51. Y. Fukushima, A. Okada, M. Kawasumi, T. Kurauchi and O. Kamigaito, “Swelling Behavior of Montmorillonite by Poly-6-Amide.” *Clay Miner.* 1988, **23**, 27–34.
 52. J. N. Coleman, U. Khan, W. J. Blau and Y. K. Gun'ko, “Small but Strong: A Review of the Mechanical Properties of Carbon Nanotube–Polymer Composites.” *Carbon* 2006, **44**, 1624–1652.
 53. M. T. Byrne and Y. K. Gun'ko, “Recent Advances in Research on Carbon Nanotube-Polymer Composites.” *Adv. Mater.* 2010, **22**, 1672–1688.
 54. M. Moniruzzaman and K. I. Winey, “Polymer Nanocomposites Containing Carbon Nanotubes.” *Macromolecules* 2006, **39**, 5194–5205.
 55. T. Ramanathan, A. A. Abdala, S. Stankovich, D. A. Dikin, M. Herrera-Alonso, R. D. Piner, D. H. Adamson, H. C. Schniepp, X. Chen, R. S. Ruoff, S. T. Nguyen, I. A. Aksay, R. K. Prud'Homme and L. C. Brinson, “Functionalized Graphene Sheets for Polymer Nanocomposites.” *Nat. Nanotechnol.* 2008, **3**, 327–331.
 56. M. A. Rafiee, J. Rafiee, Z. Wang, H. H. Song, Z. Z. Yu and N. Koratkar, “Enhanced Mechanical Properties of Nanocomposites at Low Graphene Content.” *ACS Nano* 2009, **3**, 3884–3890.
 57. J. Liang, Y. Huang, L. Zhang, Y. Wang, Y. Ma, T. Guo and Y. Chen, “Molecular-Level Dispersion of Graphene into Poly(Vinyl Alcohol) and Effective Reinforcement of Their Nanocomposites.” *Adv. Funct. Mater.* 2009, **19**, 2297–2302.

58. A. Okada and A. Usuki, "Twenty Years of Polymer-Clay Nanocomposites." *Macromol. Mater. Eng.* 2006, **291**, 1449–1476.
59. E. P. Giannelis, "Polymer Layered Silicate Nanocomposites." *Adv. Mater.* 1996, **8**, 29–35.
60. S. Pavlidou and C. D. Papaspyrides, "A Review on Polymer-Layered Silicate Nanocomposites." *Prog. Polym. Sci.* 2008, **33**, 1119–1198.
61. V. Favier, G. R. Canova, J. Y. Cavallé, H. Chanzy, A. Dufresne and C. Gauthier, "Nanocomposite Materials from Latex and Cellulose Whiskers." *Polym. Adv. Technol.* 1995, **6**, 351–355.
62. V. Favier, H. Chanzy and J. Y. Cavallé, "Polymer Nanocomposites Reinforced by Cellulose Whiskers." *Macromolecules* 1995, **28**, 6365–6367.
63. M. A. S. A. Samir, F. Alloin and A. Dufresne, "Review of Recent Research into Cellulosic Whiskers, Their Properties and Their Application in Nanocomposite Field." *Biomacromolecules* 2005, **6**, 612–626.
64. S. J. Eichhorn, A. Dufresne, M. Aranguren, N. E. Marcovich, J. R. Capadona, S. J. Rowan, C. Weder, W. Thielemans, M. Roman, S. Renneckar, W. Gindl, S. Veigel, J. Keckes, H. Yano, K. Abe, M. Nogi, A. N. Nakagaito, A. Mangalam, J. Simonsen, A. S. Benight, A. Bismarck, L. A. Berglund and T. Peijs, "Review: Current International Research into Cellulose Nanofibres and Nanocomposites." *J. Mater. Sci.* 2010, **45**, 1–33.
65. I. Siró and D. Plackett, "Microfibrillated Cellulose and New Nanocomposite Materials: A Review." *Cellulose* 2010, **17**, 459–494.
66. A. N. Nakagaito and H. Yano, "The Effect of Fiber Content on the Mechanical and Thermal Expansion Properties of Biocomposites Based on Microfibrillated Cellulose." *Cellulose* 2008, **15**, 555–559.
67. H. Yano, J. Sugiyama, A. N. Nakagaito, M. Nogi, T. Matsuura, M. Hikita and K. Handa, "Optically Transparent Composites Reinforced with Networks of Bacterial Nanofibers." *Adv. Mater.* 2005, **17**, 153–155.
68. Y. Shimazaki, Y. Miyazaki, Y. Takezawa, M. Nogi, K. Abe, S. Ifuku and H. Yano, "Excellent Thermal Conductivity of Transparent Cellulose Nanofiber/Epoxy Resin Nanocomposites." *Biomacromolecules* 2007, **8**, 2976–2978.
69. M. Nogi, K. Handa, A. N. Nakagaito and H. Yano, "Optically Transparent Bionanofiber Composites with Low Sensitivity to Refractive Index of the Polymer Matrix." *Appl. Phys. Lett.* 2005, **87**, 243110–243113.
70. M. D. Sanchez-Garcia, E. Gimenez and J. M. Lagaron, "Morphology and Barrier Properties of Solvent Cast Composites of Thermoplastic Biopolymers and Purified Cellulose Fibers." *Carbohydr. Polym.* 2008, **71**, 235–244.
71. W. G. Glasser, R. Taib, R. K. Jain and R. Kander, "Fiber-Reinforced Cellulosic Thermoplastic Composites." *J. Appl. Polym. Sci.* 1999, **73**, 1329–1340.
72. S. Ifuku, M. Nogi, K. Abe, K. Handa, F. Nakatsubo and H. Yano, "Surface Modification of Bacterial Cellulose Nanofibers for Property Enhancement of Optically Transparent Composites: Dependence on

- Acetyl-Group DS.” *Biomacromolecules* 2007, **8**, 1973–1978.
73. D. Y. Kim, Y. Nishiyama and S. Kuga, “Surface Acetylation of Bacterial Cellulose.” *Cellulose* 2002, **9**, 361–367.
 74. S. Berlioz, S. Molina-Boisseau, Y. Nishiyama and L. Heux, “Gas-Phase Surface Esterification of Cellulose Microfibrils and Whiskers.” *Biomacromolecules* 2009, **10**, 2144–2151.
 75. H. Yuan, Y. Nishiyama, M. Wada and S. Kuga, “Surface Acylation of Cellulose Whiskers by Drying Aqueous Emulsion.” *Biomacromolecules* 2006, **7**, 696–700.
 76. Y. Yoshida and A. Isogai, “Nanofibrillation of Alkyl Ketene Dimer (AKD)-Treated Cellulose in Tetrahydrofuran.” *Cellulose* 2013, **20**, 3–7.
 77. J. Majoinen, A. Walther, J. R. McKee, E. Kontturi, V. Aseyev, J. M. Malho, J. Ruokolainen and O. Ikkala, “Polyelectrolyte Brushes Grafted from Cellulose Nanocrystals Using Cu-Mediated Surface-Initiated Controlled Radical Polymerization.” *Biomacromolecules* 2011, **12**, 2997–3006.
 78. G. Morandi, L. Heath and W. Thielemans, “Cellulose Nanocrystals Grafted with Polystyrene Chains through Surface-Initiated Atom Transfer Radical Polymerization (SI-ATRP).” *Langmuir* 2009, **25**, 8280–8286.
 79. J. Yi, Q. X. Xu, X. F. Zhang and H. L. Zhang, “Temperature-Induced Chiral Nematic Phase Changes of Suspensions of Poly(*N,N*-Dimethylaminoethyl Methacrylate)-Grafted Cellulose Nanocrystals.” *Cellulose* 2009, **16**, 989–997.
 80. J. O. Zoppe, Y. Habibi, O. J. Rojas, R. A. Venditti, L. S. Johansson, K. Efimenko, M. Österberg and J. Laine, “Poly(*N*-Isopropylacrylamide) Brushes Grafted from Cellulose Nanocrystals via Surface-Initiated Single-Electron Transfer Living Radical Polymerization.” *Biomacromolecules* 2010, **11**, 2683–2691.
 81. J. O. Zoppe, M. S. Peresin, Y. Habibi, R. A. Venditti and O. J. Rojas, “Reinforcing Poly(ϵ -Caprolactone) Nanofibers with Cellulose Nanocrystals.” *ACS Appl. Mater. Interfaces* 2009, **1**, 1996–2004.
 82. H. Lönnberg, L. Fogelström, M. A. Azizi Samir, L. Berglund, E. Malmstrom and A. Hult, “Surface Grafting of Microfibrillated Cellulose with Poly(ϵ -Caprolactone) - Synthesis and Characterization.” *Eur. Polym. J.* 2008, **44**, 2991–2997.
 83. Y. Habibi, A. L. Goffin, N. Schiltz, E. Duquesne, P. Dubois and A. Dufresne, “Bionanocomposites Based on Poly(ϵ -Caprolactone)-Grafted Cellulose Nanocrystals by Ring-Opening Polymerization.” *J. Mater. Chem.* 2008, **18**, 5002–5010.
 84. N. Lin, G. J. Chen, J. Huang, A. Dufresne and P. R. Chang, “Effects of Polymer-Grafted Natural Nanocrystals on the Structure and Mechanical Properties of Poly(Lactic Acid): A Case of Cellulose Whisker-Graft-Polycaprolactone.” *J. Appl. Polym. Sci.* 2009, **113**, 3417–3425.
 85. M. Hasani, E. D. Cranston, G. Westman and D. G. Gray, “Cationic Surface Functionalization of Cellulose Nanocrystals.” *Soft Matter* 2008, **4**, 2238–2244.
 86. E. Kloser and D. G. Gray, “Surface Grafting of Cellulose Nanocrystals with Poly(Ethylene Oxide) in Aqueous Media.” *Langmuir* 2010, **26**, 13450–13456.

87. L. Rueda, B. F. d'Arlas, Q. Zhou, L. A. Berglund, M. A. Corcuera, I. Mondragon and A. Eceiza, "Isocyanate-Rich Cellulose Nanocrystals and Their Selective Insertion in Elastomeric Polyurethane." *Compos. Sci. Technol.* 2011, **71**, 1953–1960.
88. G. Siqueira, J. Bras and A. Dufresne, "Cellulose Whiskers Versus Microfibrils: Influence of the Nature of the Nanoparticle and Its Surface Functionalization on the Thermal and Mechanical Properties of Nanocomposites." *Biomacromolecules* 2009, **10**, 425–432.
89. G. Siqueira, J. Bras and A. Dufresne, "New Process of Chemical Grafting of Cellulose Nanoparticles with a Long Chain Isocyanate." *Langmuir* 2010, **26**, 402–411.
90. C. Goussé, H. Chanzy, M. Cerrada and E. Fleury, "Surface Silylation of Cellulose Microfibrils: Preparation and Rheological Properties." *Polymer* 2004, **45**, 1569–1575.
91. C. Goussé, H. Chanzy, G. Excoffier, L. Soubeyrand and E. Fleury, "Stable Suspensions of Partially Silylated Cellulose Whiskers Dispersed in Organic Solvents." *Polymer* 2002, **43**, 2645–2651.
92. A. Pei, Q. Zhou and L. A. Berglund, "Functionalized Cellulose Nanocrystals as Biobased Nucleation Agents in Poly(L-lactide) (PLLA) – Crystallization and Mechanical Property Effects." *Compos. Sci. Technol.* 2010, **70**, 815–821.
93. L. Heux, G. Chauve and C. Bonini, "Nonfloculating and Chiral-Nematic Self-Ordering of Cellulose Microcrystals Suspensions in Nonpolar Solvents." *Langmuir* 2000, **16**, 8210–8212.
94. C. Bonini, L. Heux, J. Y. Cavaille, P. Lindner, C. Dewhurst and P. Terech, "Rodlike Cellulose Whiskers Coated with Surfactant: A Small-Angle Neutron Scattering Characterization." *Langmuir* 2002, **18**, 3311–3314.
95. N. Ljungberg, C. Bonini, F. Bortolussi, C. Boisson, L. Heux and J. Y. Cavaille, "New Nanocomposite Materials Reinforced with Cellulose Whiskers in Atactic Polypropylene: Effect of Surface and Dispersion Characteristics." *Biomacromolecules* 2005, **6**, 2732–2739.
96. N. Ljungberg, J. Cavaille and L. Heux, "Nanocomposites of Isotactic Polypropylene Reinforced with Rod-Like Cellulose Whiskers." *Polymer* 2006, **47**, 6285–6292.
97. J. Araki, M. Wada and S. Kuga, "Steric Stabilization of a Cellulose Microcrystal Suspension by Poly(Ethylene Glycol) Grafting." *Langmuir* 2001, **17**, 21–27.
98. E. Lasseguette, "Grafting onto Microfibrils of Native Cellulose." *Cellulose* 2008, **15**, 571–580.
99. F. Azzam, L. Heux, J. L. Putaux and B. Jean, "Preparation by Grafting onto, Characterization, and Properties of Thermally Responsive Polymer-Decorated Cellulose Nanocrystals." *Biomacromolecules* 2010, **11**, 3652–3659.
100. R. K. Johnson, A. Zink-Sharp and W. G. Glasser, "Preparation and Characterization of Hydrophobic Derivatives of TEMPO-Oxidized Nanocelluloses." *Cellulose* 2011, **18**, 1599–1609.
101. M. Salajková, L. A. Berglund and Q. Zhou, "Hydrophobic Cellulose Nanocrystals Modified with Quaternary Ammonium Salts." *J. Mater. Chem.* 2012, **22**, 19798–19805.
102. S. Fujisawa, T. Saito and A. Isogai, "Nano-Dispersion of TEMPO-Oxidized Cellulose/Aliphatic Amine Salts in Isopropyl Alcohol." *Cellulose* 2012, **19**, 459–466.

Chapter 2

Selective Surface Modification of Cellulose Nanofibrils through TEMPO-Mediated Oxidation

2.1 Abstract

Nanoscale surface engineering of crystalline cellulose nanofibrils has been developed through selective modification of carboxyl groups on the surface of 2,2,6,6-tetramethylpiperidiny1-1-oxyl-oxidized cellulose nanofibrils (TOCNs). TOCNs were prepared from wood cellulose, and the surface carboxyl groups were selectively modified on covalent and non-covalent approaches by the use of carbodiimides and amines. When TOCNs were reacted with either *N,N'*-diisopropylcarbodiimide (DIC) or *N,N'*-dicyclohexylcarbodiimide (DCC), diisopropyl or dicyclohexyl groups were selectively introduced on the carboxyl groups via *N*-acylurea structures, respectively. Conversion ratios of carboxyl groups to *N*-acylureas were approximately 80 and 60 %, when DIC and DCC, respectively. When primary alkyl or polyethylene glycol (PEG) chains were used, they were introduced onto most of (>95%) carboxyl groups on the TOCN surfaces via ionic bondings. The carbon number of alkyl chain lengths introduced onto TOCNs varied using *n*-decyl-, *n*-dodecyl-, *n*-tetradecyl-, *n*-hexadecyl- and *n*-octadecyl-amines, and the DP_ws of PEG chains used were 23 and 48. The dispersibility of the TOCN-*N*-acylureas, alkylated-TOCNs, and PEG-TOCNs were investigated in various kinds of organic solvents. Original TOCNs are dispersed only in water or polar organic solvents. On the other hand, after surface modification, the surface-modified TOCNs were stably dispersed not only in water and polar organic solvents but also in nonpolar organic solvents such as chloroform and toluene.

2.2 Introduction

Controlling the dispersion of cellulose nanofibrils in polymer matrices is the most important in the development of high-performance polymer nanocomposites; the properties of the nanocomposites result

primarily from the dispersibility of the nanofibrils. However, it is generally difficult to disperse the nanofibrils in polymer matrices, because they have high surface energies and are prone to aggregation in various media, not only in aqueous solution but also organic media. Therefore, the development of surface-modification techniques for the dispersion of the nanofibrils is required toward their wider applications.

Stable dispersions of cellulose nanowhiskers with negatively charged sulfate groups have been prepared in polar organic solvents such as *N,N*-dimethylformamide (DMF) and dimethyl sulfoxide (DMSO).¹⁻² Okita et al. reported that 2,2,6,6-tetramethylpiperidiny-1-oxyl (TEMPO)-oxidized cellulose nanofibrils (TOCNs) were able to be stably dispersed at the individual nanofibril level in polar organic solvents such as DMF, *N,N*-dimethylacetamide (DMAc), *N*-methyl-2-pyrrolidone (NMP), 1,3-dimethyl-2-imidazolidinone (DMI) in high yields by converting the sodium carboxylate groups of the TOCNs to free carboxyl groups (TOCN-COOH).³ In these organic solvents, the sulfate or carboxyl groups on the surfaces were sufficiently dissociated, which allowed them to be individually dispersed by osmotic effects and/or electrostatic repulsion between the anionically charged fibrils. By using the organic solvent dispersions of cellulose nanowhiskers or TOCNs, mechanically enhanced polymer nanocomposites can be prepared by simple solvent casting method.⁴⁻⁷ However, the dispersibility is limited in polar organic media, and the nanofibrils were not dispersed in common low or non-polar organic solvents such as isopropyl alcohol (IPA), chloroform, and toluene, which are good solvents for a wide range of organic materials. This is likely because that the dielectric constants of these solvents are too low to sufficiently dissociate the surface sulfate or carboxyl groups.

The goal of this study was to develop a method to individually disperse cellulose nanofibrils in various kinds of organic solvents. To achieve this goal, the surface carboxyl groups of TOCNs were selectively modified on covalent and non-covalent approaches; the former involved the use of carbodiimides to form *N*-acylurea formation with the carboxyl groups, and the latter involved the formation of ionic bondings with alkyl amines or amine-terminated polyethylene glycol (PEG-NH₂).

2.3 Materials and methods

2.3.1 Materials

A never-dried softwood bleached kraft pulp (SBKP, Nippon Paper Ind., Japan), which contained approximately 90% cellulose and 10% hemicelluloses, was used as the original wood cellulose. The SBKP was stirred in a diluted HCl solution at pH ~2.5 for 2 h at 1% consistency for demineralization, and then washed repeatedly with water by filtration. TEMPO, sodium bromide, a 13% NaClO solution, DMF, DIC, DCC, *n*-decyl-, *n*-dodecyl-, *n*-tetradecyl-, *n*-hexadecyl-, *n*-octadecyl-amines (C₁₀-, C₁₂-, C₁₄-, C₁₆-, and C₁₈-amines, respectively), and other chemicals and solvents were commercial products of laboratory grade (Wako Pure Chemicals, Japan), and used as received. PEG-NH₂ (SUNBRIGHT MEPA-20H, *M_w* 2182) was obtained from NOF Corp. (Tokyo, Japan).

2.3.2 Preparation of TOCNs

TEMPO-oxidized cellulose was prepared from SBKP by the TEMPO/NaBr/NaClO system. The SBKP (1 g) was suspended in water (100 mL) containing TEMPO (0.016 g, 0.1 mmol) and sodium bromide (0.1 g, 1 mmol). The NaClO solution (10 mmol) was added to the slurry, and the mixture was stirred at room temperature and pH 10, where the pH was maintained by addition of 0.5 M sodium hydroxide solution. The TEMPO-oxidized cellulose (1 g) was treated further with sodium chlorite (1.8 g) in 0.5 M acetate buffer (90 mL) at pH 4.8 and room temperature for 2 days to convert residual C6-aldehydes to C6-carboxylates. The TEMPO-oxidized cellulose was suspended in water (100 mL) at a 0.1 w/v % solid content, and the slurry was homogenized at 7500 rpm for 1 min at room temperature using a double-cylinder-type homogenizer (Physoctron, Microtec Niton, Japan). The gel thus obtained was then sonicated for 4 min using an ultrasonic homogenizer with a 26-mm diameter probe tip at 19.5 kHz and 300 W output power (US-300T, Nissei, Japan) and converted to a transparent aqueous dispersion of TOCNs with sodium carboxylate groups (TOCN-COONa).

2.3.3 Formation of *N*-acylureas

A transparent and flowable 0.1% w/v TOCN-COOH/DMF dispersion was obtained by sonicating TOCN-COOH gels in DMF.^{3,6} DIC or DCC of 5 mol per mole of carboxyl groups of TOCN-COOH was added to the 0.1% TOCN-COOH/DMF dispersion, and the mixture was stirred at room temperature for 6, 12 and 24 h under apparently homogeneous conditions. The mixture was then poured into a mixed solution of 0.01 M HCl and ethanol (1:1 by volume). The gel-like precipitate thus formed was collected by centrifugation, and washed repeatedly with ethanol by centrifugation. Ethanol in the mixture was completely exchanged to *t*-butanol by repeated centrifugation, and then the TEMPO-oxidized cellulose reacted with either DIC or DCC was obtained by freeze-drying. Chemical structures of DIC and DCC are shown in Figure 2.1.

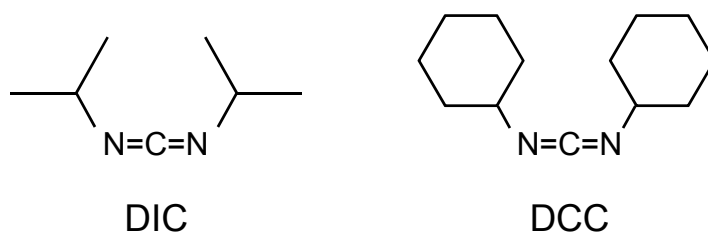


Figure 2.1. Chemical structures of *N,N'*-diisopropylcarbodiimide (DIC) and *N,N'*-dicyclohexylcarbodiimide (DCC) used in this study.

2.3.4 Amine-salt formation with alkyl amines

The TOCN-COOH was nano-dispersed in a water-IPA mixture (1:1 by vol.) by sonicating TOCN-COOH gels in the mixture.⁸ A 1 % w/v solution of C₁₀-, C₁₂-, C₁₄-, C₁₆- or C₁₈-amine in IPA was slowly added to the 0.1 w/v % homogeneous dispersion of TOCN-COOH in water-IPA mixture under continuous stirring, in which the amine/carboxyl ratio was adjusted to 1:1 by mol. All dispersions maintained the original homogeneous states after the amine additions, and the dispersions were stirred at room temperature for 1 h. When the C₁₈-amine was used, the dispersion was heated at 50 °C to completely dissolve the C₁₈-amine in the water-IPA mixture. All TOCN-COOH/amine salts homogeneously dispersed in water-IPA mixture turned to soft gels by the addition of excess water. The gels thus formed were washed with IPA to remove water and to

solvent-exchange water-IPA for each organic solvent by repeated (>5 times) centrifugation at 12,000g for 15 min. These 0.1% (w/v) amine-treated TOCN gels suspended in each organic solvent were then subjected to sonication for 1 min using an ultrasonic homogenizer (US-300T, Nihonseiki, Japan) with a 7 mm diameter probe tip at 19.5 kHz and 300 W output power.

2.3.5 Amine-salt formation with PEG amines

1 M HCl was slowly added to the TOCN-COONa/water dispersion to form TOCN-COOH. The medium was adjusted to pH ~2 and then stirred at room temperature for 30 min. The TOCN-COOH gel particles thus formed were collected and washed with water, and then solvent exchanged through ethanol into each chosen solvent by centrifugation or filtration. A 5 % w/v solution of PEG-NH₂ dissolved in each organic solvent was added to the cellulose nanofibril gel, where the molar ratio of PEG-NH₂ to the carboxyl groups of TEMPO-oxidized cellulose was adjusted to 1:1. The PEG-grafted cellulose nanofibril (PEG-TOCN) dispersions were obtained after sonication for 3 min.

2.3.6 Analyses

Light transmittance spectra of the dispersions and films were measured from 400 to 800 nm with a spectrophotometer (JASCO V-670). Fourier transform infrared (FT-IR) spectra of the TOCN films were recorded using a JASCO FT/IR-6100 spectrometer under transmission mode from 400 to 4,000 cm⁻¹ with a 4 cm⁻¹ resolution. The degree of substitutions of the carboxyl groups were evaluated by determination of nitrogen contents using an elemental analyzer (Flash 2000, Thermo Scientific, USA). X-ray diffraction patterns of pellets, which were prepared from the freeze-dried TOCN-related samples by pressing at 750 MPa for 1 min, were recorded from 10 to 30 ° of diffraction angle 2θ using the reflection method by means of a Rigaku RINT 2000 with monochromator-treated Cu K α radiation (λ 0.15418 nm) at 40 kV and 40 mA. Crystallinity indices of cellulose I were calculated from the X-ray diffraction patterns. Solid-state ¹³C NMR spectra were obtained on a CMX300 spectrometer (Varian/ Chemagnetics, USA) operating at 75.6 MHz. The

sample in a 4 mm zirconia rotor was spun at 5 kHz in a solid-state probe with the magic-angle. All spectra were obtained by using a ^1H NMR 90° pulse length of 2.5 μs , with a cross-polarization time of 1.0 ms and 60 kHz CW proton decoupling. The repetition time and accumulation times were 3 s and 24,000, respectively. The spectra were calibrated by using adamantane as an external standard. The contact angles of 2 μL water droplet on the pellet samples were measured at 23 $^\circ\text{C}$ and 50% relative humidity using a FAMES DM500 apparatus (Kyowa Interface Science Co. Ltd., Japan). Nano-dispersibility of the isolated and purified reaction products in each organic solvent was evaluated by visual observation, birefringence behavior between crosspolarizers, and light transmittance of the dispersion with an UV-Vis spectrophotometer (JASCO V-670) after ultrasonication in the organic solvent for 2 min.

2.4 Results and discussion

2.4.1 Formation of *N*-acylureas

2.4.1.1 Chemical structures of reaction products of TOCN-COOH with DIC in DMF

A transparent and flowable TOCN-COOH/DMF dispersion was obtained by the conversion of TOCN-COONa to TOCN-COOH, solvent exchange from water to DMF via acetone, and mechanical disintegration of the gel-like TOCN-COOH particles suspended in dry DMF by sonication. It was initially expected that carboxyl groups present on the TOCN surfaces could be converted to amides in the TOCN-COOH/DMF dispersion by the addition of carbodiimide such as DIC or DCC, a primary amine and 4-dimethylaminopyridine (DMAP) as an agent to prevent formation of stable *N*-acylureas, which are reported to be suitable for efficient amidation of carboxyl groups under non-aqueous systems.⁹⁻¹⁰ In preliminary experiments, various reaction conditions, where different amounts of reagents added, temperatures and times were applied, were tested to prepare TOCN-COOH derivatives with high degrees of amidation. C_8 -, C_{10} -, and C_{12} -amines were used as primary amines in the experiments. In all cases examined, the reactions proceeded under apparently homogeneous conditions, and neither formation of precipitate nor gelation of the mixture took place during the reactions. Moreover, the original birefringence behavior was observed also after the

reaction with DIC for 24 h. However, chemical structures of the reaction products after isolation and purification were clearly different from the original TOCN-COOH, the corresponding amides or TOCN/amine salts in any cases; no amides were obtained from TOCN-COOH under the reaction conditions.

The TOCN-COOH was then reacted only with DIC of 5 mol per mole of carboxyl groups of TOCN-COOH in DMF at room temperature for 1 day, and the obtained reaction product was first analyzed by FT-IR (Figure 2.2). The weight recovery ratio was >97%, and most of the recovery loss was caused by repeated washing and purification processes using centrifugation. The absorption band around 1720 cm^{-1} due to stretching vibration of free carboxyl C=O groups mostly disappeared, and new bands at 1698, 1658 and 1536 cm^{-1} due to C=ON, C=ONH and N-HCO groups, respectively,¹¹⁻¹³ appeared for the reaction product. The bands at $2750\text{--}3000\text{ cm}^{-1}$ were ascribed to C-H stretching vibration of isopropyl groups. Most of other bands remained almost unchanged after the reaction with DIC. Because the reaction product was washed thoroughly with 0.01 M HCl, it was not plausible that carboxyl groups of TOCN formed ammonium salts with DIC-derived compounds. On the other hand, it is likely from the FT-IR spectrum that the reaction product had *N*-acylurea groups, which are possible to be formed from carboxyl groups by reaction with carbodiimide and stably present in the product.¹¹⁻¹³

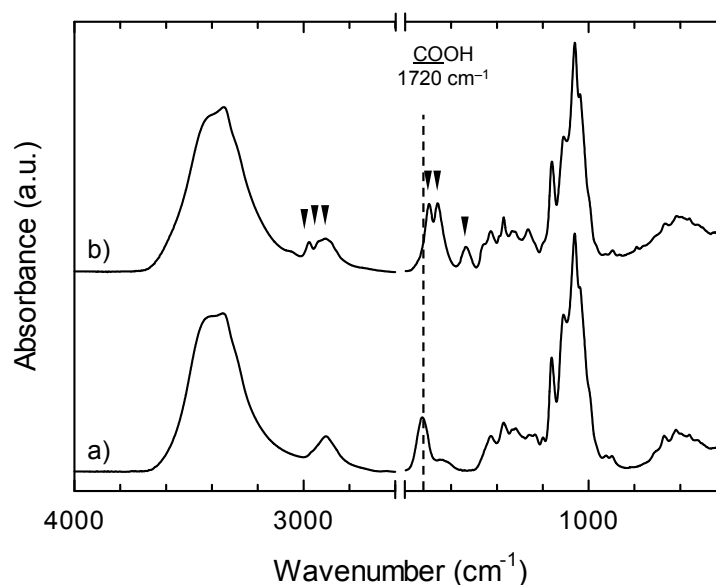


Figure 2.2. FT-IR spectra of the original TOCN-COOH (a) and reaction product of TOCN-COOH with DIC in DMF at room temperature for 1 day (b). Reproduction of image with permission from Springer (© Springer 2011).

Solid-state CP-MAS ^{13}C NMR spectra of the original TOCN-COOH and the reaction product are depicted in Figure 2.3. Although a small signal around 175 ppm due to carboxyl carbons of TOCN-COOH remained after the reaction, two new signals at 155 and 169 ppm due to two carbonyl carbons of *N*-acylurea groups appeared in the spectrum of the reaction product.^{11, 13} The signals in the range of 20–50 ppm were ascribed to $-\text{CH}_3$ and $-\text{CH}$ carbons of isopropyl moiety of the *N*-acylurea groups. The broad signals at approximately 66 and 63 ppm are ascribed to the C6 primary hydroxyl carbons inside crystalline cellulose microfibril (*C6_{cryst.}*) and microfibril surface (*C6_{surf.}*), respectively, and the signals at approximately 89 and 84 ppm were due to the C4 hydroxyl carbons inside crystalline cellulose microfibril (*C4_{cryst.}*) and microfibril surface (*C4_{surf.}*), respectively.¹⁴⁻¹⁵ The original TOCN and TOCN-*N*-acylurea in Figure 2.3 had signal area ratios *C6_{cryst.}*/*C6_{surf.}* of 0.79 and 0.78, respectively, and had signal area ratios *C4_{cryst.}*/*C4_{surf.}* of 0.47 and 0.48, respectively. Because these signal ratios were mostly unchanged before and after the *N*-acylurea formation, it can be concluded that the crystalline structure of the original TOCN was intact. Because a part of *C6_{surf.}* groups of the original wood cellulose have been converted to C6-carboxyls by TEMPO-mediated oxidation, the signal area ratios *C4_{cryst.}*/*C4_{surf.}* (0.47–0.48) were lower than those of *C6_{cryst.}*/*C6_{surf.}* (0.78–0.79).

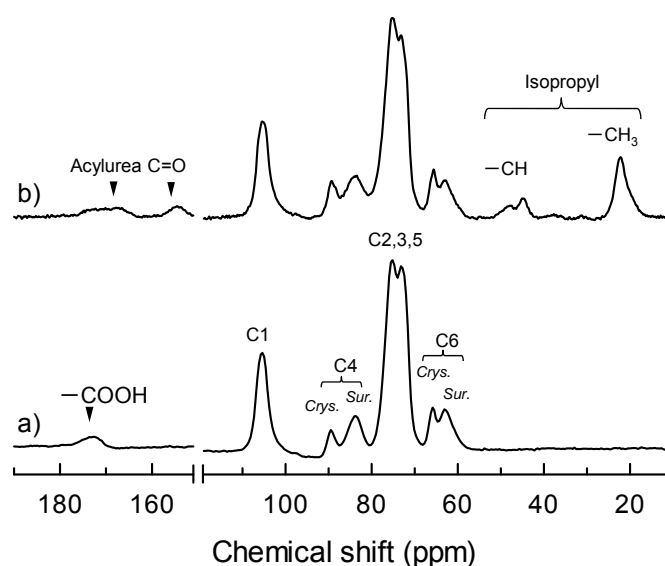


Figure 2.3. Solid state ^{13}C NMR spectra of the original TOCN-COOH (a) and reaction product of TOCN-COOH with DIC in DMF at room temperature for 1 day (b). Reproduction of image with permission from Springer (© Springer 2011).

It can be concluded from Figure 2.2 and 2.3 that carboxyl groups of TOCN-COOH react with DIC in DMF to selectively form *N*-acylurea groups (Figure 2.4), and no amidation takes place even by the coadditions of a primary amine and DMAP under the conditions examined so far. Thus, although amidation of carboxyl groups of TOCN-COOH could not be achieved by the reaction with DIC, introduction of two isopropyl moieties to one carboxyl group of TOCN-COOH or introduction of hydrophobic *N*-acylurea groups into the hydrophilic carboxyl groups of TOCN-COOH was succeeded by this reaction.

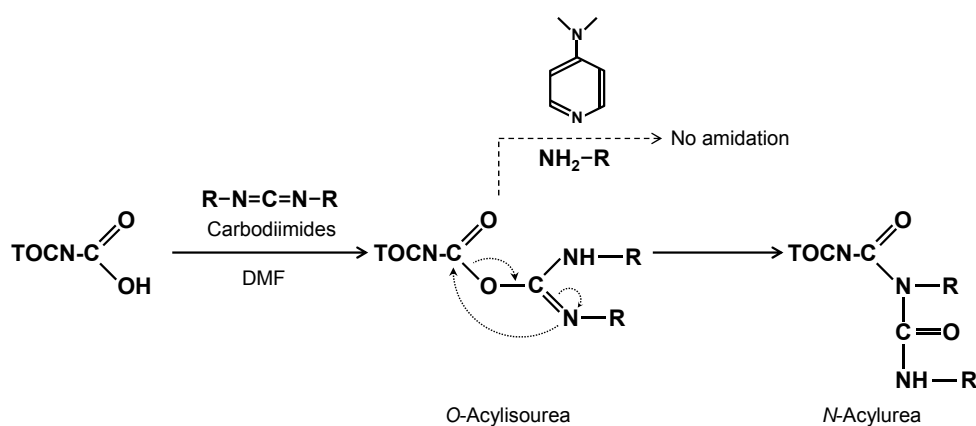


Figure 2.4. *N*-Acylation of carboxyl groups of TOCN-COOH with DIC in DMF.

2.4.1.2 The effect of reaction time on the formation of *N*-acylurea groups

Since the chemical structure of the reaction product was confirmed in the previous section, the conversion ratios of carboxyl groups of TOCN-COOH to *N*-acylurea groups by the reaction with DIC in DMF under various conditions can be calculated from nitrogen contents of the reaction products. The relationship between reaction time and the conversion ratio of carboxyl groups to *N*-acylurea groups is presented in Figure 2.5. Approximately 80% of carboxyl groups of TOCN-COOH were converted to *N*-acylurea groups after the reaction for 12 h at room temperature, and this conversion ratio was almost unchanged even after the reaction for 24 h. Because the weight recovery ratio of the product prepared by the reaction for 24 h was 97%, the yield of the product was calculated to be 83% based on the *N*-acylurea structure of the product with the COOH → *N*-acylurea conversion ratio of 78%.

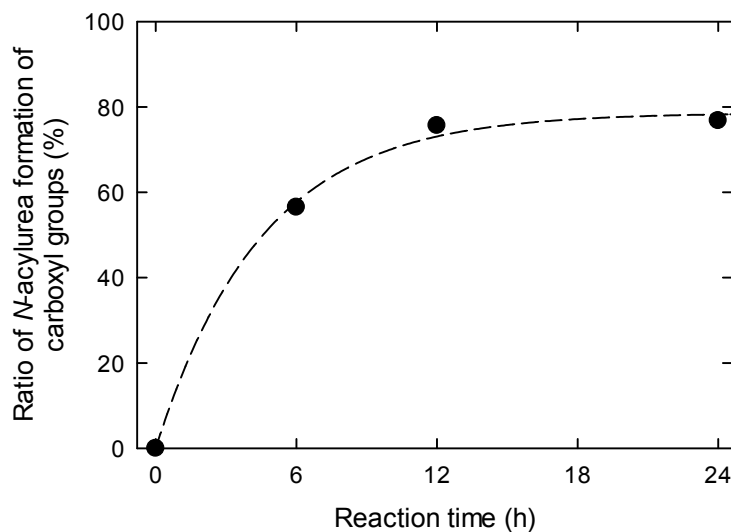


Figure 2.5. Change in conversion ratio of carboxyls of TOCN to *N*-acylurea groups during reaction with DIC in DMF at room temperature for 0–1 day. Reproduction of image with permission from Springer (© Springer 2011).

When the amounts of DIC added were 1–3 mol per mole of carboxyl groups of TOCN–COOH, the conversion ratios were lower than 20% even after the reaction for 1 day. Meanwhile, when the amounts of DIC added were increased to 7–10 mol per mole of carboxyl groups of TOCN–COOH, the conversion ratios were almost the same 80%. Thus, 5 mol per mole of carboxyl groups seemed to be the optimum addition level of DIC examined so far.

2.4.1.3 Reaction of TOCN–COOH with DCC in DMF

When DCC, which is more bulky than DIC, was used in place of DIC as the reagent for the *N*-acylurea formation of TOCN–COOH, similar results were obtained. Figure 2.6 shows the FT-IR spectrum of the reaction product prepared from TOCN–COOH with DCC of 5 mol per mole of carboxyl groups of TOCN–COOH in DMF at room temperature for 1 day.

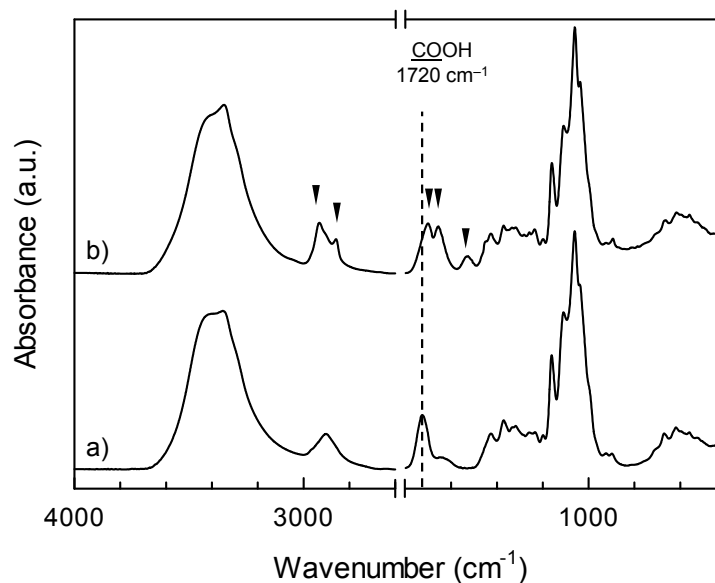


Figure 2.6. FT-IR spectra of the original TOCN-COOH (a) and reaction product of TOCN-COOH with DCC in DMF at room temperature for 1 day (b). Reproduction of image with permission from Springer (© Springer 2011).

The FT-IR spectrum was similar to that for the reaction product prepared with DIC in Figure 2.2. The increased absorption bands at 2800–3000 cm^{-1} are due to CH stretching vibrations of cyclohexyl groups. The conversion ratio of carboxyl groups of TOCN–COOH to *N*-acylurea groups was calculated to be 59% from the nitrogen content, which was lower than that for the reaction product prepared with DIC. Probably, steric factor of the bulky cyclohexyl groups of DCC resulted in the low conversion ratio. Consequently, however, formation of *N*-acylurea groups from carboxyl groups of TOCN–COOH can be intrinsically achieved with both DIC and DCC in DMF by the method presented in this paper.

2.4.1.4 Characteristics of TOCN-*N*-acylureas

X-ray diffraction patterns of freeze-dried TOCN before and after the reaction with DIC at room temperature for 1 day are shown in Figure 2.7. The original cellulose I crystal structure with a relatively low crystallinity of wood cellulose was maintained in the reaction product. The original TOCN and TOCN-*N*-acylurea in Figure 2.7 had crystal widths of 2.8 and 2.7 nm, respectively, when calculated from the full width

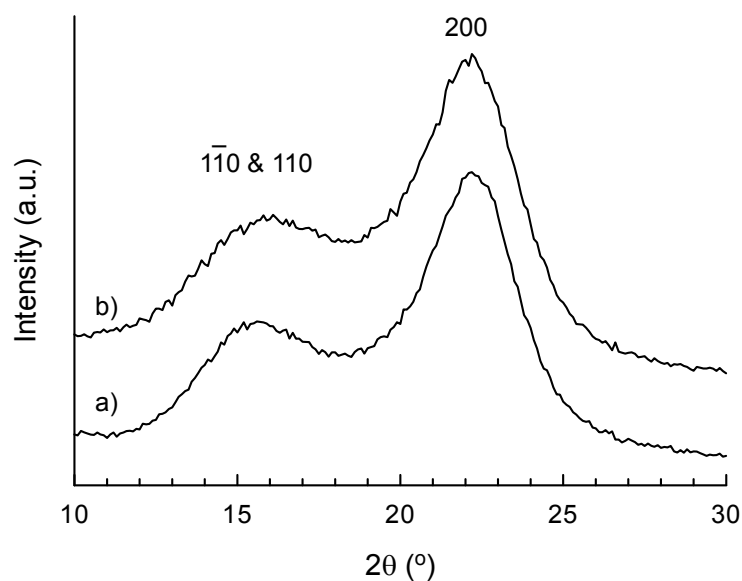


Figure 2.7. X-ray diffraction patterns of the original TOCN-COOH (a) and reaction product of TOCN with DIC in DMF at room temperature for 1 day (b). Reproduction of image with permission from Springer (© Springer 2011).

at half maximum of the (2 0 0) diffraction peak by Scherrer's equation. As a result, approximately 80 and 60% of carboxyl groups present on the crystalline cellulose microfibril surfaces of TOCN-COOH can be converted to *N*-acylurea groups by the reaction with DIC and DCC, respectively, in DMF without significant reduction of the original crystallinity or crystal width of cellulose I. The solid-state ^{13}C NMR spectrum of the reaction product (Figure 2.3) also supports the same conclusion.

The nano-dispersibility of the TOCN-*N*-acylureas in organic solvents was evaluated for freeze-dried or solvent-exchanged and thus never-dried TOCN-*N*-acylureas prepared with DIC and DCC at the conversion ratios of 78 and 59%, respectively. DMF, IPA and dioxane were used as the dispersion solvents, and ultrasonic treatment was applied to the suspensions for 2 min. When the freeze-dried TOCN-*N*-acylureas were used, no homogeneous dispersions were obtained and the mixtures always contained gel-like particles or precipitates. Thus, the once-freeze dried TOCN-*N*-acylureas could be no longer dispersed at the individual nanofibril level in these organic solvents, probably because some inter-fibrillar hydrogen bonds are formed during freeze-drying process. On the other hand, when the never-dried TOCN-*N*-acylurea gels were solvent-exchanged to DMF and sonicated in fresh DMF for 2 min, transparent and flowable dispersions with

birefringence behavior between cross-polarizers were obtained for TOCN-*N*-acylureas prepared with both DIC and DCC, showing that nano-dispersion of the TOCN-*N*-acylureas can be achieved by the solvent exchange method (Figure 2.8a). However, the TOCN-*N*-acylureas could not be completely nano-dispersed in IPA or dioxane even by the solvent-exchange method, and some gels were observed at the upper internal wall of the sample bottles. The TOCN-*N*-acylureas dispersed in DMF at the nanofibril level had high light transmittances of >95% at 600 nm (Figure 2.8b). Moreover, the nano-dispersion states of TOCN-*N*-acylureas in DMF were maintained without formation of any aggregates or gels for at least 3 months at room temperature, showing that the nano-dispersion states are highly stable.

Nano-dispersion mechanisms in DMF are different between TOCN-COOH and TOCN-*N*-acylureas. Dissociation of carboxyl groups and the subsequent electrostatic repulsion of TOCN-COOH elements in DMF is the primary reason for the nano-dispersion in DMF, which has a high dielectric constant of 36.7.³ On the other hand, solvation of *N*-acylurea groups (and maybe C2-OH and C3-OH groups as well) with DMF molecules is likely to bring about the nano-dispersion of TOCN-*N*-acylureas. Moreover, free carboxyl groups

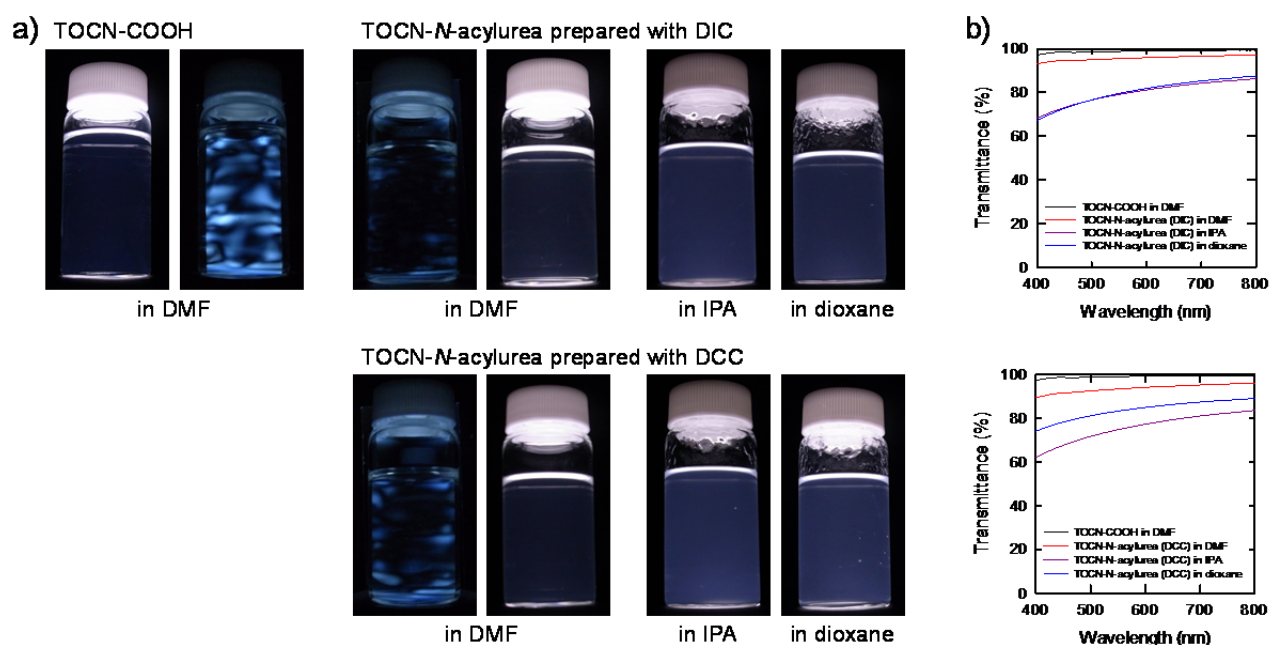


Figure 2.8. Photographs of dispersions of the original TOCN-COOH in DMF, TOCN-*N*-acylureas in DMF, IPA, and dioxane, taken with or without crossed-polarizers (a). Light transmittance spectra of the dispersions in DMF, IPA, and dioxane. Reproduction of image with permission from Springer (© Springer 2011).

were still remained on the TOCN surfaces even after the reactions, which might have played a role on dispersing TOCN-*N*-acylureas. These mechanisms may be less effective in nano-dispersion than those of TOCN-COOH, resulting in slightly lower light transmittances of TOCN-*N*-acylureas in DMF (Figure 2.8b).

2.4.1.5 Hydrophobicity of the TOCN-*N*-acylureas

Contact angles of water droplet on TOCN increased from approximately 45° to 82° and 85° after the reaction with DIC and DCC, respectively (Figure 2.9). Hydrophobicity of TOCN was thus increased due to the introduction of hydrophobic diisopropyl and dicyclohexyl groups onto the TOCN surface via *N*-acylurea structures. However, water-contact angles on the TOCN-*N*-acylureas gradually decreased by wetting expansion as time goes by. This may stem from hydrophilicity of unreacted carboxyl and hydroxyl groups remaining on the surface of TOCNs after the reaction. The TOCN reacted with DCC had a little higher water-contact angle than that with DIC, although the TOCN reacted with DCC exhibited lower conversion ratio of carboxyl groups. This is probably because cyclohexyl groups have higher hydrophobicity than isopropyls. As a result, hydrophobic nature can be introduced to TOCN by conversion of hydrophilic carboxyl groups to hydrophobic *N*-acylurea groups.

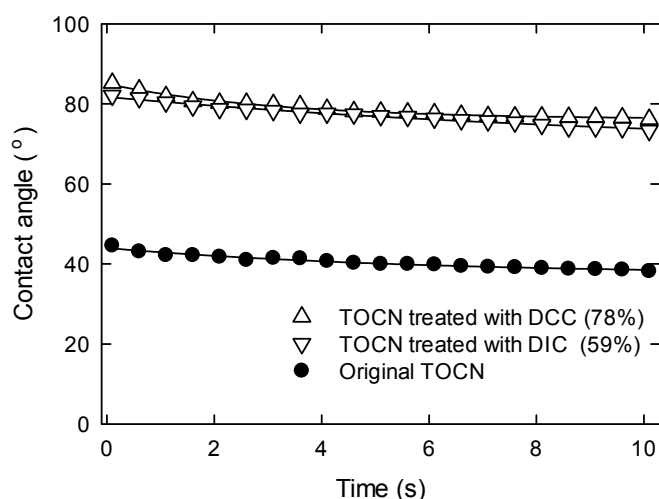


Figure 2.9. Contact angle of water droplet on the pellets made of original TOCN and TOCN modified with DIC or DCC. The number shown in parentheses indicate the conversion ratio of carboxyl groups to *N*-acylureas. Reproduction of image with permission from Springer (© Springer 2011).

2.4.2 Amine-salt formation with alkyl amines

2.4.2.1 Chemical structures of alkylated TOCNs

Because TOCN-COOH was found to be dispersed at the individual nanofibril level in water-IPA mixture with 1:1 by vol. (but not nano-dispersed in pure IPA), formation of TOCN-COOH/alkyl amine salts proceeded homogeneously without any precipitates in the water-IPA mixture by adding the amine/IPA solutions. When the C₁₈-amine was used, heating of the dispersion at 50 °C was required to keep the homogeneous dispersion state without precipitation of the C₁₈-amine in the mixture. To remove water in the dispersions and to solvent-exchange the water-IPA mixture for pure IPA as a dispersion medium, the TOCN-COOH/amine salts were precipitated as soft gels by addition of excess water to the homogeneous dispersions, and the gel-like precipitates thus formed were sufficiently washed with IPA for solvent exchange.

Figure 2.10 presents FT-IR spectra of the original TOCN-COOH film and the alkylated TOCN films. The absorption band due to carbonyl stretching of free carboxyl groups of TOCN-COOH at 1720 cm⁻¹ mostly shifted to that due to carboxylate groups at 1600 cm⁻¹ by the amine salt formation. The shoulder and small bands at 1640 and 1540 cm⁻¹, respectively, are due to N-H stretching vibrations of protonated amine salt groups. The bands at 2800–3000 cm⁻¹ are ascribed to C-H stretching vibrations of methyl and methylene groups of alkyl amines. The relative absorbance peaks at 2890 and 2855 cm⁻¹ due to C-H stretching vibration of methylene groups to those at 1000–1200 cm⁻¹ due to cellulose backbones increased with increasing the carbon number of the alkyl amines used for neutralization of the TOCN-COOH. Other absorption bands due to crystalline cellulose remained unchanged.

These FT-IR spectra indicate that most of the carboxyl groups of TOCN-COOH formed the amine salt structures in the films. Nitrogen contents of selfstanding films of the TOCN-COOH/amine salts showed that the degrees of the amine salt formation or those of introduction of amines to carboxyl groups were 95–99% (Figure 2.10). Thus, more than 95% of carboxyl groups of TOCN-COOH were converted to the corresponding alkyl amine salts in the present scheme, where the moles of alkyl amines added were adjusted to the same as those of carboxyl groups of TOCN-COOH in the dispersions. It was confirmed by X-ray diffraction analysis that the crystallinity and crystal width of the original cellulose I of TOCN-COONa were unchanged before

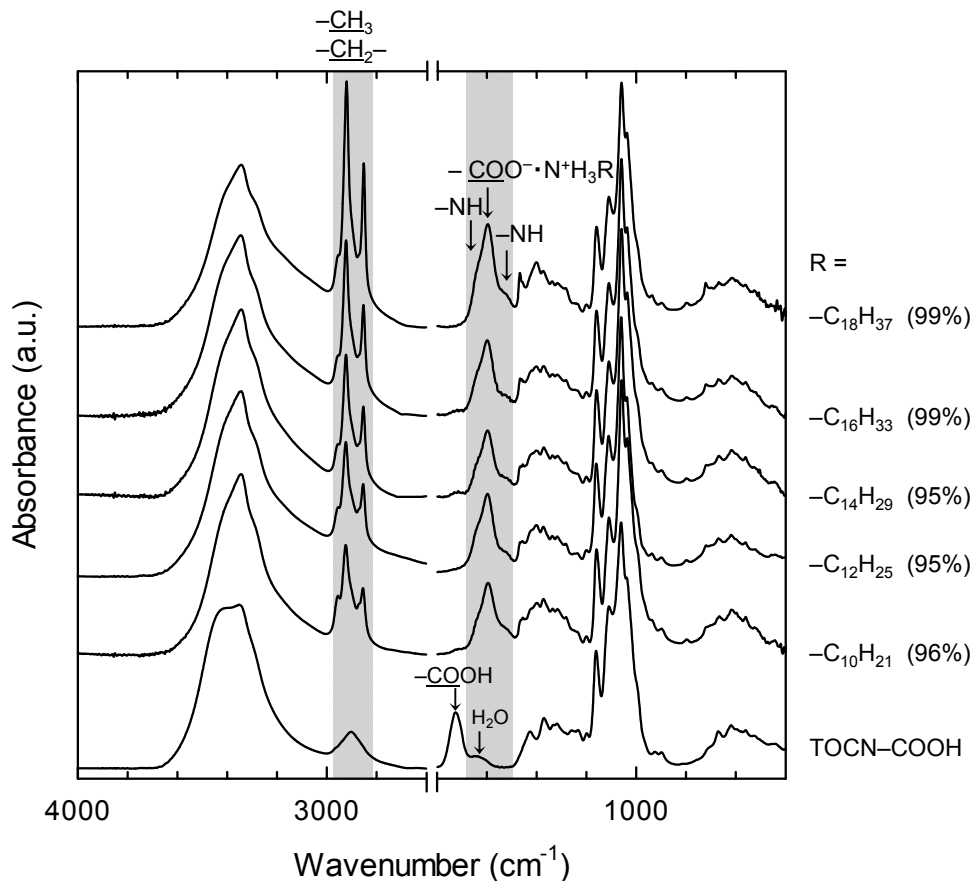


Figure 2.10. FT-IR spectra of TOCN-COOH and alkylated TOCN films. Percentages in parentheses are the conversion ratios from TOCN-COOH to TOCN-COOH/alkyl-amine salts, calculated from their nitrogen contents. Reproduction of image with permission from Springer (© Springer 2012).

and after the amine salt formation in all cases.¹⁶ As a result, long alkyl chains can be positionselectively and almost stoichiometrically introduced into carboxyl groups present on the TOCN surfaces via the amine salt formation.

2.4.2.2 Nano-dispersibility of alkylated TOCNs in IPA

The gel-like precipitates of TOCN-COOH/alkyl amine salts in IPA were then mechanically disintegrated by ultrasonication, and flowable dispersions of alkylated TOCNs were successfully obtained (Figure 2.11). When the C₁₂-, C₁₄- and C₁₆-amines were used for neutralization of carboxyl groups of TOCN, the dispersions showed high transparencies (>97% at 600 nm) and clear birefringence (Figure 2.11c), indicating that these

salts were dispersed at the individual nanofibril level in IPA.¹⁷ These dispersions of alkylated TOCNs stably maintained the transparent dispersion states at room temperature for more than 3 months. In the cases of the C10-amine, the light-transmittance became lower; the C₁₀-TOCN forms some fibril aggregates in IPA. The light-transmittance of the C₁₈-TOCN dispersion was the lowest in the dispersions examined; complete individualization of nanofibrils of this salt in IPA could not be achieved. Thus, the number or length of carbon chains of primary amines used for the salt formation of TOCN-COOH influences the nano-dispersibility of the alkylated TOCNs in IPA, and the C₁₂-, C₁₄- and C₁₆-amines are adequate for nano-dispersion of the alkylated TOCNs in IPA. Because neither TOCN-COONa nor TOCN-COOH can be dispersed at individual nanofibril level in pure IPA,³ introduction of hydrophobic alkyl chains to carboxyl groups of TOCN-COOH as amine salts makes the nano-dispersion of TOCN in IPA possible. Probably, alkyl chains of the alkyl amine salts densely introduced into the TOCN surfaces are effectively interacted with IPA molecule, resulting in the complete nano-dispersion of the alkylated TOCNs in IPA.

As shown in Figure 2.11, nano-dispersion of TOCN in IPA was achieved, when the C₁₂-, C₁₄- and C₁₆-amines are used. On the other hand, neither C₁₀- nor C₁₈- amine could give a highly transparent dispersion,

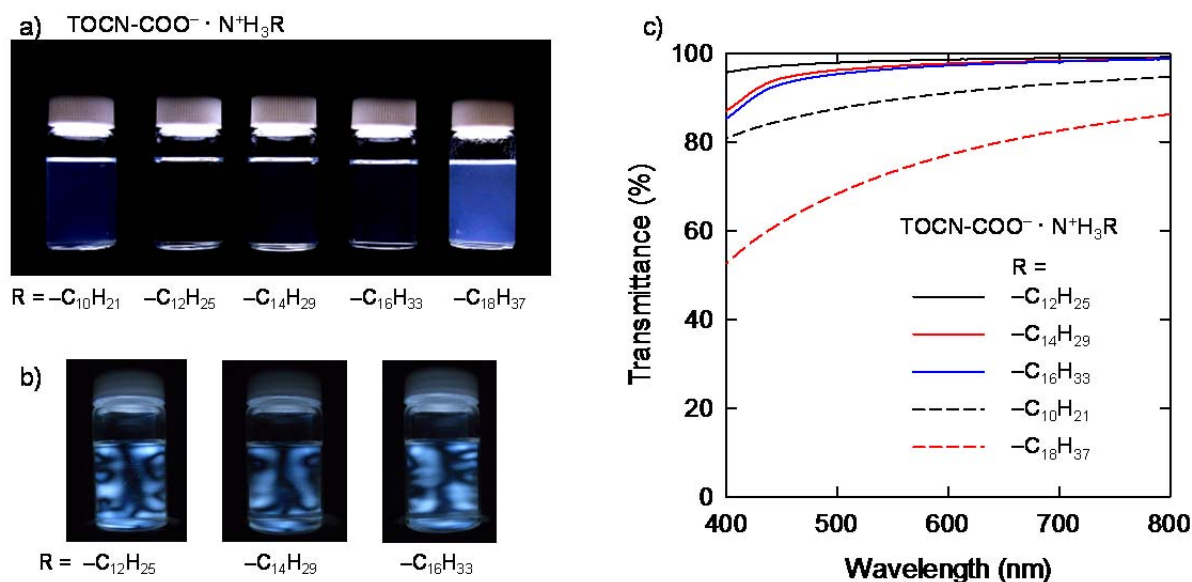


Figure 2.11. Photographs of 0.1% w/v dispersions of alkylated TOCNs in IPA (a), three of them taken between crossed-polarizers (b), and UV-Vis transmittance spectra of the dispersions (c). Reproduction of image with permission from Springer (© Springer 2012).

although almost all carboxyl groups of TOCN-COOH were converted to the corresponding amine salts in both cases (Figure 2.10). The alkyl chain length of the C₁₀-amine may be too short for each TOCN to be sufficiently interacted with IPA. In the case of the C₁₈-amine, its solubility in IPA may be originally low at room temperature.

As described in the previous paragraph, when the C₁₂-, C₁₄- and C₁₆-amines are used, alkylated TOCNs are successfully nano-dispersed in IPA, keeping the integrity of the original crystal structure of TOCN. These alkylated TOCNs were also dispersed in ethanol and polar organic solvents such as DMF, DMAc, and NMP. On the other hand, when the same dispersion protocol of the alkylated TOCNs was applied to other organic solvents such as chloroform, toluene and tetrahydrofuran (THF), the alkylated TOCNs could not be dispersed at the individual nanofibril level in any of these solvents.

2.4.2.3 Preparation of alkylated TOCN films

The film properties of alkylated TOCNs were studied using the C₁₂-, C₁₄-, and C₁₆-TOCNs. Flexible and highly transparent self-standing films of these alkylated TOCNs were successfully obtained by casting and drying of the dispersions in IPA. Figure 2.12a shows the photograph of C₁₂-TOCN films, and the film showed high optical transparency (89% light-transmittance at 600 nm). Because IPA has a boiling point of 82.4 °C, which is lower than that of water, evaporation energies required to make dried films from the IPA dispersions of the alkylated TOCNs are lower than those for the aqueous TOCN-COONa or TOCN-COOH dispersions. Time-dependent hydrophobic nature of the alkylated TOCN films was evaluated by measuring water-contact angles in comparison with the TOCN-COONa film (Figure 2.12b). The TOCN-COONa film is highly hydrophilic due to abundant sodium carboxylate groups densely present on the TOCN surfaces, and had an initial water-contact angle of 54°. This value gradually decreased with time by partial spreading of water droplet on the film and partial absorption of water into the film. In contrast, the alkylated TOCN films had high water contact angles of 85°, and these values were unchanged for more than 10 seconds, showing that the film has sufficiently hydrophobic nature. This is because the hydrophilic TOCNs are densely covered with the

alkyl chains. Thus, hydrophilic nature of TOCN films can be converted to hydrophobic by the formation of alkyl amine salts on the TOCN surfaces.

The densities, moisture contents, and tensile properties of the self-standing films prepared from the dispersions of TOCN-COONa in water and C₁₂-TOCN in IPA are listed in Table 2.1. The C₁₂-TOCN film had clearly lower mechanical properties and lower film density than those of the TOCN-COONa film probably due to a decrease in the amount of inter-fibrillar hydrogen bonds. The moisture content of the C₁₂-TOCN film was lower due to the introduction of hydrophobic long alkyl chains in large quantity. The 50 μm thick PET films coated with ~1 μm thick TOCN-COONa and C₁₂-TOCNs were subjected to oxygen transmission rate measurement at 23 °C and 0% RH. The oxygen permeability of the PET films decreased from 15.5 to 0.0015 mL m⁻² day⁻¹ kPa⁻¹ by coating with TOCN-COONa, showing that the TOCN-COONa layer has excellent oxygen barrier properties. In contrast, coating of the C₁₂-TOCN did not improve the oxygen barrier property of the PET film at all. Because the film density of the C₁₂-TOCN was as low as 1.33 (Table 2.1), it is likely that pore sizes in the film are larger and thus oxygen molecules easily permeate through the film, whereas the TOCN-COONa film has a denser structure with much smaller pore sizes.¹⁸ Thus, the introduction of abundant long-alkyl chains to TOCN by the formation of amine salts has a negative impact on oxygen barrier properties of the TOCN films.

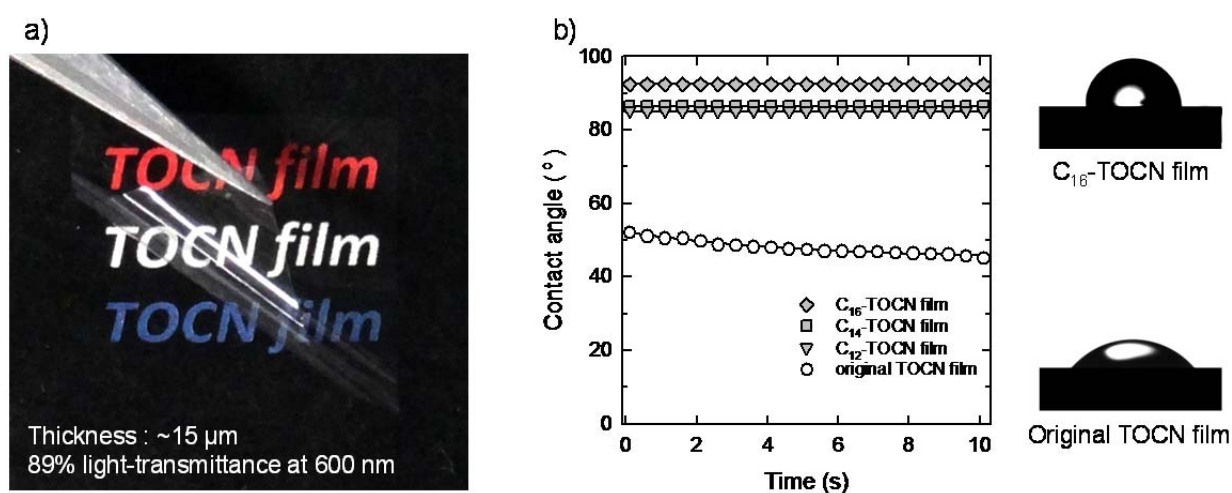


Figure 2.12. Photograph of self-standing film of C₁₂-TOCN film (a), and time-dependent changes in contact angle of water droplet on the films of TOCN-COONa and alkylated TOCN films (b). Reproduction of image with permission from Springer (© Springer 2012).

Table 2.1. Fundamental and mechanical properties of self-standing films of TOCN-COONa and C₁₂-TOCN.

	Density (g cm ⁻³)	Tensile strength (MPa)	Young's modulus (GPa)	Elongation at break (%)	Moisture content (%)
TOCN-COONa	1.44	247 ± 11	9.4 ± 1.0	6.7 ± 0.4	11.0
C ₁₂ -TOCN	1.33	83 ± 8.6	3.4 ± 4.3	4.1 ± 0.6	4.2

The mechanical and oxygen barrier properties of the C₁₂-TOCN films are clearly inferior to those of the TOCN-COONa films. However, IPA is one of the good solvents for most monomers of plastics and also some polymers. Thus, the alkylated TOCNs in IPA are expected to be used as nano-fillers for preparation of fiber-reinforced plastics. This is because complete dispersion of fillers at the individual nanofiber level with high aspect ratios is one of the necessary conditions to achieve the maximum mechanical properties of the fiber-reinforced plastics and nanocomposites with smaller filler-addition levels.

2.4.3 Amine-salt formation with PEG amines

2.4.3.1 Nano-dispersibility of PEG-TOCNs in non-polar organic solvents

A PEG-NH₂ (M_w 2182) was grafted onto TOCN surfaces via ionic bonding with their abundant C6-carboxyl groups. The PEG-grafted cellulose nanofibrils were dispersed at the individual nanofibril level in chloroform, tetrahydrofuran (THF) and toluene and showed birefringence when observed between cross-polarizers¹⁷ (Figure 2.13a). The dispersions were optically transparent with a light transmittance of more than 94% at 600 nm (Figure 2.13b). Original TOCNs without the surface-modification were not dispersible in these solvents at all. Thus, stable dispersion of the nanofibrils at the individual level in the organic solvents was achieved by grafting the PEG chains densely on the TOCN surfaces via ionic bonds.

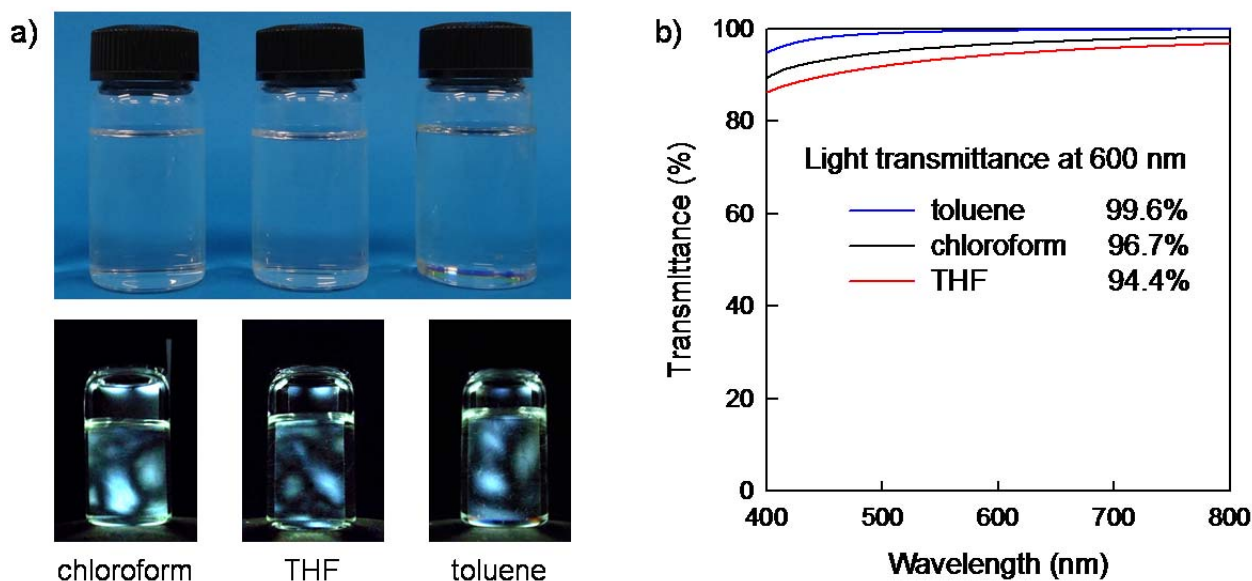


Figure 2.13. Photographs of 0.4 % w/v PEG-TOCN/organic solvent dispersions taken with and without cross polarizers (a) and UV-Vis transmittance spectra of the PEG-TOCN dispersions. The difference in light transmittance is due to that in refractive index between TEMPO-oxidized cellulose nanofibril and the solvent. The refractive indices of TEMPO-oxidized cellulose nanofibril, toluene, chloroform, and THF are 1.54, 1.49, 1.44, and 1.40, respectively, at 25°C; a larger difference in refractive index causes higher light scattering. Reproduction of image with permission from American Chemical Society (©American Chemical Society 2013).

2.4.3.2 Chemical structure of PEG-TOCNs

The PEG chains were selectively and densely grafted to C6-carboxyl groups on the TOCN surfaces at a 1:1 molar ratio, which was evaluated from FT-IR spectra (Figure 2.14) and nitrogen contents determined by elemental analysis. The PEG-grafted cellulose nanofibril/organic solvent dispersions maintained their original nano-dispersion states for at least six months. Generally, for colloidal dispersions stabilized by end-grafted chains, the repulsive forces between grafted chains ultimately arise from high osmotic pressures inside the brushes.¹⁹⁻²² The thickness of the resulting PEG layers on each cellulose nanofibril surface was theoretically calculated and estimated to be ~11 nm (Appendix),²²⁻²³ indicating that the grafted PEG chains stretched away from the cellulose nanofibril surface due to the highly dense grafting.

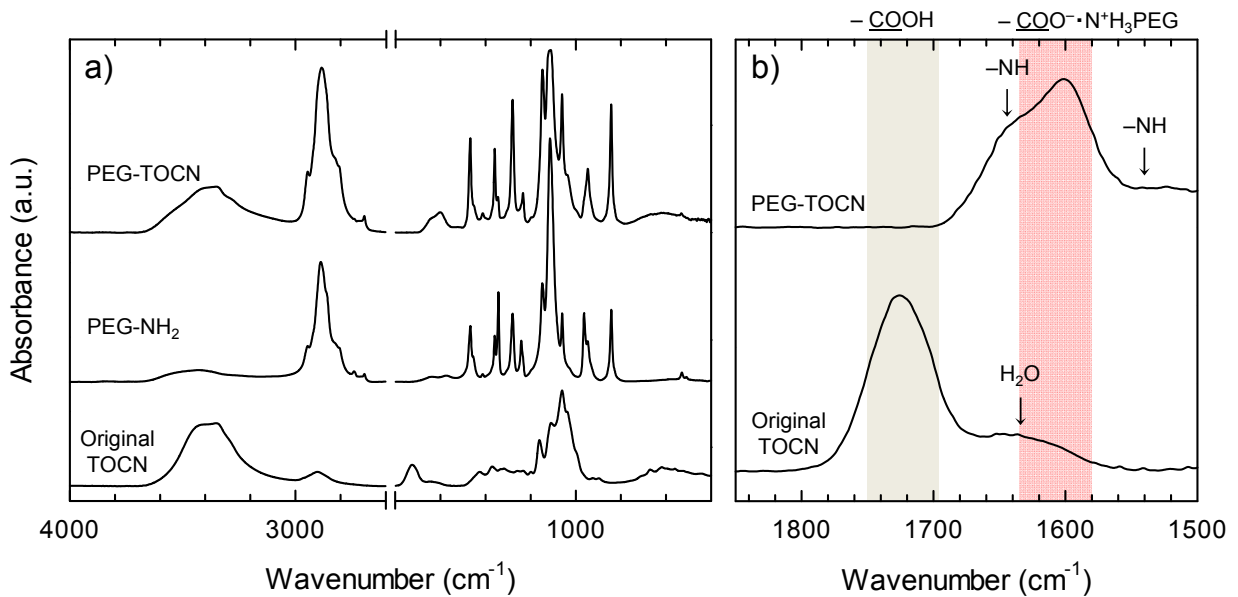


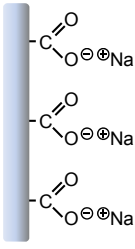
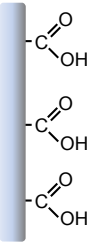
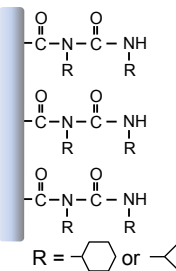
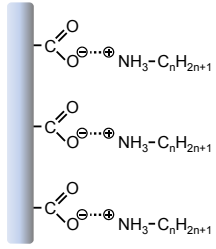
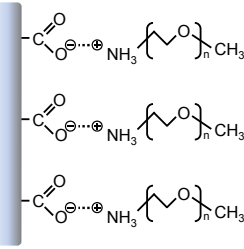
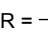
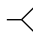
Figure 2.14. FT-IR spectra of original TOCN film, PEG-NH₂, and PEG-TOCN film at 4000–400 cm⁻¹ (a) and 1850–1500 cm⁻¹.

The repulsive force between grafted polymer layers was dependent on the thickness and density of the polymer brush layer. When another amine-terminated PEG sample with a shorter chain length of M_w 1176 was used as the grafting agent, the nanofibril/organic solvent dispersions were unstable in the organic solvents, and formed gels within one week at room temperature after sonication. In this study, therefore, long PEG chains (M_w 2182) were grafted on the TOCN surfaces in high density, which may have provided effective repulsion between the cellulose nanofibrils due to higher osmotic pressure, resulting in their stable and complete dispersion at the individual nanofibril level. Some surface modifications of TOCNs or nanowhiskers have been investigated so far. However, in these studies, the surface-modified nanocelluloses could not be dispersed at the individual nano-element level in nonpolar organic solvents such as chloroform and toluene and instead existed as bundles of nano-elements,^{16, 24-28} probably due to a low density of the grafted-chains on the nanocellulose surfaces or shortness of the grafting chain length. Therefore, surface-selective grafting of long PEG chains onto TOCN surfaces at high density allows the nano-dispersibility in these organic solvents.

2.4.4 Dispersibility of surface-modified TOCNs in organic solvents

The dispersibilities of original TOCNs and surface-modified TOCNs were summarized in Table 2.2. The dispersibilities were tested by birefringence examinations between crossed polarizers. As reported by Okita et al.,³ TOCN-COONa and TOCN-COOH are dispersible only in aqueous and polar organic solvents, which

Table 2.2. Dispersibilities of original TOCNs and surface-modified TOCNs in various organic solvents.

	TOCN-COONa	TOCN-COOH	TOCN- <i>N</i> -acylureas	Alkylated TOCN	PEG-TOCN
					
			R =  or 	n = 12, 14, and 16	n = 48 or 23
Water	○	○	×	×	○
DMSO	○	×	×	×	○
DMI	×	○	○	○	○
DMAc	×	○	○	○	○
DMF	×	○	○	○	○
NMP	×	○	○	○	○
ethanol	×	×	×	○	○
IPA	×	×	×	○	○
acetonitrile	×	×	×	×	○
methanol	×	×	×	×	○
acetone	×	×	×	×	○
THF	×	×	×	×	○
chloroform	×	×	×	×	○
toluene	×	×	×	×	○
hexane	×	×	×	×	×

have high dielectric constants. Even after the introduction of hydrophobic isopropyl and cyclohexyl groups via *N*-acylurea structures, the TOCN-*N*-acylureas are not dispersed in the other organic solvents such as dioxane and IPA. When alkyl chains were densely introduced onto the TOCN surfaces, the alkylated TOCNs were dispersed at the individual nanofibril level in ethanol and IPA. This is likely because that the length of alkyl chains was longer than that of isopropyl or cyclohexyl groups on the surface of the TOCN-*N*-acylureas. However, the alkylated TOCNs were still not dispersed in nonpolar organic solvents such as chloroform and toluene. On the other hand, when PEG-NH₂ which has longer chains than the alkyl chains were used as grafting agent, the PEG-TOCNs were for the first time dispersed in nonpolar organic solvents such as chloroform and toluene. The PEG-TOCNs were dispersed not only in nonpolar organic solvents, but also in aqueous and various polar organic solvents.

Figure 2.15 shows nano-dispersion map of original TOCNs and surface-modified TOCNs/organic solvent in terms of dielectric constant and viscosity of the organic solvent. As reported by Okita et al., TOCN-COONa and TOCN-COOH are only dispersible in organic solvents which have high dielectric constant and high viscosity. The dielectric constant plays a significant role on dissociating surface carboxyl groups of

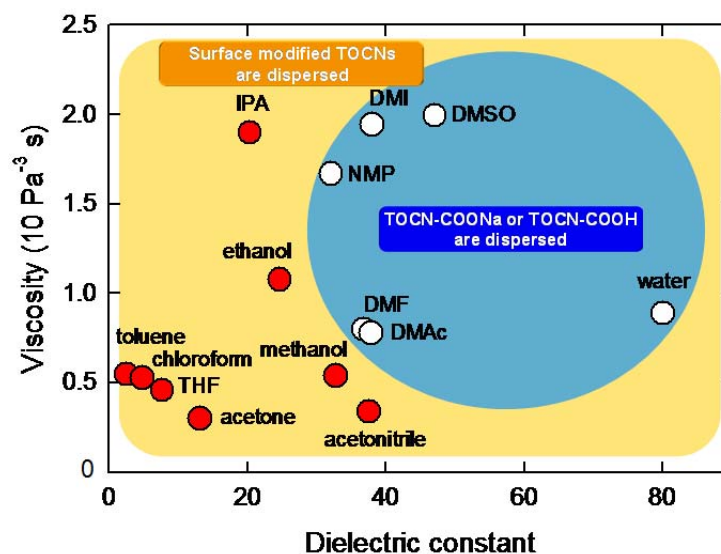


Figure 2.15. Nano-dispersion map of original TOCNs and surface-modified TOCNs/organic solvent in terms of dielectric constant and viscosity of the organic solvent.

TOCN-COONa and TOCN-COOH. The viscosity increases shear stress during mechanical treatment, and thermodynamically stabilizes the dispersion. On the other hand, surface modification of TOCNs allowed stable dispersions in various kinds of organic solvents. As noted above, the repulsive force between grafted polymer layers was dependent on the thickness and density of the polymer brush layer. Therefore, the dense layers of long alkyl or PEG chains allowed TOCNs to be dispersed by high osmotic pressure between the layers.

2.5 Conclusions

The nano-dispersibility of cellulose nanofibrils in organic solvents was modulated by selective surface modification of TOCNs. The surface carboxyl groups of TOCNs were densely modified via either *N*-acylurea structures or ionic bondings, without changing the crystal structure and crystal width of the original TOCNs. Formation of *N*-acylurea groups from carboxyl groups of TOCN-COOH was achieved using TOCN-COOH/DMF dispersions by reaction with DIC or DCC at room temperature. When DIC and DCC of 5 mol per mole of carboxyl groups of TOCN-COOH was used as the reagent in the reaction at room temperature for 1 day, the conversion ratio from carboxyls to *N*-acylurea groups was reached to be approximately 80 and 60%, respectively. Dispersion of TOCN-*N*-acylureas in polar organic solvents was accomplished by sonication. Introduction of long alkyl or PEG chains via simple ionic bondings was achieved by mixing TOCN-COOH and the amines. The introduction was selective to surface carboxyl groups of TOCNs, and the conversion ratios from free carboxyl groups to amine salt groups were more than 95%. When the C12-, C14- and C16-amines are used, the alkylated TOCNs were dispersed at the individual nanofibril level in ethanol and IPA. When PEG-NH₂ was introduced onto the TOCN surfaces, the PEG-TOCNs were stably dispersed not only in water and polar organic solvents but also in nonpolar organic solvents such as chloroform and toluene.

2.6 References

1. D. Viet, S. Beck-Candanedo and D. G. Gray, "Dispersion of Cellulose Nanocrystals in Polar Organic Solvents." *Cellulose* 2006, **14**, 109–113.
2. O. van den Berg, J. R. Capadona and C. Weder, "Preparation of Homogeneous Dispersions of Tunicate Cellulose Whiskers in Organic Solvents." *Biomacromolecules* 2007, **8**, 1353–1357.
3. Y. Okita, S. Fujisawa, T. Saito and A. Isogai, "TEMPO-Oxidized Cellulose Nanofibrils Dispersed in Organic Solvents." *Biomacromolecules* 2011, **12**, 518–522.
4. M. A. S. A. Samir, F. Alloin, J. Y. Sanchez, N. El Kissi and A. Dufresne, "Preparation of Cellulose Whiskers Reinforced Nanocomposites from an Organic Medium Suspension." *Macromolecules* 2004, **37**, 1386–1393.
5. N. E. Marcovich, M. L. Auad, N. E. Bellesi, S. R. Nutt and M. I. Aranguren, "Cellulose Micro/Nanocrystals Reinforced Polyurethane." *J. Mater. Res.* 2006, **21**, 870–881.
6. S. Fujisawa, T. Ikeuchi, M. Takeuchi, T. Saito and A. Isogai, "Superior Reinforcement Effect of TEMPO-Oxidized Cellulose Nanofibrils in Polystyrene Matrix: Optical, Thermal, and Mechanical Studies." *Biomacromolecules* 2012, **13**, 2188–2194.
7. H. Liu, D. Liu, F. Yao and Q. Wu, "Fabrication and Properties of Transparent Polymethylmethacrylate/Cellulose Nanocrystals Composites." *Bioresour. Technol.* 2010, **101**, 5685–5692.
8. S. Fujisawa, Y. Okita, H. Fukuzumi, T. Saito and A. Isogai, "Preparation and Characterization of TEMPO-Oxidized Cellulose Nanofibril Films with Free Carboxyl Groups." *Carbohydr. Polym.* 2011, **84**, 579–583.
9. T. S. Yokum, J. Alsina and G. Barany, "Solid-Phase Syntheses of Heterocycles Containing the 2-Aminothiophenol Moiety." *J. Comb. Chem.* 2000, **2**, 282–292.
10. P. J. Costanzo and F. L. Beyer, "Thermoresponsive, Optically Active Films Based on Diels-Alder Chemistry." *Chem. Mater.* 2007, **19**, 6168–6173.
11. P. Angelova, K. Kostova, K. Hinrichs and D. Tsankov, "A Convenient Synthesis of Long-Chain 4-Substituted Benzyloxycarbonyl Alkanethiols for the Formation of Self Assembled Monolayers on Metal Substrates." *Cent. Eur. J. Chem.* 2005, **3**, 658–667.
12. D. F. Detar and Silverst.R, "Reactions of Carbodiimides .I. Mechanisms of Reactions of Acetic Acid with Dicyclohexylcarbodiimide." *J. Am. Chem. Soc.* 1966, **88**, 1013–1019.
13. G. W. Buchanan, M. F. Rastegar and G. Enright, "Reaction of R_F-palmitic acid-F₁₃ with Dicyclohexylcarbodiimide." *J. Fluorine Chem.* 2007, **128**, 1026–1028.
14. L. Heux, E. Dinand and M. R. Vignon, "Structural Aspects in Ultrathin Cellulose Microfibrils Followed by ¹³C CP-MAS NMR." *Carbohydr. Polym.* 1999, **40**, 115–124.
15. R. J. Viëtor, R. H. Newman, M. A. Ha, D. C. Apperley and M. C. Jarvis, "Conformational Features of Crystal-Surface Cellulose from Higher Plants." *Plant J.* 2002, **30**, 721–731.
16. R. K. Johnson, A. Zink-Sharp and W. G. Glasser, "Preparation and Characterization of Hydrophobic Derivatives of TEMPO-Oxidized Nanocelluloses." *Cellulose* 2011, **18**, 1599–1609.

17. M. M. de Souza Lima and R. Borsali, "Rodlike Cellulose Microcrystals: Structure, Properties, and Applications." *Macromol. Rapid Commun.* 2004, **25**, 771–787.
18. H. Fukuzumi, T. Saito, S. Iwamoto, Y. Kumamoto, T. Ohdaira, R. Suzuki and A. Isogai, "Pore Size Determination of TEMPO-Oxidized Cellulose Nanofibril Films by Positron Annihilation Lifetime Spectroscopy." *Biomacromolecules* 2011, **12**, 4057-4062.
19. S. T. Milner, "Polymer Brushes." *Science* 1991, **251**, 905–914.
20. E. P. K. Currie, W. Norde and M. A. Cohen Stuart, "Tethered Polymer Chains: Surface Chemistry and Their Impact on Colloidal and Surface Properties." *Adv. Colloid Interface Sci.* 2003, **100-102**, 205–265.
21. P. G. de Gennes, "Polymers at an Interface; a Simplified View." *Adv. Colloid Interface Sci.* 1987, **27**, 189–209.
22. J. N. Israelachvili, *Intermolecular and Surface Forces*. 2nd ed.; Academic Press: London, 1991.
23. P. G. de Gennes, "Conformations of Polymers Attached to an Interface." *Macromolecules* 1980, **13**, 1069–1075.
24. J. Araki, M. Wada and S. Kuga, "Steric Stabilization of a Cellulose Microcrystal Suspension by Poly(Ethylene Glycol) Grafting." *Langmuir* 2001, **17**, 21–27.
25. E. Lasseguette, "Grafting onto Microfibrils of Native Cellulose." *Cellulose* 2008, **15**, 571–580.
26. F. Azzam, L. Heux, J. L. Putaux and B. Jean, "Preparation by Grafting onto, Characterization, and Properties of Thermally Responsive Polymer-Decorated Cellulose Nanocrystals." *Biomacromolecules* 2010, **11**, 3652–3659.
27. M. Salajková, L. A. Berglund and Q. Zhou, "Hydrophobic Cellulose Nanocrystals Modified with Quaternary Ammonium Salts." *J. Mater. Chem.* 2012, **22**, 19798–19805.
28. S. Fujisawa, T. Saito and A. Isogai, "Nano-Dispersion of TEMPO-Oxidized Cellulose/Aliphatic Amine Salts in Isopropyl Alcohol." *Cellulose* 2012, **19**, 459–466.

Chapter 3

Preparation and Characterization of PEG-TOCN/PLLA Nanocomposites

3.1 Abstract

Surface grafting of crystalline and ultrafine cellulose nanofibrils with poly(ethylene glycol) (PEG) chains via ionic bonds was achieved by a simple ion-exchange treatment. The PEG-grafted 2,2,6,6-tetramethylpiperidiny-1-oxyl -oxidized cellulose nanofibrils (TOCNs) exhibited nanodispersibility in organic solvents such as chloroform, toluene, and tetrahydrofuran. Then, the PEG-grafted TOCN (PEG-TOCN)/chloroform dispersion and poly(L-lactide) (PLLA)/chloroform solution were mixed, and the PEG-TOCN/PLLA composite films with various blend ratios were prepared by casting the mixtures on a plate and drying. The tensile strength, Young's modulus, and work of fracture of the composite films were remarkably improved, despite low TOCN addition levels (<1 wt %). The highly efficient nanocomposite effect was explained in terms of achievement of nanodispersion states of the PEG-TOCNs in the PLLA matrix. Moreover, some attractive interactions mediated by the PEG chains were likely to be formed between the TOCNs and PLLA molecules in the composites, additionally enhancing the efficient nanocomposite effect.

3.2 Introduction

Biopolymer/filler nanocomposites have been extensively studied primarily for the preparation of light-weight/ultrahigh-strength materials alternative to heavy steel and petroleum-based high-gas barrier films. When rigid nanoparticles such as carbon nanotubes,¹⁻³ nanoclays⁴⁻⁶ and graphene⁷⁻⁸ are used as nanofillers in polymer matrices, the resultant nanocomposites exhibit some improvement of their material properties when compared with neat polymers or conventional micro-composites.

In nature, plant cellulose microfibrils, which are present in plant cell walls and individually consist of 30–40

fully extended cellulose chains, have high elastic moduli (~ 140 GPa),¹¹ high tensile strengths (2–3 GPa),¹² and high aspect ratios (~ 3 nm and >1 μ m in width and length, respectively),¹³ and thereby contribute to the principal structural support of living plant bodies. Much effort has been dedicated to the use of cellulose microfibrils as reinforcing fillers in polymer nanocomposites because of their potential as mechanical reinforcing nano-elements. However, cellulose nanofibrils inherently have two main issues as a nanofiller: (i) low dispersibility in polymer matrix and (ii) poor interfacial interaction with the matrix. Therefore, surface modification of cellulose nanofibrils is necessary to take advantage of the unique properties in polymer nanocomposites.

In this chapter, our goal was to evaluate the previously described polyethylene glycol (PEG) was grafted onto 2,2,6,6-tetramethylpiperidiny-1-oxyl (TEMPO)-oxidized cellulose nanofibril (TOCN) surfaces and the PEG-TOCNs were used as reinforcements in poly (*L*-lactid) (PLLA). In general, cellulose nanofibril/PLLA nanocomposite materials show brittle behaviour because of insufficient attractive interactions between hydrophilic cellulose and hydrophobic PLLA matrix. Therefore, the interface should be carefully engineered to achieve the transfer of the mechanical load to individual cellulose nanofibrils. Bulota et al. recently reported that partial acetylation of the resulting cellulose nanofibrils leads to an increase in toughness of cellulose/poly(*L*-lactide) (PLLA) nanocomposites. However, improvement of both stiffness and toughness (resistance to fracture) still remains a challenge for these composites.⁹⁻¹⁰ Here, we report on the successful preparation of cellulose nanofibril/PLLA nanocomposites with enhanced stiffness, tensile strength, and toughness using the PEG-TOCNs. The idea is to improve the nano-dispersibility of TEMPO-oxidized cellulose nanofibrils in hydrophobic polymer matrix and the attractive interactions between the nanofiller and matrix polymer, by grafting long PLLA-miscible polymer chains efficiently and densely onto the TOCN surfaces using their abundant C6-carboxyl groups as anchoring sites (Figure 3.1).

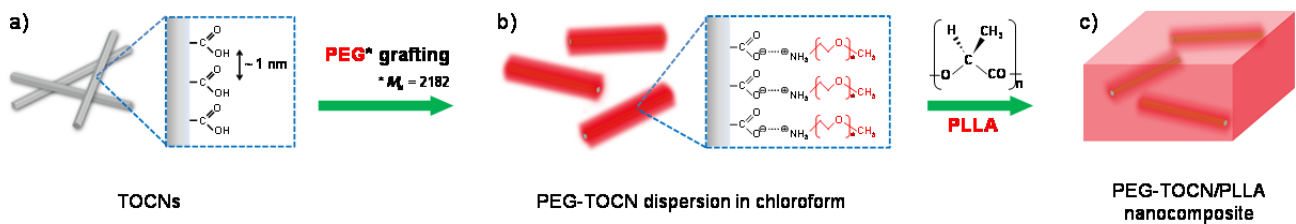


Figure 3.1. Schematic illustration of the process for the preparation of PEG-TOCN/PLLA nanocomposite films. a) Original TOCNs. b) PEG-TOCNs dispersed in chloroform. c) PEG-TOCN/PLLA nanocomposite film.

3.3 Materials and methods

3.3.1 Materials

A never-dried softwood bleached kraft pulp (Nippon Paper Ind. Co., Japan), which contained approximately 90% cellulose and 10% hemicelluloses, was used as the original wood cellulose. PEG-NH₂ (SUNBRIGHT MEPA-20H, M_w 2182) was obtained from NOF Corp. (Tokyo, Japan). All other reagents were purchased from Wako Pure Chemicals, Co., Japan and used as received. Poly(L-lactide) (PLLA) (Lacty[®]) with M_w and M_n of 94,000 and 45,000, respectively, was supplied by Toyota Motor Co., Japan.

3.3.2 Preparation of PEG-TOCN dispersions in chloroform

Cellulose nanofibrils were obtained using a TEMPO/NaBr/NaClO system with 3.8 mmol NaClO per gram of cellulose. Oxidation with sodium chlorite at pH 4.8 was subsequently carried out to convert the small amount of aldehyde groups remaining after the TEMPO-mediated oxidation. The TEMPO-oxidized cellulose thus obtained had a carboxylate content of 1.30 mmol g⁻¹, which was determined by conductivity titration. The TEMPO-oxidized cellulose was then suspended in water at 0.1 w/v%. This suspension was homogenized at 7500 rpm for 1 min at room temperature using a double-cylinder-type homogenizer (Phycotron, Microtec Nition Co. Ltd., Japan), and then sonicated for 4 min to be convert it to a transparent TOCN/water dispersion using an ultrasonic homogenizer (26 mm probe tip diameter, US-300T, Nissei, Japan). The TOCN/water

dispersion was centrifuged at 12000 g for 20 min to remove the small amount of partly fibrillated or unfibrillated fraction (<10%). 1 M HCl was slowly added to the TOCN/water dispersion to form TOCNs with free carboxyl groups. The medium was adjusted to pH ~2 and then stirred at room temperature for 30 min. The TOCN gel particles thus formed were collected and washed with water, and then solvent exchanged through ethanol into each chosen solvent by centrifugation or filtration. A 5 % w/v solution of PEG-NH₂ dissolved in chloroform was added to the TOCN gel, where the molar ratio of PEG-NH₂ to the carboxyl groups of TEMPO-oxidized cellulose was adjusted to 1:1. The PEG-grafted TOCN (PEG-TOCN) dispersion was obtained after sonication for 3 min.

3.3.3 Preparation of PEG-TOCN/PLLA nanocomposites

PEG-TOCN/PLLA nanocomposite films were prepared by casting mixtures of PLLA/chloroform solution and PEG-TOCN/chloroform dispersion. PLLA was dissolved in chloroform solution at a concentration of 20 mg mL⁻¹. The PLLA/chloroform solution and the PEG-TOCN/chloroform dispersion were mixed in different ratios and stirred for 30 min. The mixtures were cast in poly(fluoro acetate) petri dishes and dried at 30 °C followed by vacuum-drying at room temperature for 24 h. The films were then hot pressed at 175 °C for 1 min and rapidly quenched to obtain the final PEG-TOCN/PLLA nanocomposite films having various weight ratios of the two components.

3.3.4 Analyses

Light transmittance spectra of the PEG-TOCN/organic solvent dispersions were measured from 400 to 800 nm with a spectrophotometer (JASCO V-670). For transmission electron microscopy (TEM) observation of film cross-sections, the film was sectioned at 90° relative to the film surface using a Leica Ultracut-E microtome equipped with a diamond knife. The approximately 100 nm thick sections were stained with 0.5% uranyl acetate on a carbon support grid, and then observed by TEM using a JEOL JEM-2000EX microscope at an accelerating voltage of 200 kV. Fourier transform infrared (FT-IR) spectra of the films were recorded using a JASCO

FT/IR-6100 spectrometer under transmission mode from 400 to 4000 cm^{-1} with a 4 cm^{-1} resolution. Differential scanning calorimetry (DSC) measurements were carried out using a Perkin-Elmer DSC 8500 instrument at a heating rate of 10 $^{\circ}\text{C min}^{-1}$. Tensile tests of the films, which were $\sim 150 \mu\text{m}$ in thickness, were carried out using a Shimadzu EZ-TEST tensile tester equipped with a 500 N load cell. Specimens of 30 mm and 2 mm length and width, respectively, were measured at 20 mm min^{-1} and a 10 mm span length, and at least 5 specimens were measured for each sample.

3.4 Results and discussion

Nanocomposite films were prepared by casting and drying mixtures of PEG-TOCN/chloroform dispersion and PLLA/chloroform solution in various ratios. The films were quenched after hot-pressing to obtain PEG-TOCN/PLLA composite films with an amorphous PLLA matrix, because the crystallinity of the PLLA matrix also affects the resultant mechanical properties of the composites. The nanocomposite films, which were ca. 100–150 μm in thickness, showed high optical transparency (Figure 3.2a); the light transmittance of the nanocomposite containing 1.0 wt% cellulose nanofibril was 89% at 600 nm, and that of the neat PLLA was 90%. Cellulose nanofibrils with widths of $\sim 3 \text{ nm}$ were homogeneously distributed and individually dispersed in the

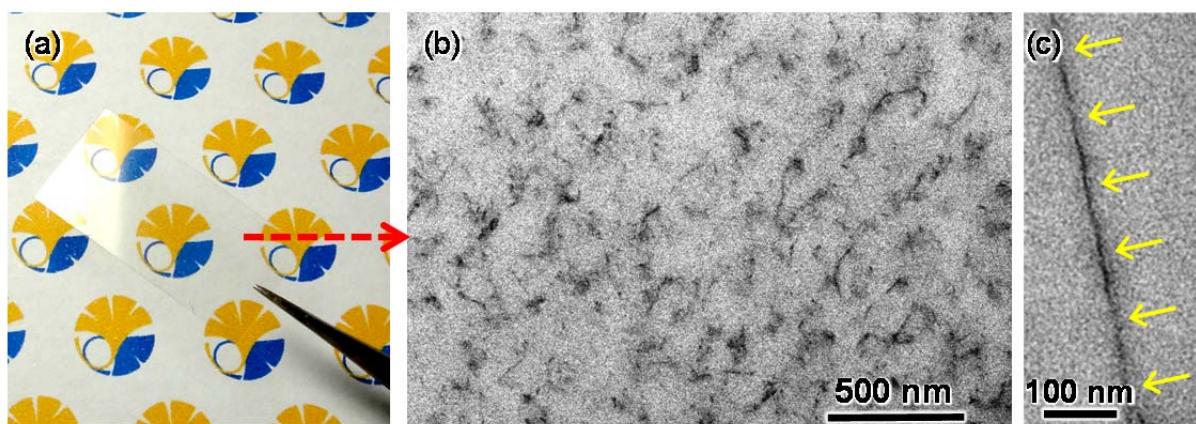


Figure 3.2. a) Photograph of PEG-TOCN/PLLA nanocomposite film containing 1.0 wt % TOCNs. b,c) Cross-sectional TEM image of PEG-TOCN/PLLA nanocomposite film containing 1.0 wt % cellulose nanofibrils.

Table 3.1. Thermal properties of PEG-TOCN/PLLA nanocomposites (1st run).

Sample	TOCN content (wt %)	T_g (°C)	ΔH_c^a (J/g)	ΔH_m^b (J/g)	X_c^c (%)
PLLA	-	58.8	33.0	33.0	0
PEG-TOCN/PLLA nanocomposite	0.1	54.5	39.0	39.1	0
	0.25	54.3	39.7	39.7	0
	0.5	54.2	38.1	38.4	0
	1.0	53.0	36.7	37.0	0

^a Melting enthalpy of PLLA component. ^b Crystallization enthalpy of PLLA component. ΔH_c and ΔH_m were calculated based on the weight fraction of PLLA component in the composites. ^c Degree of crystallinity of PLLA component in the composites, which was calculated from ΔH_c and ΔH_m (Supporting Information).

PLLA matrix (Figure 3.2b and c); dispersion of the PEG-TOCNs in chloroform allowed sufficient corresponding nano-dispersion of cellulose nanofibrils in the PLLA matrix. Accordingly, the nanocomposites had high optical transparency.

Table 3.1 shows the thermal characteristics of the PEG-TOCN/ PLLA nanocomposites obtained by DSC analysis (Figure 3.3). The crystallinities of the PLLA matrices of all composites were estimated to be zero based on the melting and crystallization enthalpies. Note that the cellulose nanofibril contents of the composites

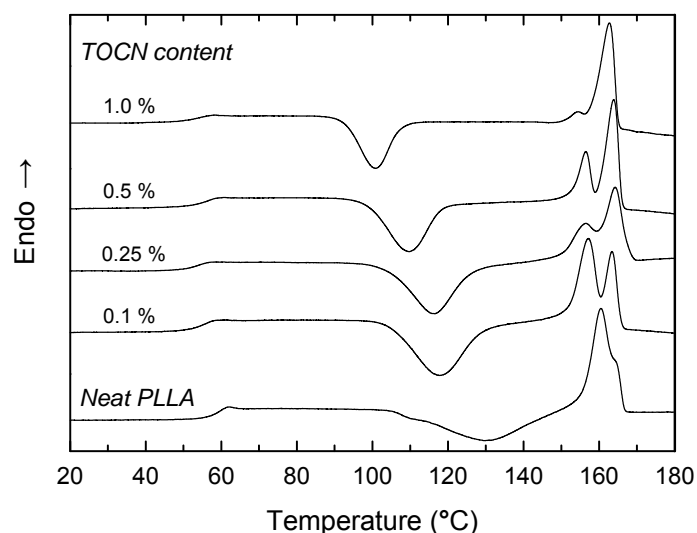


Figure 3.3. DSC curves of neat PLLA and PEG-TOCN/PLLA nanocomposite films with different TOCN contents obtained from the 1st heating run at 10 °C min⁻¹. Reproduction of image with permission from American Chemical Society (©American Chemical Society 2013).

expressed in this chapter correspond to those without grafted PEG moiety. The glass transition temperature (T_g) of the PLLA matrix decreased with increasing PEG-TOCN content, indicating that the PEG-TOCNs were sufficiently miscible with PLLA molecules in the nanocomposites. Therefore, attractive interactions were likely present between cellulose nanofibrils and PLLA molecules, which were mediated by the surface-grafted PEG chains. Moreover, the cold crystallization temperature decreased with the filler addition, indicating that PEG-TOCNs effectively acted as a nucleating agent for PLLA. A detailed investigation of the nucleating properties is reported in the following chapter.

The mechanical properties of the nanocomposite films were investigated by tensile testing. Figure 3.4a shows the stress-strain curves of the nanocomposites, and the obtained tensile properties at different TOCN contents are shown in Figure 3.4b–d and Table 2. The nanocomposite containing only 0.1 wt % TOCNs showed better mechanical properties than those of the neat PLLA film, and the properties were continuously improved

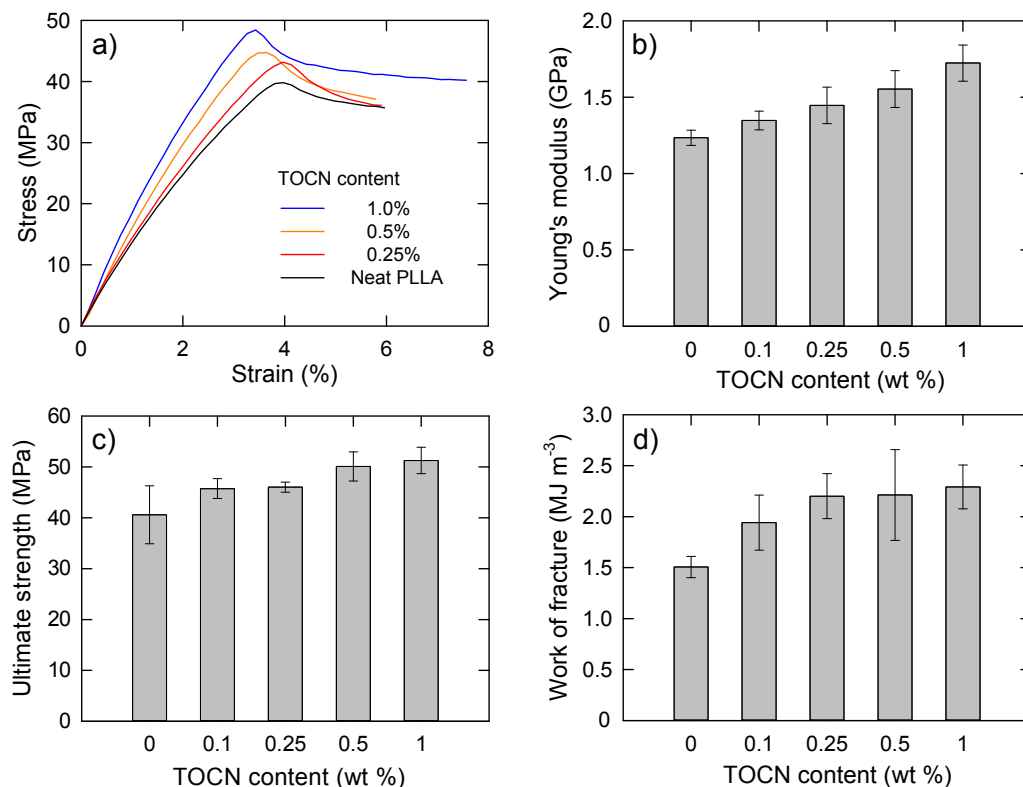


Figure 3.4. Mechanical properties of nanocomposite films with different TOCN contents: a) stress-strain curves, b) Young's moduli, c) ultimate tensile strengths, and d) work of fractures. Reproduction of image with permission from American Chemical Society (©American Chemical Society 2013).

Table 3.2. Tensile properties of PEG-TOCN/PLLA composite films.

Sample	TOCN content (wt %)	Young's modulus (GPa)	Ultimate tensile strength (MPa)	Work of fracture (MJ m ⁻³)
Neat PLLA film	–	1.23 ± 0.05	40.6 ± 5.7	1.51 ± 0.11
PEG-TOCN/PLLA composite film	0.1	1.35 ± 0.06	45.7 ± 2.0	1.94 ± 0.27
	0.25	1.45 ± 0.12	46.0 ± 1.0	2.20 ± 0.22
	0.5	1.55 ± 0.12	50.1 ± 2.9	2.21 ± 0.45
	1.0	1.72 ± 0.12	51.3 ± 2.6	2.29 ± 0.22

up to 1.0 wt % TOCN content. The Young's modulus, ultimate tensile strength, and work of fracture of the nanocomposite containing 1.0 wt % TOCNs was increased by 40%, 26%, and 52%, respectively, compared with the neat PLLA film. In this study, the PLLA matrices in the composites were controlled to be amorphous, and it was found that the PEG molecules themselves did not affect the mechanical properties of the PLLA film at all.⁴³ Thus, the observed improvement in mechanical properties of the PEG-TOCN/PLLA composites was likely to be due to a nano-reinforcement effect by the crystalline TOCNs.

In Figure 3.5, the increase in Young's modulus of the PEG-TOCN/PLLA composites versus the volume content of TOCNs was plotted with those of previously reported cellulose/PLLA composites,⁹⁻¹⁷ even though other nanocomposites had different crystallinities of PLLA matrix. In the case of previously reported nanocellulose/PLLA composites, cellulose loadings of >10 wt% (or ~8 vol%) have been required to achieve increases in Young's modulus comparable to those of the nanocomposites reported in this paper. Moreover, the increases in Young's modulus of the nanocomposites presented in this paper were in good agreement with those calculated using the Voigt-Reuss and Halpin-Tsai models commonly used to predict Young's moduli for polymer nanocomposites (Appendix), indicating that the TOCNs are homogeneously nano-dispersed in the PLLA matrix and attractively interacted with the polymer molecules. Thus, the nanocomposites prepared by the combination of TOCNs and position-selective PEG grafting presented in this study showed a superior reinforcement effect according to theoretical predictions, probably due to high nano-dispersibility of the PEG-TOCNs at the individual nanofibril level in the PLLA matrix and the presence of attractive interactions between the two components.

Furthermore, the work of fracture of the nanocomposite containing 1.0 wt% TOCNs also increased by 52% in comparison with that of the neat PLLA film, probably due to attractive interactions between the PEG-TOCNs and PLLA matrix molecules. In general, the addition of crystalline nanocelluloses to polymer matrix leads to increases in both the Young's modulus and brittleness of the resulting composites because there are almost no attractive interactions between hydrophilic nanocellulose elements and hydrophobic PLLA matrix. In contrast, our results indicate that attractive interfacial interactions present between PLLA matrix polymers and cellulose nanofibrils, mediated by the grafted PEG chains. It has been reported that surface modification of carbon nanotubes lead to increase in Young's modulus, tensile strength, and toughness of the resultant carbon nanotube/polymer nanocomposites, because the functionalization results in an extremely high polymer/nanotube interfacial shear strength.¹⁸ Therefore grafted PEG layers are likely to have played a significant role in the observed remarkable improvement of stress transfer efficiency in the present composite.

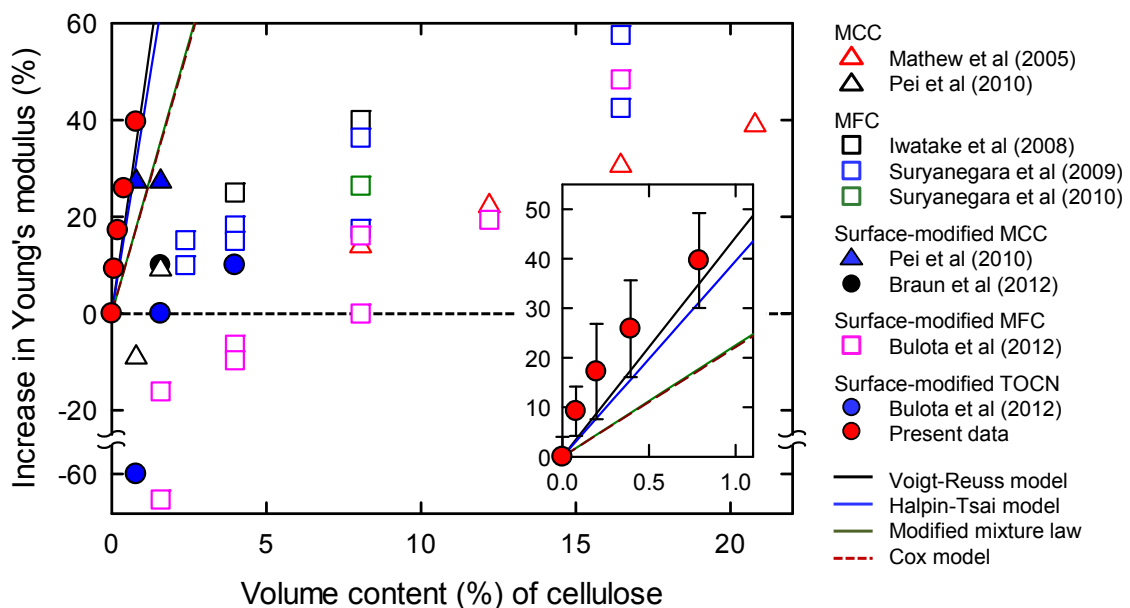


Figure 3.5. Increase in Young's modulus versus cellulose volume content for various cellulose/PLLA composites. MCC: microcrystalline cellulose, MFC: microfibrillated cellulose, and TOCN: TEMPO-oxidized cellulose nanofibril. Lines represent the theoretical predictions for the present nanocomposites by Voigt-Reuss model (black solid line), Halpin-Tsai model (blue solid line), the modified mixture law (green solid line), and Cox model (brown dashed line) (see Appendix). An E_m value of 1.23 GPa was determined from the tensile test data. For TOCN, E_f of 145 GPa¹⁹ and d_f of 3 nm²⁰ were used, and a l_f value of 1087 nm was the average length measured from TEM images. Reproduction of image with permission from American Chemical Society (©American Chemical Society 2013).

3.5 Conclusions

We have shown a novel procedure for the fabrication of bio-based polymer nanocomposite materials, and demonstrated that achievement of sufficient nano-dispersion states of cellulose nanofibrils in PLLA matrix and attractive interfacial interactions between cellulose nanofibrils and PLLA molecules efficiently enhances the improvement of the stiffness, strength, and toughness of the nanocellulose/polymer composites. The mechanical properties of the cellulose nanofibril/polymer composites could be modulated by changing the type of grafted chains. Thus, the surface-engineering of TOCNs developed in this study is expected to prove versatility towards novel green nanocomposite materials. This technique, i.e. enhancement of the nano-dispersibility of cellulose nanofibrils and incorporation of attractive cellulose/polymer interactions by densely grafting PEG chains onto the TOCN surfaces, is simple and effective, and has potential for future green material applications.

3.6 References

1. J. N. Coleman, U. Khan, W. J. Blau and Y. K. Gun'ko, "Small but Strong: A Review of the Mechanical Properties of Carbon Nanotube–Polymer Composites." *Carbon* 2006, **44**, 1624–1652.
2. J. N. Coleman, U. Khan and Y. K. Gun'ko, "Mechanical Reinforcement of Polymers Using Carbon Nanotubes." *Adv. Mater.* 2006, **18**, 689–706.
3. M. T. Byrne and Y. K. Gun'ko, "Recent Advances in Research on Carbon Nanotube-Polymer Composites." *Adv. Mater.* 2010, **22**, 1672–1688.
4. T. D. Fornes, P. J. Yoon, D. L. Hunter, H. Keskkula and D. R. Paul, "Effect of Organoclay Structure on Nylon 6 Nanocomposite Morphology and Properties." *Polymer* 2002, **43**, 5915–5933.
5. H. S. Lee, P. D. Fasulo, W. R. Rodgers and D. R. Paul, "Tpo Based Nanocomposites. Part 1. Morphology and Mechanical Properties." *Polymer* 2005, **46**, 11673–11689.
6. A. Okada and A. Usuki, "Twenty Years of Polymer-Clay Nanocomposites." *Macromol. Mater. Eng.* 2006, **291**, 1449–1476.
7. T. Ramanathan, A. A. Abdala, S. Stankovich, D. A. Dikin, M. Herrera-Alonso, R. D. Piner, D. H. Adamson, H. C. Schniepp, X. Chen, R. S. Ruoff, S. T. Nguyen, I. A. Aksay, R. K. Prud'Homme and L. C. Brinson, "Functionalized Graphene Sheets for Polymer Nanocomposites." *Nat. Nanotechnol.* 2008, **3**, 327–331.
8. M. A. Rafiee, J. Rafiee, Z. Wang, H. H. Song, Z. Z. Yu and N. Koratkar, "Enhanced Mechanical Properties of Nanocomposites at Low Graphene Content." *ACS Nano* 2009, **3**, 3884–3890.
9. M. Bulota, K. Kreitsmann, M. Hughes and J. Paltakari, "Acetylated Microfibrillated Cellulose as a Toughening Agent in Poly(Lactic Acid)." *J. Appl. Polym. Sci.* 2012, **126**, E449–E458.
10. M. Bulota and M. Hughes, "Toughening Mechanisms in Poly(Lactic) Acid Reinforced with

- TEMPO-Oxidized Cellulose.” *J. Mater. Sci.* 2012, **47**, 5517–5523.
11. A. P. Mathew, K. Oksman and M. Sain, “Mechanical Properties of Biodegradable Composites from Poly Lactic Acid (PLA) and Microcrystalline Cellulose (MCC).” *J. Appl. Polym. Sci.* 2005, **97**, 2014–2025.
 12. A. Iwatake, M. Nogi and H. Yano, “Cellulose Nanofiber-Reinforced Polylactic Acid.” *Compos. Sci. Technol.* 2008, **68**, 2103–2106.
 13. L. Suryanegara, A. N. Nakagaito and H. Yano, “The Effect of Crystallization of PLA on the Thermal and Mechanical Properties of Microfibrillated Cellulose-Reinforced PLA Composites.” *Compos. Sci. Technol.* 2009, **69**, 1187–1192.
 14. L. Suryanegara, A. N. Nakagaito and H. Yano, “Thermo-Mechanical Properties of Microfibrillated Cellulose-Reinforced Partially Crystallized PLA Composites.” *Cellulose* 2010, **17**, 771–778.
 15. K. Larsson, L. A. Berglund, M. Ankerfors and T. Lindström, “Polylactide Latex/Nanofibrillated Cellulose Bionanocomposites of High Nanofibrillated Cellulose Content and Nanopaper Network Structure Prepared by a Papermaking Route.” *J. Appl. Polym. Sci.* 2012, **125**, 2460–2466.
 16. A. Pei, Q. Zhou and L. A. Berglund, “Functionalized Cellulose Nanocrystals as Biobased Nucleation Agents in Poly(L-lactide) (PLLA) – Crystallization and Mechanical Property Effects.” *Compos. Sci. Technol.* 2010, **70**, 815–821.
 17. B. Braun, J. R. Dorgan and L. O. Hollingsworth, “Supra-Molecular Ecobionanocomposites Based on Polylactide and Cellulosic Nanowhiskers: Synthesis and Properties.” *Biomacromolecules* 2012, **13**, 2013–2019.
 18. D. Blond, V. Barron, M. Ruether, K. P. Ryan, V. Nicolosi, W. J. Blau and J. N. Coleman, “Enhancement of Modulus, Strength, and Toughness in Poly(Methyl Methacrylate)-Based Composites by the Incorporation of Poly(Methyl Methacrylate)-Functionalized Nanotubes.” *Adv. Funct. Mater.* 2006, **16**, 1608–1614.
 19. S. Iwamoto, W. Kai, A. Isogai and T. Iwata, “Elastic Modulus of Single Cellulose Microfibrils from Tunicate Measured by Atomic Force Microscopy.” *Biomacromolecules* 2009, **10**, 2571–2576.
 20. T. Saito, R. Kuramae, J. Wohlert, L. A. Berglund and A. Isogai, “An Ultrastrong Nanofibrillar Biomaterial: The Strength of Single Cellulose Nanofibrils Revealed via Sonication-Induced Fragmentation.” *Biomacromolecules* 2013, **14**, 248–253.

Chapter 4

Comparison of Mechanical Reinforcement Effects of Surface-Modified Cellulose Nanofibrils and Carbon Nanotubes in PLLA Composites

4.1 Abstract

Cellulose nanofibrils were prepared using 2,2,6,6-tetramethylpiperidiny1-1-oxyl (TEMPO)-mediated oxidation of wood cellulose, and the surfaces of the resulting TEMPO-oxidized cellulose nanofibrils (TOCNs) were grafted with amine-terminated polyethylene glycol (PEG) chains via ionic bonds. PEG-TOCN/PLLA composite films were prepared by casting mixtures of various ratios of PEG-TOCN/chloroform dispersion and PLLA/chloroform solution. The mechanical reinforcement properties of PEG-TOCNs prepared using PEG-NH₂ of two different PEG chain lengths were evaluated using tensile tests and compared against those of PEG-grafted single-walled carbon nanotubes (PEG-SWCNT). PEG-TOCNs were individually dispersed in the PLLA matrix so that the Young's modulus increased with PEG-TOCN content, following theoretically predicted values. In contrast, the PEG-SWCNT formed aggregates in the PLLA matrix, probably owing to heterogeneous distribution of carboxyl groups. As a result, PEG-TOCN/PLLA composites showed superior properties to those of PEG-SWCNT/PLLA composites in terms of optical transparency, strength, and toughness.

4.2 Introduction

Recently, polymer nanocomposites have attracted considerable interest over the decades. By the incorporation of nanometer-sized stiff particles, such as carbon nanotubes,¹⁻³ graphene,⁴⁻⁶ and nanoclays,⁷⁻⁹ into a polymer, mechanical properties of polymers, such as strength, elastic modulus, and thermal deformation can be substantially improved with a small amount of the fillers. In particular, carbon nanotubes have been shown

to enhance mechanical properties of polymer.¹⁻³ Because of the extraordinary mechanical properties of the nanotubes such as high elastic modulus (~ 1 TPa)¹⁰⁻¹² and high strength (4–20 GPa),¹³⁻¹⁵ incorporation of carbon nanotubes into a polymer can effectively enhance its mechanical properties with only a small amount of the nanotubes.

Cellulose holds great potential as a renewable alternative to carbon nanotubes. Cellulose forms unique crystalline nanofibrils, called cellulose microfibrils,¹⁶ which have high elastic modulus (130–150 GPa),¹⁷⁻¹⁹ and high strength (2–6 GPa).²⁰ Moreover, the nanofibrils have large specific surface areas and high aspect ratio (>300) with small width (2–20 nm), that are comparable to those of single-walled carbon nanotubes (SWCNTs). If the reinforcement potential of cellulose nanofibrils is fully realized, the nanofibrils are attractive as environmentally-friendly alternatives to conventional fillers.

The goal of this chapter was to investigate the mechanical reinforcement properties of 2,2,6,6-tetramethylpiperidiny-1-oxyl (TEMPO)-oxidized cellulose nanofibrils (TOCNs) grafted with PEGs of two different chain lengths in a PLLA matrix. Their performance was compared with that of carboxylic acid-functionalized SWCNTs (SWCNT-COOH), the width, length, and average surface COOH density of which are comparable with those of TOCN. PEG chains were grafted onto the TOCNs and SWCNTs (PEG-SWCNTs), and the mechanical properties of PEG-TOCN/PLLA and PEG-SWCNT/PLLA were compared. In addition, the effect of PEG chain length on stress-transfer efficiency in the PEG-TOCN/PLLA composites during tensile testing was evaluated.

4.3 Materials and methods

4.3.1 Materials

A never-dried softwood bleached kraft pulp (Nippon Paper Ind., Japan), which contained approximately 90% cellulose and 10% hemicelluloses, was used as the original wood cellulose. Two kinds of PEG-NH₂, PEG(23)-NH₂ and PEG(48)-NH₂ (SUNBRIGHT MEPA-20H, $n = 23$ and MEPA-10H, $n = 48$, respectively) were purchased from NOF Corp. (Japan) (see Figure 4.1). Carboxylic acid-functionalized single-walled carbon

nanotubes (SWCNT-COOH, diameter: 4–5 nm, length: 0.5–1.5 μm) were purchased from Sigma Aldrich, and used without further purification. SWCNT-COOH had carboxyl content of 1.90 mmol/g, which was determined by conductivity titration. PLLA with M_w of 110,000 and M_n of 80,000 (Lacty) was supplied from the Toyota Motor Corp. All other reagents were purchased from Wako Pure Chemicals, Co. Ltd., and used as received.

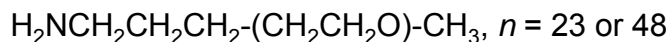


Figure 4.1. Chemical structures of two PEG-NH₂ samples used in this study.

4.3.2 Preparation of PEG-TOCN and PEG-SWCNT dispersions in chloroform

A TOCN-COONa/water dispersion was prepared according to the procedure reported in the previous chapter (Chapter 2). To the dispersion, 1 M HCl was slowly added to form TOCN-COOH gel particles. The pH of the medium was adjusted to ~ 2 and then stirred at room temperature for 30 min. The gel particles were collected and washed with water, and then solvent exchanged to chloroform through ethanol by repeated soaking and centrifugation.⁴⁹ 5 w/v % solutions of PEG(23)-NH₂ and PEG(48)-NH₂ in chloroform were prepared, and then each of them was added to the TOCN-COOH gel in chloroform, where the molar ratio of PEG-NH₂ to carboxyl group of TOCN-COOH was adjusted to 1:1. The dispersions of two PEG-grafted TOCNs with different grafting chain lengths, PEG(23)-TOCN and PEG(48)-TOCN, in chloroform were prepared by sonication of the mixtures for 3 min at temperature below 20 °C. A PEG(48)-grafted SWCNT (PEG(48)-SWCNTs) dispersed in chloroform was prepared according to the method used for preparation of the PEG-TOCN/chloroform dispersions but with sonication for 15 min.

4.3.3 Preparation of PEG-TOCN/PLLA and PEG-SWCNT/PLLA composite films

PLLA was dissolved in chloroform with a concentration of 20 mg mL⁻¹. Three kinds of composite films with different filler contents were prepared by casting of the mixture of a PLLA solution and one of the dispersions of PEG(23)-TOCN, PEG(48)-TOCN, and PEG(48)-SWCNT in chloroform with various ratios. The mixtures of

PLLA and the filler dispersion were stirred for 30 min, and poured in poly(fluoroacetate) petri dishes and dried at 30 °C followed by vacuum-drying at room temperature for >1 week. All composite films were quenched immediately after hot pressing at 180 °C for 1 min, to obtain amorphous PLLA matrices.

4.3.4 Analyses

Light transmittance spectra of the films were measured from 400 to 800 nm with a spectrophotometer (JASCO V-670). Fourier transform infrared (FT-IR) spectra of the films were recorded using a JASCO FT/IR-6100 spectrometer under transmission mode from 400 to 4000 cm^{-1} with a 4 cm^{-1} resolution. Spectra for the original SWCNT-COOH and PEG(48)-SWCNT were obtained using the KBr disk method. Differential scanning calorimetry (DSC) measurements were carried out using a Perkin-Elmer DSC 8500 instrument at a heating rate of 10 °C min^{-1} . Transmission electron microscopy (TEM) observation was performed using a JEOL JEM-2000EX microscope at an accelerating voltage of 200 kV. The PEG-TOCN/PLLA and PEG-SWCNT/PLLA films with approximately 100 nm in thickness were stained with uranyl acetate and lead citrate, respectively, on a carbon support grid, and then observed by TEM. Tensile tests of films with ~150 μm thickness were carried out using a Shimadzu EZ-TEST tensile tester equipped with a 500 N load cell. Specimens with 30 mm length and 2 mm width were measured at 20 mm min^{-1} and a 10 mm span length, and at least 5 specimens were measured for each sample. Scanning electric microscopy (SEM) observation of the fracture surfaces pre-coated with metallic osmium by a Meiwa Fosis Neoc-ST (Japan) was performed at accelerating voltage of 1.0 kV using a field emission-SEM (Hitachi S-4800).

4.4 Results and discussion

4.4.1 PEG-TOCN and PEG-SWCNT dispersions in chloroform.

TOCN-COOH and SWCNT-COOH were grafted with PEG-NH₂ by forming ionic bonds between carboxyl and amine groups (Figure 4.2a, b). Note that the width, length, and average surface COOH density of

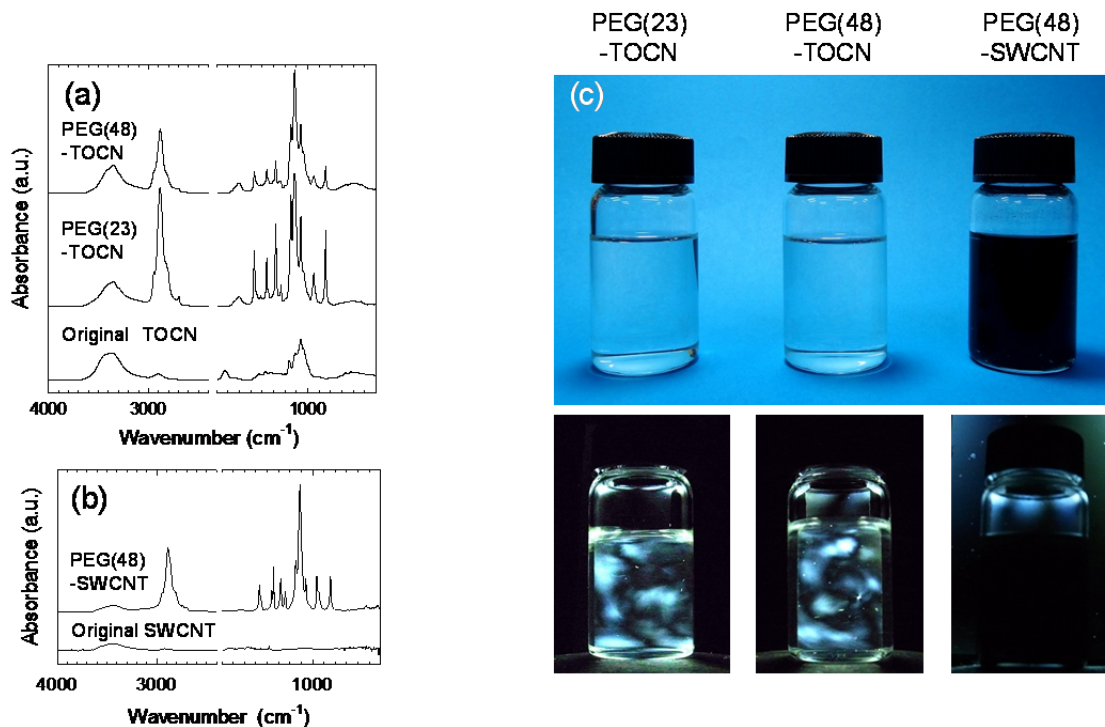


Figure 4.2. FT-IR spectra of (a) original TOCN, PEG(48)-TOCN, and PEG(23)-TOCN films, and (b) original SWCNT and PEG(48)-SWCNT in the region of 400–4000 cm⁻¹. (c) Photographs of 0.1 w/v % PEG(23)-TOCN (left), PEG(48)-TOCN (center), and PEG(48)-SWCNT (right) dispersions in chloroform taken with and without crossed polarizers.

SWCNT-COOH is comparable to those of TOCN-COOH. The PEG-TOCNs and PEG-SWCNT were nanodispersed in chloroform for preparation of composites with PLLA. In order to investigate the effect of grafted chain length on interfacial stress transfer efficiency in the composite, two PEG-NH₂ samples were used as grafting agents: PEG(23)-NH₂ and PEG(48)-NH₂ having number-average degrees of polymerization of 23 and 48, respectively. These two PEG chains were grafted onto TOCN-COOH and PEG(48) was grafted on SWCNT-COOH, and thus three types of dispersions, PEG(23)-TOCN, PEG(48)-TOCN and PEG(48)-SWCNT dispersions in chloroform, were successfully prepared by sonicating TOCN-COOH/PEG-NH₂ or SWCNT-COOH/PEG-NH₂ mixtures in chloroform (Figure 4.2c).

PEG(23)-TOCN and PEG(48)-TOCN were readily dispersed in chloroform, and the dispersions showed high transparency of >97% at 600 nm and clear birefringence, indicating that they were dispersed at the

individual nanofibril level in chloroform.²¹ Generally, cellulose nanofibrils cannot be dispersed at the individual nanofibril level in non-polar organic solvents. In this study, by grafting long PEG chains onto the surfaces, TOCNs were individually nanodispersed; the repulsive forces between grafted PEG chains arise from high osmotic pressures inside the brushes.²²⁻²⁵ Although birefringence in PEG(48)-SWCNTs were not observed between crossed polarizers, they formed a stable dispersion in chloroform. Because neither the original TOCN-COOH nor SWCNT-COOH is dispersible in chloroform without PEG-NH₂, they were stabilized by osmotic pressure within the surface PEG layers.

4.4.2 PEG-TOCN and PEG-SWCNT/PLLA composite films.

The PEG-TOCN/chloroform or PEG-SWCNT/chloroform dispersion was mixed with a PLLA/chloroform solution, and the mixture was stirred at room temperature to produce a homogeneous PEG-TOCN/PLLA or PEG-SWCNT/PLLA mixture. The composite films were formed by casting and drying the mixtures. In this study, all composite films were melted and immediately quenched to obtain amorphous PLLA matrices, which can make clear the effect of filler addition on mechanical properties of the composite films. This is because mechanical properties of PLLA and PLLA composites are significantly affected by the PLLA crystallinity, which should not be taken into account in this study.

Figure 4.3a shows photograph of PEG(23)-TOCN/PLLA, PEG(48)-TOCN/PLLA and PEG(48)-SWCNT/PLLA composite films with different filler contents. Note that the filler contents in this study were given as the weight percentage (wt %) of the fillers without grafted PEG moiety, compared to entire weight of the composites. The thicknesses of the films were 150–200 μm . At any weight content, PEG(23)-TOCN/PLLA and PEG(48)-TOCN/PLLA composite films were optically transparent, and the light transmittance at 600 nm wavelength was above 87 %, which is comparable to that of neat PLLA film, while the light transmittance rate of PEG(48)-SWCNT/PLLA composite films significantly decreased with increasing SWCNT content (Figure 4.3b).

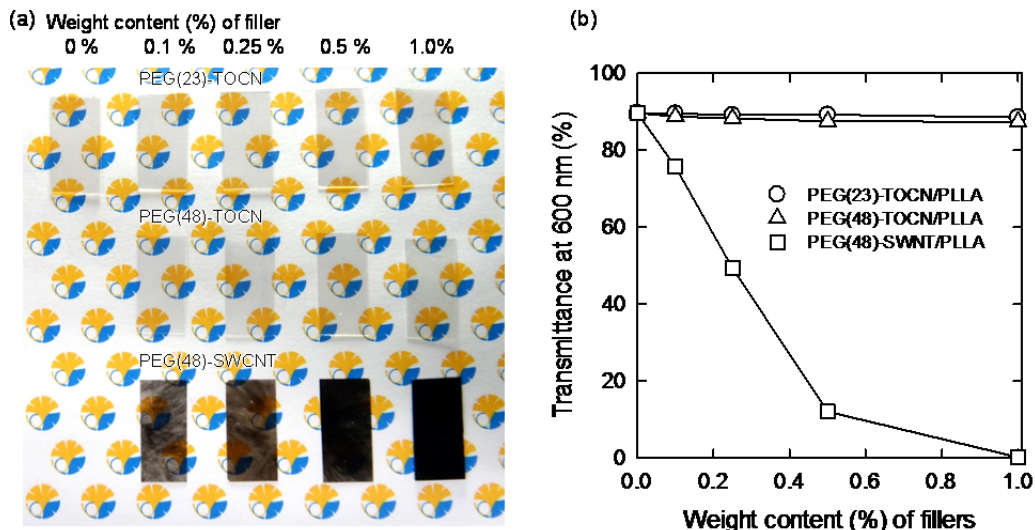


Figure 4.3. (a) Photograph of PEG(23)-TOCN/PLLA, PEG(48)-TOCN/PLLA, and PEG(48)-SWCNT/PLLA composite films, and (b) light transmittance ratios of the films at 600 nm.

TEM images of film cross-sections suggested that PEG-TOCNs were homogeneously and individually dispersed in the PLLA matrices (Figure 4.4); the PEG-TOCN dispersions in chloroform allowed nanodispersibility in the hydrophobic PLLA matrix. On the other hand, SWCNTs existed as bundles at the same weight content, due to their strong aggregation tendency. Even though average surface density of carboxyl groups on SWCNT-COOH is as high as that on TOCN, PEG-SWCNT showed lower dispersibility in the PLLA matrix probably due to heterogeneous distribution of carboxyl groups in SWCNT-COOH. In contrast, it has been proved that carboxyl groups are regularly present on TOCN surfaces; every one of two glucosyl units are oxidized to glucuronosyl units by the TEMPO-mediated oxidation.²⁶

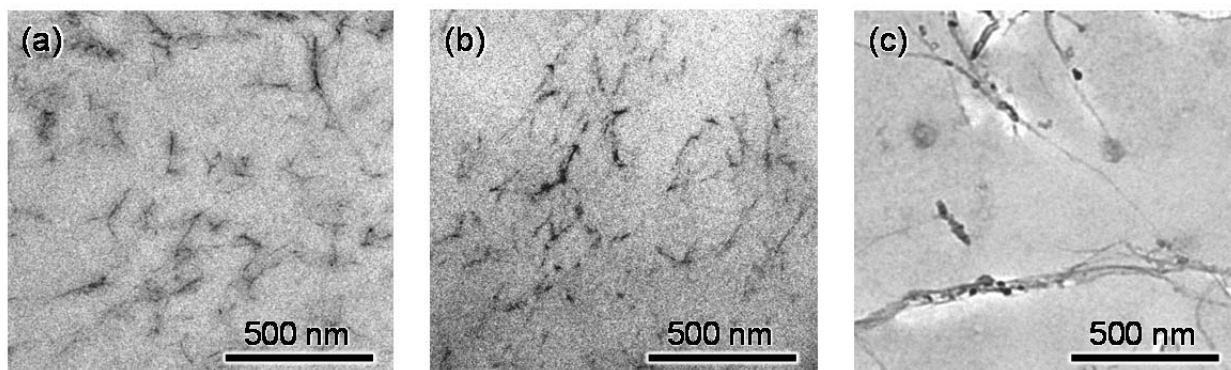


Figure 4.4. TEM images of film cross-sections of (a) PEG(23)-TOCN/PLLA, (b) PEG(48)-TOCN/PLLA, and (c) PEG(48)-SWCNT/PLLA composites containing 1 wt % of fillers. Reproduction of image with permission from Elsevier (© Elsevier 2013).

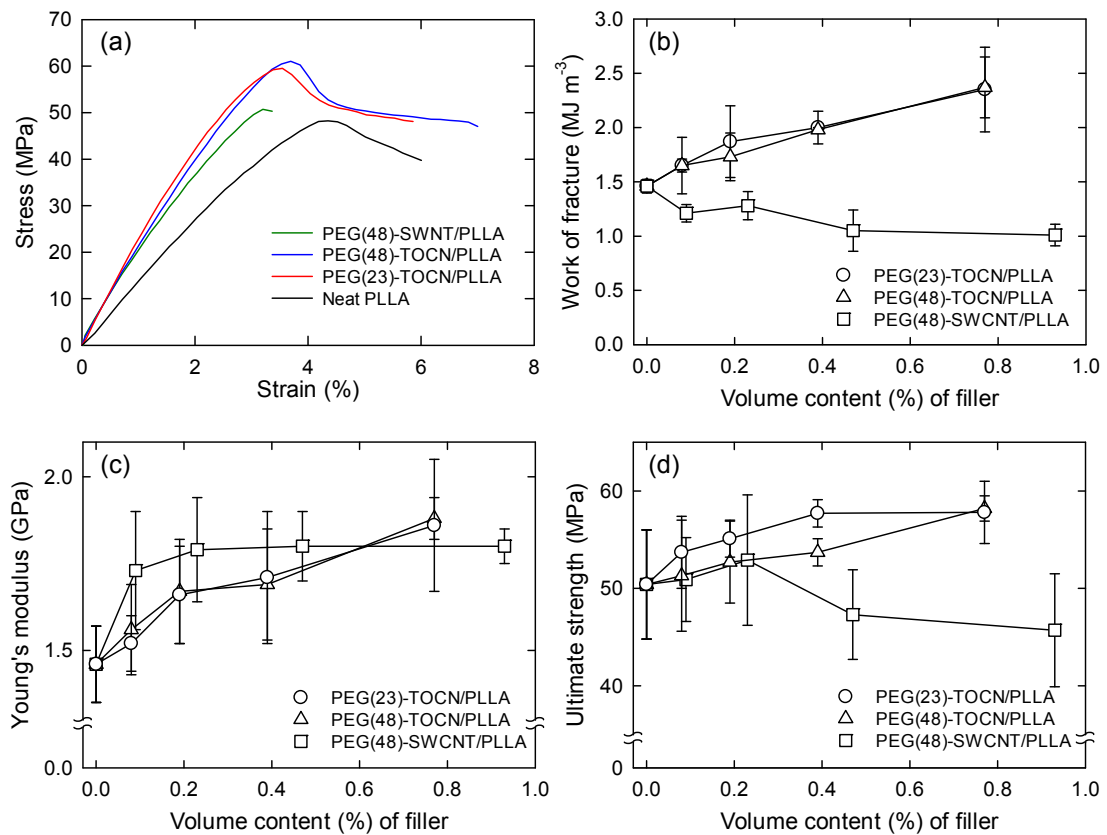


Figure 4.5. Tensile properties of PEG(23)-TOCN/PLLA, PEG(48)-TOCN/PLLA and PEG(48)-SWCNT/PLLA composite films with different filler contents: a) stress-strain curves of neat PLLA and the composites containing 1.0 wt % of fillers, b) work of fractures, c) Young's moduli, and d) ultimate tensile strengths. Error bars represent the standard deviation. Reproduction of image with permission from Elsevier (© Elsevier 2013).

Figure 4.5a shows tensile properties of PEG(23)-TOCN/PLLA, PEG(48)-TOCN/PLLA and PEG(48)-SWCNT/PLLA composite films with different filler contents, where volume content of fillers were calculated supposing that the densities of PLLA, TOCN, and SWCNT are 1.26, 1.63,²⁷ and 1.35 g cm⁻³,² respectively. Remarkably, with only 0.1 wt % of TOCN, not only Young's modulus and ultimate tensile strength but also work of fracture (or toughness) increased for the PEG-TOCN/PLLA composites. The mechanical properties were continuously improved with increasing TOCN content up to 1.0 wt % (Table 4.1). The Young's modulus, tensile strength, and work of fracture of the composite were increased by 29, 15, and 62 % at 1.0 wt % (or 0.77 vol %) of TOCN. This enhancement was clearly due to the reinforcement by TOCNs, because PLLA

Table 4.1. Thermal properties of PEG(23)-TOCN/PLLA, PEG(48)-TOCN/PLLA, and PEG(48)-SWCNT/PLLA nanocomposites (first run).

	Weight content of fillers	ΔH_c^a	ΔH_m^b	X_c^c
	(wt %)	(J/g)	(J/g)	(%)
Neat PLLA	-	26.4	26.4	0
PEG(23)-TOCN/PLLA	0.1	36.1	36.4	0
	0.25	34.7	34.7	0
	0.5	37.8	37.8	0
	1.0	37.5	37.7	0
PEG(48)-TOCN/PLLA	0.1	39.1	39.2	0
	0.25	39.9	39.9	0
	0.5	38.4	38.7	0
	1.0	37.3	37.6	0
PEG(48)-SWCNT/PLLA	0.1	39.9	40.0	0
	0.25	41.4	41.5	0
	0.5	39.9	40.0	0
	1.0	38.6	38.6	0

^a Melting enthalpy of PLLA component. ^b Crystallization enthalpy of PLLA component. ΔH_c and ΔH_m were calculated based on the weight fraction of PLLA component in the composites. ^c Degree of crystallinity of PLLA component in the composites was calculated from ΔH_c and ΔH_m .

matrices in the composites were equally amorphous (Table 4.2), and PEG chains themselves did not play a role in the mechanical improvement at all.²⁸

Generally, cellulose-based composites with hydrophobic polymer show brittle behavior because of low interaction between the two components. In this study, surface-grafted PEG chains mediated interactions between TOCNs and PLLA matrix, which led to good stress transfer from the soft matrix to stiff TOCNs. No significant difference in mechanical properties was observed between PEG(23)-TOCN/PLLA and PEG(48)-TOCN/PLLA composites, indicating that the PEG chain with DP_w 23 is long enough for the efficient stress-transfer from PLLA molecules to TOCN elements in this nanocomposite system, which is likely due to interfacial shear strength improved by surface PEG chains.

In contrast, the addition of PEG(48)-SWCNT led to a marked reduction in toughness of the composite (Figure 4.5b). Work of fracture of 1.46 MJ m^{-3} for neat PLLA decreased to 1.01 MJ m^{-3} at 1.0 wt % (or 0.93 vol %) SWCNT content. The Young's modulus sharply increased with only 0.1 wt % loading of SWCNT due to extraordinary high Young's modulus of SWCNTs ($\sim 1 \text{ TPa}$).¹⁰⁻¹² However, further addition of PEG(48)-SWCNT resulted in saturation of the modulus and a decrease of the tensile strength because of the aggregation behavior of nanotube elements in the PLLA composites as has been reported before.²⁹⁻³¹

In SEM images of the tensile fracture surfaces (Figure 4.6), there were many cracks on the tensile fracture surface of PEG(48)-SWCNT/PLLA composite. Generally, aggregation of SWCNT bundles in polymer matrix is inevitable in any cases, and the composites show brittle properties due to SWCNT slippage between the bundles (Figure 4.6d). In contrast, PEG-TOCN/PLLA composites had relatively smooth fracture surface over a wide

Table 4.2. Tensile properties of PEG(23)-TOCN/PLLA, PEG(48)-TOCN/PLLA and PEG(48)-SWCNT/PLLA nanocomposite films

Sample	Weight content	Volume content	Young's modulus (GPa)	Ultimate strength (MPa)	Work of fracture (MJ m^{-3})
	of fillers (wt%)	of fillers (vol%)			
Neat PLLA	–	–	1.46 ± 0.11	50.4 ± 5.6	1.46 ± 0.06
PEG(23)-TOCN/PLLA	0.1	0.08	1.52 ± 0.08	53.7 ± 3.7	1.65 ± 0.06
	0.25	0.19	1.66 ± 0.14	55.1 ± 1.9	1.87 ± 0.33
	0.5	0.39	1.71 ± 0.19	57.7 ± 1.4	2.00 ± 0.15
	1.0	0.77	1.86 ± 0.19	57.8 ± 3.2	2.35 ± 0.39
PEG(48)-TOCN/PLLA	0.1	0.08	1.56 ± 0.13	51.3 ± 5.7	1.65 ± 0.26
	0.25	0.19	1.67 ± 0.15	52.7 ± 4.2	1.73 ± 0.22
	0.5	0.39	1.69 ± 0.16	53.7 ± 1.4	1.98 ± 0.02
	1.0	0.77	1.88 ± 0.06	58.2 ± 1.3	2.37 ± 0.28
PEG(48)-SWCNT/PLLA	0.1	0.09	1.73 ± 0.17	50.9 ± 4.3	1.21 ± 0.08
	0.25	0.23	1.79 ± 0.15	52.9 ± 6.7	1.28 ± 0.13
	0.5	0.47	1.80 ± 0.10	47.3 ± 4.6	1.05 ± 0.19
	1.0	0.93	1.80 ± 0.05	45.7 ± 5.8	1.01 ± 0.10

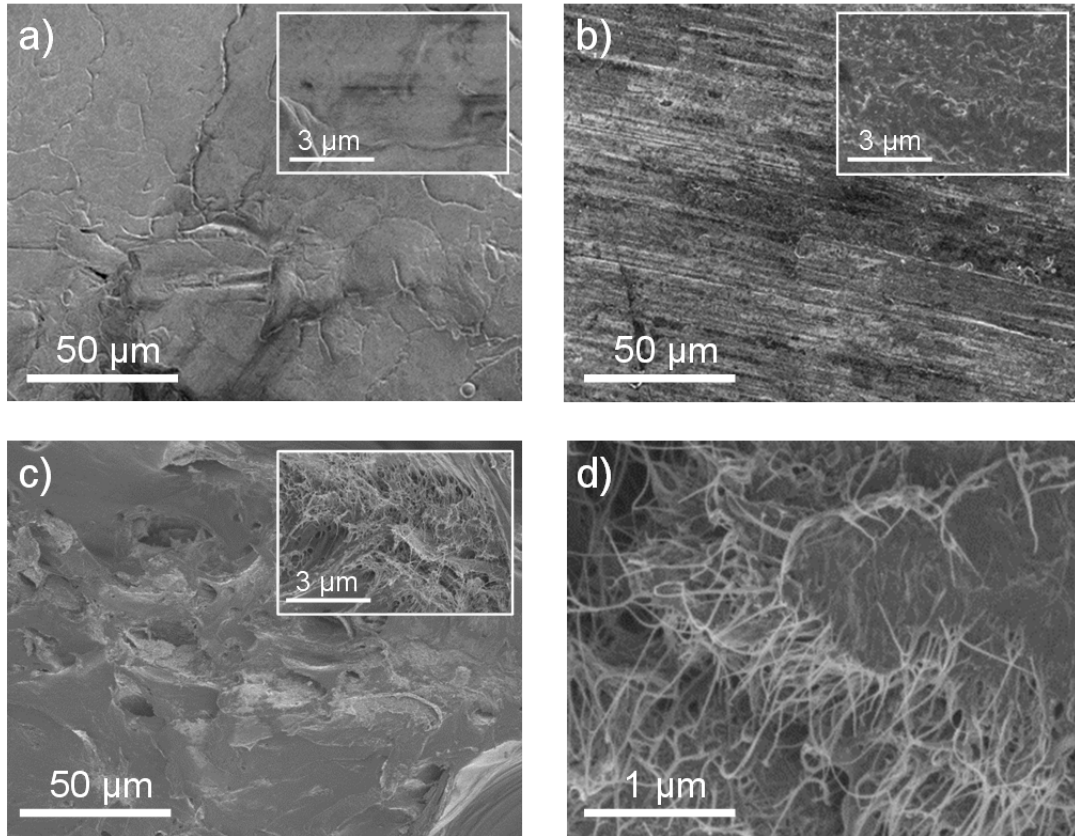


Figure 4.6. SEM images of tensile fracture surfaces: (a) 1.0 wt % PEG(23)-TOCN/PLLA, (b) 1.0 wt % PEG(48)-TOCN/PLLA, and (c, d) 1.0 wt % PEG(48)-SWCNT/PLLA composite films. Reproduction of image with permission from Elsevier (© Elsevier 2013).

range, indicating that crack generation was suppressed in the composites, because individually dispersed TOCNs strongly interacted with the PLLA molecules in the matrix.

4.4.3 Model approach

In order to evaluate the reinforcement efficiency of PEG-TOCN in PLLA, model approach was employed. Because TOCNs are considered to be randomly laminated in the PEG-TOCN/PLLA composites, the well-established Voigt-Reuss model³²⁻³³ and Halpin-Tsai model³³⁻³⁵ were used to calculate the theoretical Young's modulus of the composites. The modulus predicted from the Voigt-Reuss model (E_{VR}) is described as

$$E_{VR} = \frac{3}{8}[V_f E_f + (1 - V_f)E_m] + \frac{5}{8} \left[\frac{E_f E_m}{E_f(1 - V_f) + E_m V_f} \right] \quad (1)$$

where E_f and E_m are the moduli of the filler and matrix, and V_f is the volume fraction of the filler. The Halpin-Tsai model, which takes into account the aspect ratio of the reinforcing fillers, is described as

$$E_{HT} = \frac{3}{8} \left[\frac{1 + 2(l_f/d_f)\eta_L V_f}{1 - \eta_L V_f} E_m \right] + \frac{5}{8} \left[\frac{1 + 2\eta_T V_f}{1 - \eta_T V_f} E_m \right] \quad (2)$$

where E_{HT} is Young's modulus of the composite, and η_L and η_T are expressed as follows

$$\eta_L = \frac{(E_f/E_m) - 1}{(E_f/E_m) + 2(l_f/d_f)} \quad (3)$$

$$\eta_T = \frac{(E_f/E_m) - 1}{(E_f/E_m) + 2} \quad (4)$$

where l_f and d_f are the average length and width of the filler, respectively. In this study, the E_m value of 1.46 GPa was determined from tensile test data (Table 4.2). For TOCN, E_f of 145 GPa¹⁹ and d_f of 3 nm²⁰ were used, and the l_f value of 1087 nm was average length measured from TEM images. For SWCNT, E_f of 1 TPa was used,³⁶ and d_f and l_f were assumed to be 4.5 nm and 1.0 μ m, respectively, based on the catalog values.

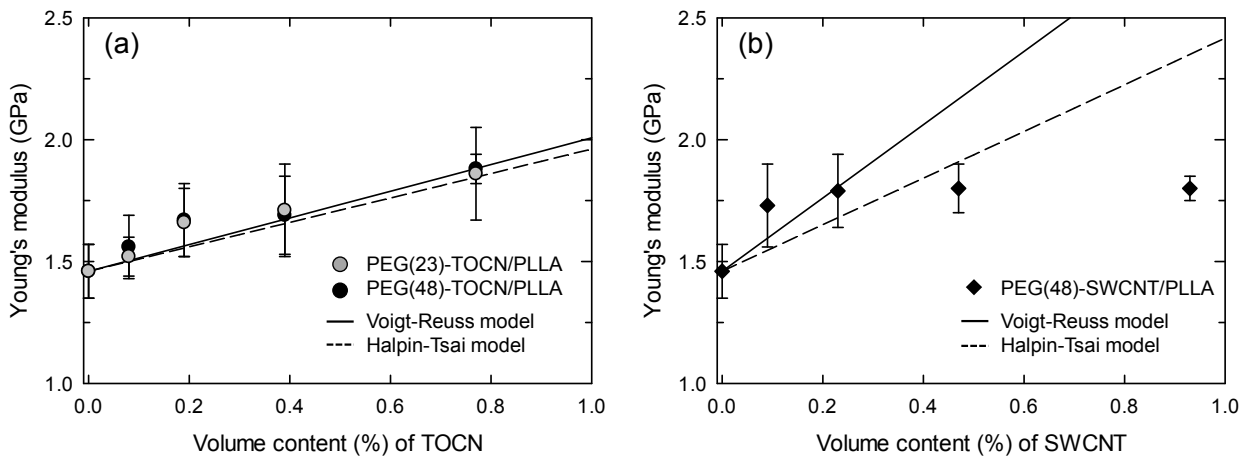


Figure 4.7. Young's modulus of the composites versus filler volume content: (a) PEG(23)-TOCN/PLLA and PEG(48)-TOCN/PLLA s, and (b) PEG(48)-SWCNT/PLLA. Lines present the theoretical predictions for the composites by Voigt-Reuss model (black solid line) and Halpin-Tsai model (black dashed line). Reproduction of image with permission from Elsevier (© Elsevier 2013).

In Figure 4.7, Young's moduli of the PEG(23)-TOCN/PLLA, PEG(48)-TOCN/PLLA, and PEG(48)-SWCNT/PLLA composites were plotted versus the volume content of fillers. The modulus of PEG(48)-SWCNT/PLLA composite did not follow either Voigt-Reuss or Halpin-Tsai model at higher SWCNT contents, probably due to the aggregation of SWCNTs (see Figure 4.6d again). On the other hand, those of PEG-TOCN/PLLA nanocomposites found to be in good agreement with both of the theories. This clearly indicates that the applied stress was ideally transferred to individual TOCNs, which have a high elastic modulus, high strength, and extraordinarily large specific surface areas approaching $900 \text{ m}^2 \text{ g}^{-1}$, and thus the nanocomposite achieved not only higher Young's modulus and strength, but also higher work of fracture.

4.5 Conclusions

We have shown the reinforcing potential of plant cellulose microfibrils through surface modification of TOCNs. TOCN surfaces were densely and selectively grafted with PEG(23)-NH₂ or PEG(48)-NH₂, which enabled them to be dispersed in chloroform. With the aid of the surface grafting, both PEG-TOCNs were individually dispersed and strongly interacted with surrounding PLLA matrix, so that the resultant nanocomposites showed higher stiffness, strength, and toughness, compared with neat PLLA, whereas PEG(48)-SWCNT/PLLA became brittle with increasing the SWCNT content up to 1.0 wt %. Although individual SWCNTs potentially have extraordinary mechanical properties such as higher tensile strength and ~10 times higher Young's modulus than cellulose nanofibrils, they are prone to aggregate in various media, and therefore the material properties are dominated by the bundle properties. On the other hand, TOCN surfaces can be finely grafted, which enables us to fully take advantage of the reinforcing potential of cellulose nanofibrils. We expect that this facile and efficient way to modify cellulose nanofibril surfaces could be applied in the development of sustainable and lightweight/high-strength nanocomposite materials.

4.6 References

1. J. N. Coleman, U. Khan, W. J. Blau and Y. K. Gun'ko, "Small but Strong: A Review of the Mechanical Properties of Carbon Nanotube–Polymer Composites." *Carbon* 2006, **44**, 1624–1652.
2. M. T. Byrne and Y. K. Gun'ko, "Recent Advances in Research on Carbon Nanotube-Polymer Composites." *Adv. Mater.* 2010, **22**, 1672–1688.
3. M. Moniruzzaman and K. I. Winey, "Polymer Nanocomposites Containing Carbon Nanotubes." *Macromolecules* 2006, **39**, 5194–5205.
4. T. Ramanathan, A. A. Abdala, S. Stankovich, D. A. Dikin, M. Herrera-Alonso, R. D. Piner, D. H. Adamson, H. C. Schniepp, X. Chen, R. S. Ruoff, S. T. Nguyen, I. A. Aksay, R. K. Prud'Homme and L. C. Brinson, "Functionalized Graphene Sheets for Polymer Nanocomposites." *Nat. Nanotechnol.* 2008, **3**, 327–331.
5. M. A. Rafiee, J. Rafiee, Z. Wang, H. H. Song, Z. Z. Yu and N. Koratkar, "Enhanced Mechanical Properties of Nanocomposites at Low Graphene Content." *ACS Nano* 2009, **3**, 3884–3890.
6. J. Liang, Y. Huang, L. Zhang, Y. Wang, Y. Ma, T. Guo and Y. Chen, "Molecular-Level Dispersion of Graphene into Poly(Vinyl Alcohol) and Effective Reinforcement of Their Nanocomposites." *Adv. Funct. Mater.* 2009, **19**, 2297–2302.
7. A. Okada and A. Usuki, "Twenty Years of Polymer-Clay Nanocomposites." *Macromol. Mater. Eng.* 2006, **291**, 1449–1476.
8. E. P. Giannelis, "Polymer Layered Silicate Nanocomposites." *Adv. Mater.* 1996, **8**, 29–35.
9. S. Pavlidou and C. D. Papaspyrides, "A Review on Polymer-Layered Silicate Nanocomposites." *Prog. Polym. Sci.* 2008, **33**, 1119–1198.
10. M. M. J. Treacy, T. W. Ebbesen and J. M. Gibson, "Exceptionally High Young's Modulus Observed for Individual Carbon Nanotubes." *Nature* 1996, **381**, 678–680.
11. J. P. Lu, "Elastic Properties of Single and Multilayered Nanotubes." *J. Phys. Chem. Solids* 1997, **58**, 1649–1652.
12. R. S. Ruoff and D. C. Lorents, "Mechanical and Thermal-Properties of Carbon Nanotubes." *Carbon* 1995, **33**, 925–930.
13. Y. Y. Huang, T. P. J. Knowles and E. M. Terentjev, "Strength of Nanotubes, Filaments, and Nanowires from Sonication-Induced Scission." *Adv. Mater.* 2009, **21**, 3945–3948.
14. T. Taniguchi and K. Okamura, "New Films Produced from Microfibrillated Natural Fibres." *Polym. Int.* 1998, **47**, 291–294.
15. D. Klemm, F. Kramer, S. Moritz, T. Lindstrom, M. Ankerfors, D. Gray and A. Dorris, "Nanocelluloses: A New Family of Nature-Based Materials." *Angew. Chem. Int. Edit.* 2011, **50**, 5438–5466.
16. Y. Nishiyama, "Structure and Properties of the Cellulose Microfibril." *J. Wood. Sci.* 2009, **55**, 241–249.
17. I. Sakurada, Y. Nukushina and T. Ito, "Experimental Determination of the Elastic Modulus of Crystalline Regions in Oriented Polymers." *J. Polym. Sci.* 1962, **57**, 651–660.

18. A. Sturcova, G. R. Davies and S. J. Eichhorn, "Elastic Modulus and Stress-Transfer Properties of Tunicate Cellulose Whiskers." *Biomacromolecules* 2005, **6**, 1055–1061.
19. S. Iwamoto, W. Kai, A. Isogai and T. Iwata, "Elastic Modulus of Single Cellulose Microfibrils from Tunicate Measured by Atomic Force Microscopy." *Biomacromolecules* 2009, **10**, 2571–2576.
20. T. Saito, R. Kuramae, J. Wohler, L. A. Berglund and A. Isogai, "An Ultrastrong Nanofibrillar Biomaterial: The Strength of Single Cellulose Nanofibrils Revealed via Sonication-Induced Fragmentation." *Biomacromolecules* 2013, **14**, 248–253.
21. M. M. de Souza Lima and R. Borsali, "Rodlike Cellulose Microcrystals: Structure, Properties, and Applications." *Macromol. Rapid Commun.* 2004, **25**, 771–787.
22. S. T. Milner, T. A. Witten and M. E. Cates, "Theory of the Grafted Polymer Brush." *Macromolecules* 1988, **21**, 2610–2619.
23. S. T. Milner, "Polymer Brushes." *Science* 1991, **251**, 905–914.
24. E. P. K. Currie, W. Norde and M. A. Cohen Stuart, "Tethered Polymer Chains: Surface Chemistry and Their Impact on Colloidal and Surface Properties." *Adv. Colloid Interface Sci.* 2003, **100-102**, 205–265.
25. P. G. de Gennes, "Polymers at an Interface; a Simplified View." *Adv. Colloid Interface Sci.* 1987, **27**, 189–209.
26. M. Hirota, K. Furihata, T. Saito, T. Kawada and A. Isogai, "Glucose/Glucuronic Acid Alternating Co-Polysaccharides Prepared from TEMPO-Oxidized Native Celluloses by Surface Peeling." *Angew. Chem. Int. Edit.* 2010, **49**, 7670–7672.
27. Y. Nishiyama, P. Langan and H. Chanzy, "Crystal Structure and Hydrogen-Bonding System in Cellulose I β from Synchrotron X-Ray and Neutron Fiber Diffraction." *J. Am. Chem. Soc.* 2002, **124**, 9074–9082.
28. O. Martin and L. Averous, "Poly(Lactic Acid): Plasticization and Properties of Biodegradable Multiphase Systems." *Polymer* 2001, **42**, 6209–6219.
29. M. A. L. Manchado, L. Valentini, J. Biagiotti and J. M. Kenny, "Thermal and Mechanical Properties of Single-Walled Carbon Nano Tubes-Polypropylene Composites Prepared by Melt Processing." *Carbon* 2005, **43**, 1499–1505.
30. J. N. Coleman, M. Cadek, K. P. Ryan, A. Fonseca, J. B. Nagy, W. J. Blau and M. S. Ferreira, "Reinforcement of Polymers with Carbon Nanotubes. The Role of an Ordered Polymer Interfacial Region. Experiment and Modeling." *Polymer* 2006, **47**, 8556–8561.
31. D. Blond, V. Barron, M. Ruether, K. P. Ryan, V. Nicolosi, W. J. Blau and J. N. Coleman, "Enhancement of Modulus, Strength, and Toughness in Poly(Methyl Methacrylate)-Based Composites by the Incorporation of Poly(Methyl Methacrylate)-Functionalized Nanotubes." *Adv. Funct. Mater.* 2006, **16**, 1608–1614.
32. P. Laborde-Lahoz, W. Maser, T. Martínez, A. Benito, T. Seeger, P. Cano, R. G. d. Villoria and A. Miravete, "Mechanical Characterization of Carbon Nanotube Composite Materials." *Mech. Adv. Mater. Struct.* 2005, **12**, 13–19.

33. R. Guzmán de Villoria and A. Miravete, “Mechanical Model to Evaluate the Effect of the Dispersion in Nanocomposites.” *Acta Mater.* 2007, **55**, 3025–3031.
34. X. F. Zhang, T. Liu, T. V. Sreekumar, S. Kumar, V. C. Moore, R. H. Hauge and R. E. Smalley, “Poly(Vinyl Alcohol)/SWNT Composite Film.” *Nano Lett.* 2003, **3**, 1285–1288.
35. J. C. H. Affdl and J. L. Kardos, “The Halpin-Tsai Equations: A Review.” *Polym. Eng. Sci.* 1976, **16**, 344–352.
36. E. W. Wong, P. E. Sheehan and C. M. Lieber, “Nanobeam Mechanics: Elasticity, Strength, and Toughness of Nanorods and Nanotubes.” *Science* 1997, **277**, 1971–1975.

Chapter 5

The effect of PEG-TOCNs on the crystallization behavior and thermo-mechanical properties of PLLA

5.1 Abstract

The abilities of surface-grafted cellulose nanofibrils for the nucleation of poly(L-lactide) (PLLA) were investigated. Cellulose nanofibrils with a width of ~3 nm were obtained from wood cellulose via the oxidation using 2,2,6,6-tetramethylpiperidiny-1-oxyl (TEMPO) as a catalyst and successive mechanical treatment. The TEMPO-oxidized cellulose nanofibril (TOCN) surfaces were selectively modified with amine-terminated poly(ethylene glycol) chains, via simple ionic bonds (PEG-TOCN). The PEG-TOCN/PLLA composite films were prepared using a solvent casting method with chloroform. The isothermal and non-isothermal crystallization kinetics of the PLLA in the composites were studied using differential scanning calorimetry and polarized optical microscopy. The PEG chains were densely immobilized on the surface of the cellulose nanofibril templates, which had extraordinarily large specific surface areas. As a result, the surface-PEG layers effectively increased the rate of crystallization of the PLLA in the composites. Because of the increased degree of crystallinity after the isothermal crystallization, the composites showed better heat resistance than neat PLLA.

5.2 Introduction

Poly(L-lactide) (PLLA) is one of the most widely used biodegradable polymers. Because of its biocompatibility and renewability, PLLA is attractive for wide range of applications, including packaging,¹⁻³ and medical⁴⁻⁶ applications. However, a major drawback of PLLA is its low heat resistance. Although the crystallization of PLLA itself is a simple and effective way to solve the problem, the crystallization rate of PLLA is very low. Therefore, the use of neat PLLA typically results in an amorphous or very low-crystallinity

material; the resultant material is easily distorted at its glass transition temperature (T_g) of $\sim 60^\circ\text{C}$, which limits its potential for applications.

Much effort has been dedicated to enhancing the crystallization of PLLA. The addition of nucleating agents is an effective method for increasing the crystallization rate of PLLA. Some micro- or nano-elements such as talc,⁷⁻⁹ montmorillonite,¹⁰⁻¹¹ carbon nanotubes,¹²⁻¹⁵ and graphene¹⁵⁻¹⁷ are known to act as nucleating agents for the crystallization of PLLA. These nucleating agents have large specific surface areas, and are thus efficient in inducing the crystallization of PLLA on their surfaces. Organic compounds such as benzenetricarboxylamide derivatives¹⁸ and polysaccharide derivatives¹⁹ have recently been shown to play an effective role as nucleating agents for PLLA. In addition to these nucleating agents, plasticizers such as poly(ethylene glycol) (PEG) can also enhance the crystallization.²⁰⁻²² PEG chains increase the polymer chain mobility, which leads to an increase in the crystallization of PLLA via a reduction in the energy required for the chain folding process during crystallization.²³⁻²⁴

Cellulose nanofibrils are promising candidates for renewable nucleating agents for PLLA, and originate from naturally occurring cellulose microfibrils,²⁵ which have high aspect ratios (>300) with small widths of 2–20 nm and high crystal moduli (130–150 GPa).²⁶⁻²⁸ It has been reported that these nanofibrils act as effective nucleating agents when they are incorporated in semi-crystalline polymers such as PLLA,²⁹⁻³¹ polypropylene,³²⁻³⁵ and poly(3-hydroxybutyrate-co-3-hydroxyvalerate).³⁶ Since the crystallization is initiated on their surfaces, the dispersibility of the nanofibrils in polymer matrices significantly affects the nucleation rate.²⁹⁻³⁰ However, it is typically difficult to disperse hydrophilic cellulose nanofibrils in a hydrophobic polymer matrix without any aggregation.

In the previous chapter, we showed a method that was used to achieve the individual dispersion of cellulose nanofibrils in a hydrophobic PLLA matrix via the surface modification of 2,2,6,6-tetramethylpiperidiny-1-oxyl (TEMPO)-oxidized cellulose nanofibrils (TOCNs).³⁷ Carboxyl groups are exposed in high densities on the surface of TOCNs,³⁸⁻³⁹ and these groups can be used as selective anchoring sites for many kinds of functional groups.⁴⁰⁻⁴⁶ When long PEG chains are grafted onto the carboxyl groups, the PEG-grafted TOCNs (PEG-TOCNs) can be dispersed at the individual nanofibril level in a PLLA matrix,

and the resultant PEG-TOCN/PLLA composites show enhanced mechanical properties with only small amounts of the PEG-TOCNs added.

In this chapter, we demonstrated the nucleating abilities of the PEG-TOCNs for the crystallization of PLLA. TOCNs were prepared from wood cellulose, and the surface carboxyl groups were selectively modified with PEG chains via simple ionic bonds. Two PEGs with different chain lengths were used as grafting agents to evaluate the effects on the nucleating properties. PEG-TOCN/PLLA composites containing 0.5 and 1.0 wt % of TOCNs were prepared by casting and drying mixtures of the PEG-TOCN dispersions and the PLLA solutions in chloroform. The crystallization behaviour of the PEG-TOCN/PLLA composites was investigated under isothermal and non-isothermal conditions.

5.3 Materials and methods

5.3.1 Materials

A never-dried softwood bleached kraft pulp (Nippon Paper Ind., Japan), which contained approximately 90% cellulose and 10% hemicelluloses, was used as the original wood cellulose. Two amine-terminated PEGs, PEG(23)-NH₂ and PEG(48)-NH₂ (Sunbright MEPA-10Hand MEPA-20H with $n = 23$ and $n = 48$, respectively) were obtained from NOF Corp. (Japan). PLLA with $M_w = 94,000$ and $M_n 45,000$ (Lacty[®]) was supplied from Toyota Motor Corp., Japan. All other reagents were purchased from Wako Pure Chemicals, Co. Ltd., Japan, and used as received.

5.3.2 Preparation of PEG-TOCN/PLLA composite films

PEG(23)-TOCN/PLLA and PEG(48)-TOCN/PLLA nanocomposite films were prepared by casting the PEG(23)-TOCN/PLLA and PEG(48)-TOCN/PLLA mixtures in chloroform, respectively, according to the procedure reported in the previous chapter (Chapter 4).

5.3.3 Analyses

Thermal analysis of the samples was carried out using a Perkin-Elmer differential scanning calorimetry (DSC) 8500 instrument. Samples (2–3 mg) were sealed in aluminium pans. For the non-isothermal crystallization study, the samples were heated to 185°C, maintained at this temperature for 2 min, and then rapidly cooled to 0°C. The parameters were collected during the second heating run from 0 to 185°C at a heating rate of 20°C min⁻¹. In the isothermal study, samples were heated to 185°C, and then maintained at this temperature for 2 min to erase any thermal history. The samples were then quenched to a desired crystallization temperature (85, 90, 95, 100, 105, 110, 115, and 120°C), and then held at that temperature until the isothermal crystallization was complete. The degree of crystallinity (X_c) of the PLLA after isothermal crystallization for 60 min was calculated from the DSC heating curve using the following equation:

$$X_c = \frac{\Delta H_m - \Delta H_{cc}}{\Delta H_m^\infty} \times 100 (\%) \quad (5.1)$$

where ΔH_{cc} and ΔH_m are the cold crystallization enthalpy and melting enthalpy, respectively, and ΔH_m^∞ is the theoretical melting enthalpy of 100% crystallized PLLA (93.0 J g⁻¹).⁴⁷ Wide-angle X-ray diffraction (WAXD) measurements were carried out using a Rigaku RINT2000 diffractometer with Cu K α radiation ($\lambda = 1.5418 \text{ \AA}$) at 40 kV and 40 mA. The spherulite morphology of the PLLA crystal was observed using a Nikon E600 POL polarized microscope equipped with two hot stages. The sample was initially melted at 185°C for 2 min on one of the stages, and was then immediately transferred to another stage that had been preheated to the desired crystallization temperature (85–120°C). The images were captured using Motic Image Plus 2.2S software. Tensile tests were carried on films with a thickness of ~150 μm using a Shimadzu EZ-TEST tensile tester equipped with a 500 N load cell. Specimens with a length of 30 mm and a width of 2 mm were measured at an extension rate of 20 mm min⁻¹ with a 10 mm span length. At least 5 specimens were measured for each sample. Thermal mechanical analysis (TMA) was carried out using a 0.03 N load in a nitrogen atmosphere, at temperatures from 30 to 140°C, with a heating rate of 5°C min⁻¹ using a Shimadzu thermomechanical analyser (Shimadzu, Japan, TMA-60). The change in specimen length with temperature was recorded, and the linear coefficient of thermal expansion (CTE) was calculated.

5.4 Results and discussion

5.4.1 Non-isothermal crystallization behavior

Two PEG-NH₂ samples, PEG(23)-NH₂ and PEG(48)-NH₂ with average degrees of polymerization of 23 and 48, respectively, were grafted onto the TOCN surfaces via ionic bonds. The PEG(23)-TOCN and PEG(48)-TOCN were individually dispersed in chloroform, and then mixed with PLLA/chloroform solutions. The PEG(23)-TOCN/PLLA and PEG(48)-TOCN/PLLA composite films were prepared simply by casting the PEG(23)-TOCN/PLLA-chloroform and PEG(48)-TOCN/PLLA-chloroform mixtures, respectively.

The addition of PEG(23)-TOCN and PEG(48)-TOCN significantly increased the crystallization rate of PLLA under heating. The cold crystallization peaks of PLLA became sharp, and the cold crystallization temperature (T_{cc}) decreased from 134 to 120 and 111°C by the addition of 1.0% PEG(23)-TOCNs and PEG(48)-TOCNs, respectively (Table 5.1 and Figure 5.1). In this study, the weight contents were based on the contents of TOCN without PEG moieties. The cold crystallization enthalpy (ΔH_{cc}) increased with increasing PEG-TOCN contents. In contrast, no such nucleating effect was observed in the PEG/PLLA blends (without TOCN) at these weight contents. The T_g of the PLLA matrix decreased with increasing PEG contents, which showed that the PEG chains were sufficiently miscible in the PLLA matrix in this system.

Table 5.1. Thermal properties of PEG-TOCN/PLLA nanocomposites and PEG/PLLA blends in the second heating run (heating rate 20 °C min⁻¹).

Sample	Weight content (wt %)		T_g (°C)	T_{cc} (°C)	ΔH_{cc} (J g ⁻¹)	T_m (°C)	ΔH_m (J g ⁻¹)
	TOCN	PEG					
Neat PLLA	0	0	58.3	134.0	10.6	160.0	10.6
1.0 % PEG(23)-TOCN/PLLA nanocomposite	1.0	1.5	50.5	120.0	39.8	157.5, 162.2	39.8
PEG(23)/PLLA blend	0	1.5	48.9	129.3	10.5	158.8	10.5
1.0 % PEG(48)-TOCN/PLLA nanocomposite	1.0	3.0	51.9	111.3	40.8	155.5, 162.5	40.9
PEG(48)/PLLA blend	0	3.0	49.1	129.5	19.0	158.3	19.0

T_g : glass transition temperature T_{cc} : cold crystallization temperature, ΔH_{cc} : cold crystallization enthalpy, T_m : melting temperature, ΔH_m : melting enthalpy. ΔH_{cc} and ΔH_m were calculated based on the weight content of PLLA component.

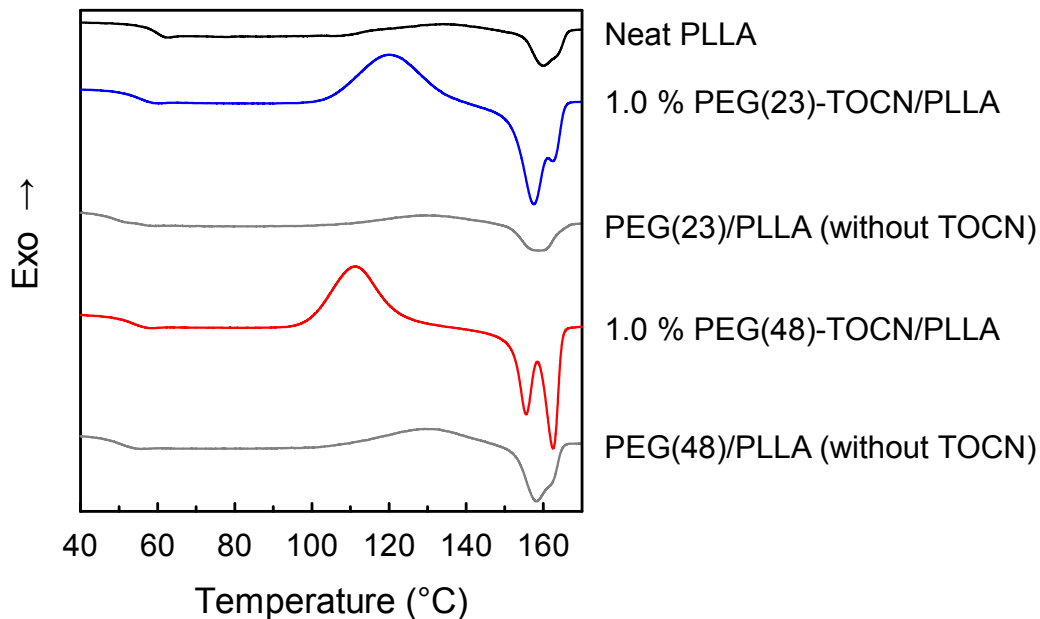


Figure 5.1. DSC curves of PLLA and the 1.0 % PEG-TOCN/PLLA nanocomposites and PEG/PLLA blends in the second heating run (heating rate: $20\text{ }^{\circ}\text{C min}^{-1}$). The weight contents were based on the contents of TOCN without PEG moiety (see Table 5.1).

PEG chains are typically used as a plasticizing agent for PLLA, and can significantly increase the cold crystallization rate of PLLA (by $>10\text{ wt }%$),²⁰⁻²² the PEG chains enhance the chain mobility of PLLA as the density of PEG chains increases, which leads to a reduction in the energy required for the chain folding process during crystallization.²³⁻²⁴ In this study, the PEG chains, which were not immobilized on the surface of the TOCNs, did not enhance the cold crystallization at all, probably due to the low PEG density in the matrix. However, when the PEG chains were densely anchored on the TOCN surfaces ($\sim 1.4\text{ chains nm}^{-2}$), the chains significantly enhanced the crystallization rate of the PLLA; the rate increased as the PEG content in the composite films was increased (Table 5.1). This demonstrated that the sufficiently dispersed PEG-TOCN elements with large surface areas efficiently initiated the nucleation of PLLA. Moreover, the PLLA mobility may have been increased by the dense PEG layers on the TOCN surfaces, which resulted in a reduction in the energy required during crystallization. In addition, double melting behaviour was observed in the PEG-TOCN/PLLA composites (Fig. 5.1), which is explainable in terms of melting-recrystallization-remelting phenomenon.

5.4.2 Isothermal crystallization behavior

The isothermal crystallization behaviour of the composites was investigated using DSC. Neat PLLA and the PEG-TOCN/PLLA composites were melted at 185°C for 2 min, and subsequently cooled to different isothermal crystallization temperatures (T_c). Figure 5.2 shows the crystallization half-time ($t_{1/2}$) as a function of the crystallization temperature T_c , which ranged from 85 to 120°C. $t_{1/2}$ is defined as the time at which the relative crystallinity (X_t) reaches 50% of the total crystallinity, and can be calculated using the following equation:

$$X_t = \frac{\int_0^t (dH/dt) dt}{\int_0^\infty (dH/dt) dt} \times 100 \quad (\%) \quad (5.2)$$

The addition of PEG-TOCN enhanced the isothermal crystallization of PLLA to a remarkable degree. At any T_c , the $t_{1/2}$ of PLLA decreased with the addition of PEG-TOCN (Fig. 5.2). The minimum $t_{1/2}$ value for the neat PLLA and the PEG-TOCN/PLLA composites was observed at approximately 100°C. PEG(23)-TOCN/PLLA and PEG(48)-TOCN/PLLA showed a minimum $t_{1/2}$ of 4.8 and 4.7 min, respectively, at

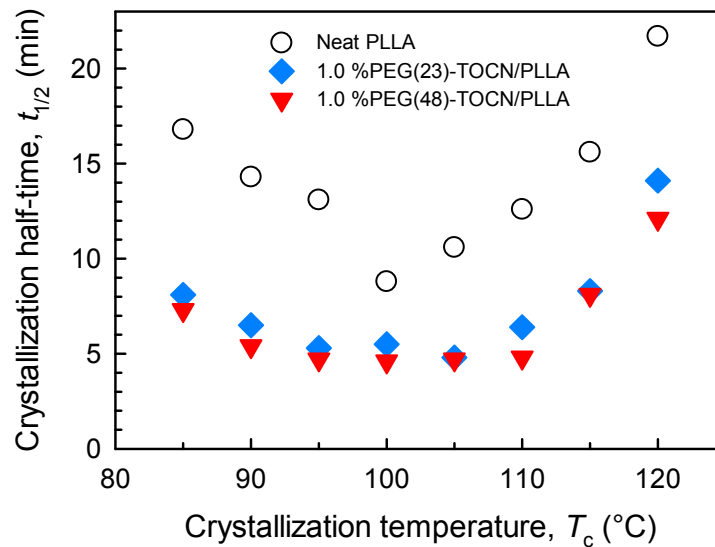


Figure 5.2. The crystallization half time ($t_{1/2}$) of PLLA film, 1.0 % PEG(23)-TOCN/PLLA, and 1.0 % PEG(48)-TOCN/PLLA nanocomposites.

Table 5.2. $t_{1/2}$ values for neat PLLA and PEG-TOCN/PLLA composites at various T_c values.

	$t_{1/2}$ (min) at T_c							
	85 °C	90 °C	95 °C	100 °C	105 °C	110 °C	115 °C	120 °C
Neat PLLA	16.8	14.3	13.1	8.8	10.6	12.6	15.6	21.7
0.5 % PEG(23)-TOCN/PLLA	12.9	9.2	7.8	7.6	7.3	8.1	13.4	16.6
without TOCN	20.0	10.7	11.2	7.7	9.4	9.0	15.0	21.7
1.0 % PEG(23)-TOCN/PLLA	8.1	6.5	5.3	5.5	4.8	6.4	8.3	14.1
without TOCN	11.5	9.4	6.7	7.6	6.1	8.6	9.9	15.1
0.5 % PEG(48)-TOCN/PLLA	12.3	8.3	6.5	5.7	5.7	7.3	10.0	16.5
without TOCN	20.0	12.3	11.3	8.6	9.1	11.3	13.8	18.8
1.0 % PEG(48)-TOCN/PLLA	7.3	5.4	4.7	4.6	4.7	4.8	8.1	12.1
without TOCN	9.3	7.3	6.6	5.7	6.0	8.2	9.9	15.7

105°C, whereas that of PLLA was 10.6 min. These values are comparable with that of the composite containing 1 % silylated cellulose crystals ($t_{1/2} = 4.2$ min at 110 °C)³⁰ or that of the composite containing 1 % nanocellulose prepared by aqueous counter collision ($t_{1/2} = 3.4$ min at 130 °C)²⁹. In contrast, when only PEG molecules without TOCNs were added to the PLLA matrix, the enhancement in isothermal crystallization was not as significant as that achieved using the PEG-TOCNs (Table 5.2). Thus, the isothermal crystallization of PLLA was effectively enhanced by PEG-TOCNs.

The crystallization kinetics of the samples were described using the well-known Avrami theory.⁴⁸⁻⁵⁰ In the Avrami equation, X_t is described as:

$$X_t = 1 - \exp(-kt^n) \quad (5.3)$$

where n is the Avrami exponent and k is the rate constant of crystallization. In this equation, n is dependent on the crystal shape and the nucleation process. Equation (5.3) can be rearranged to give the following equation:

$$[-\ln(1-X_t)] = \ln k + n \ln t \quad (5.4)$$

The parameter n can be obtained from the slope of plots of $\ln[-\ln(1-X_t)]$ versus $\ln t$.

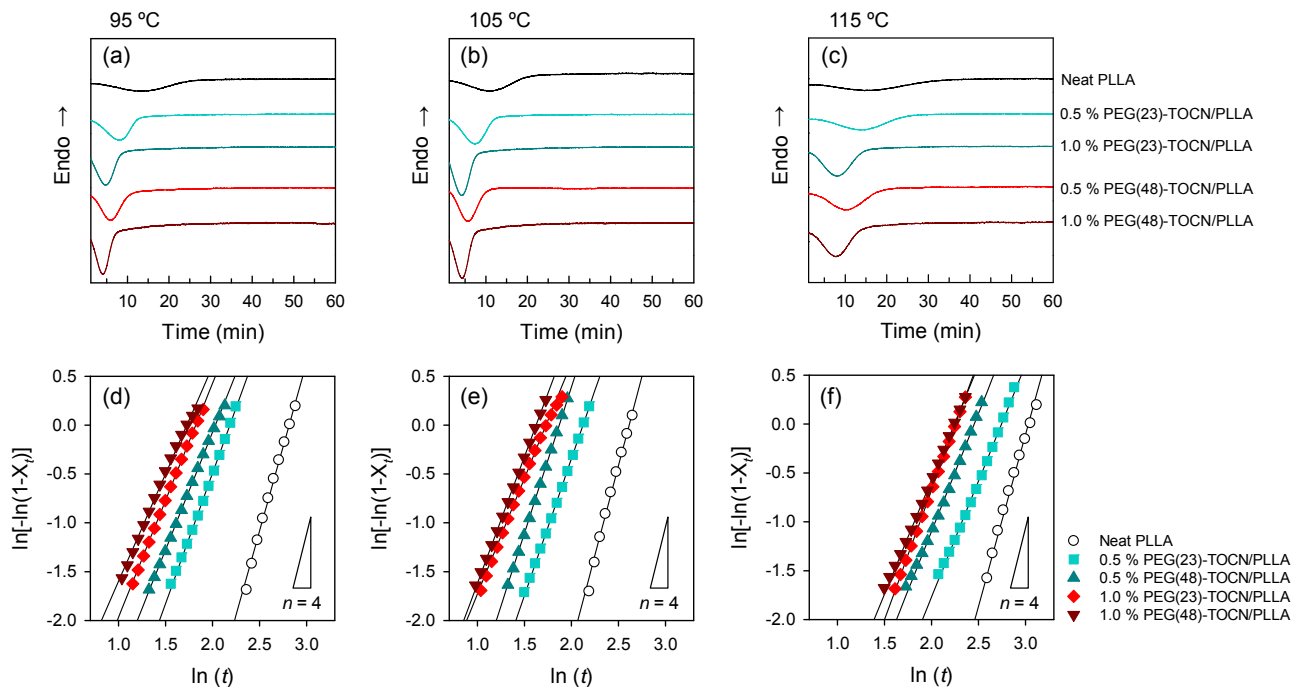


Figure 5.3. Isothermal crystallization curves obtained using DSC, and corresponding Avrami plots of $\ln[-\ln(1-X_t)]$ versus $\ln(t)$ at different temperatures; (a, d) 95 °C, (b, e) 105 °C, and (c, f) 115 °C.

Figure 5.3 shows isothermal crystallization curves for neat PLLA and PEG-TOCN/PLLA composites at 95, 105, and 115 °C and the corresponding Avrami plots. The isothermal peaks became sharper after the addition of the PEG-TOCNs, which clearly showed that they enhanced the isothermal crystallization of PLLA. The n and X_c values obtained from the isothermal peaks are listed in Table 5.3. The Avrami exponent n was obtained using a linear fitting of the X_t data in the range of 20–70%. This exponent predicts the nucleation mechanism and growth dimensions. For the neat PLLA, n was close to 4, indicating homogeneous nucleation with a three-dimensional growth.⁵¹ In contrast, the n values of the PEG-TOCN/PLLA composites were in the range of 2.2–2.7, which revealed that the growth of the PLLA crystals occurred with homogeneous nucleation in one or two dimensions in the composites.

The crystal growth of the neat PLLA and PEG-TOCN/PLLA composites was observed using polarized optical microscopy at different T_c values (Figure 5.4). The PEG-TOCN/PLLA composites showed a significantly higher nucleation density than the neat PLLA, because the nucleation was enhanced on the TOCN surfaces. Moreover, no three-dimensional spherulites were observed for the composites; this was

Table 5.3. Isothermal crystallization kinetics parameters at 95, 105, and 115 °C. X_c was calculated based on the weight content of PLLA component.

Sample	$T_c = 95\text{ °C}$		$T_c = 105\text{ °C}$		$T_c = 115\text{ °C}$	
	n	X_c (%)	n	X_c (%)	n	X_c (%)
Neat PLLA	3.4	28.5	3.5	32.2	3.7	30.2
0.5 % PEG(23)-TOCN	2.7	32.4	2.8	37.0	2.4	38.0
1.0 % PEG(23)-TOCN	2.4	33.6	2.4	39.5	2.7	41.7
0.5 % PEG(48)-TOCN	2.4	32.6	3.0	37.1	2.4	39.6
1.0 % PEG(48)-TOCN	2.2	33.7	2.6	40.1	2.3	42.1

different from the behaviour observed for the neat PLLA. This was likely because the dense PEG-TOCN networks in the composites prohibited the three-dimensional growth of the PLLA spherulites in the composites. In a previous study, it was demonstrated that TOCNs with a width of ~ 3 nm and a length of ~ 1 μm formed a network throughout a polymer matrix (i.e., via percolation) with a TOCN content of only 0.31 vol % (0.5 wt %).⁵²

In this study, it is likely that dense TOCN networks were formed in the composites with 1.0 wt % TOCN contents. As a result, the TOCN network in the PLLA matrix restricted the dimensionality of the crystal growth of PLLA (which is consistent with the lower n values of the composites, as discussed previously). The size of the PLLA spherulites in the neat PLLA films increased with crystallization temperature, and the nucleation rate was lower. In contrast, the crystal size in the PEG-TOCN/PLLA composites was apparently unchanged with temperature in the presence of the TOCN networks. The X_c value increased up to 42.1 % with the addition of PEG-TOCNs (Table 2), which is as high as that of the composite containing 25 w/w % microcrystalline cellulose ($X_c = 44.5\%$)⁵³. The X_c value slightly increased with the addition of PEG-TOCNs (Table 5.3). The WAXD patterns showed that the addition of PEG-TOCNs did not change the crystal forms of the neat PLLA at all during isothermal crystallization (Figure 5.5). Thus, the PEG-TOCNs increased not only the crystallization rate but also the X_c of PLLA, without changing the crystal structure.

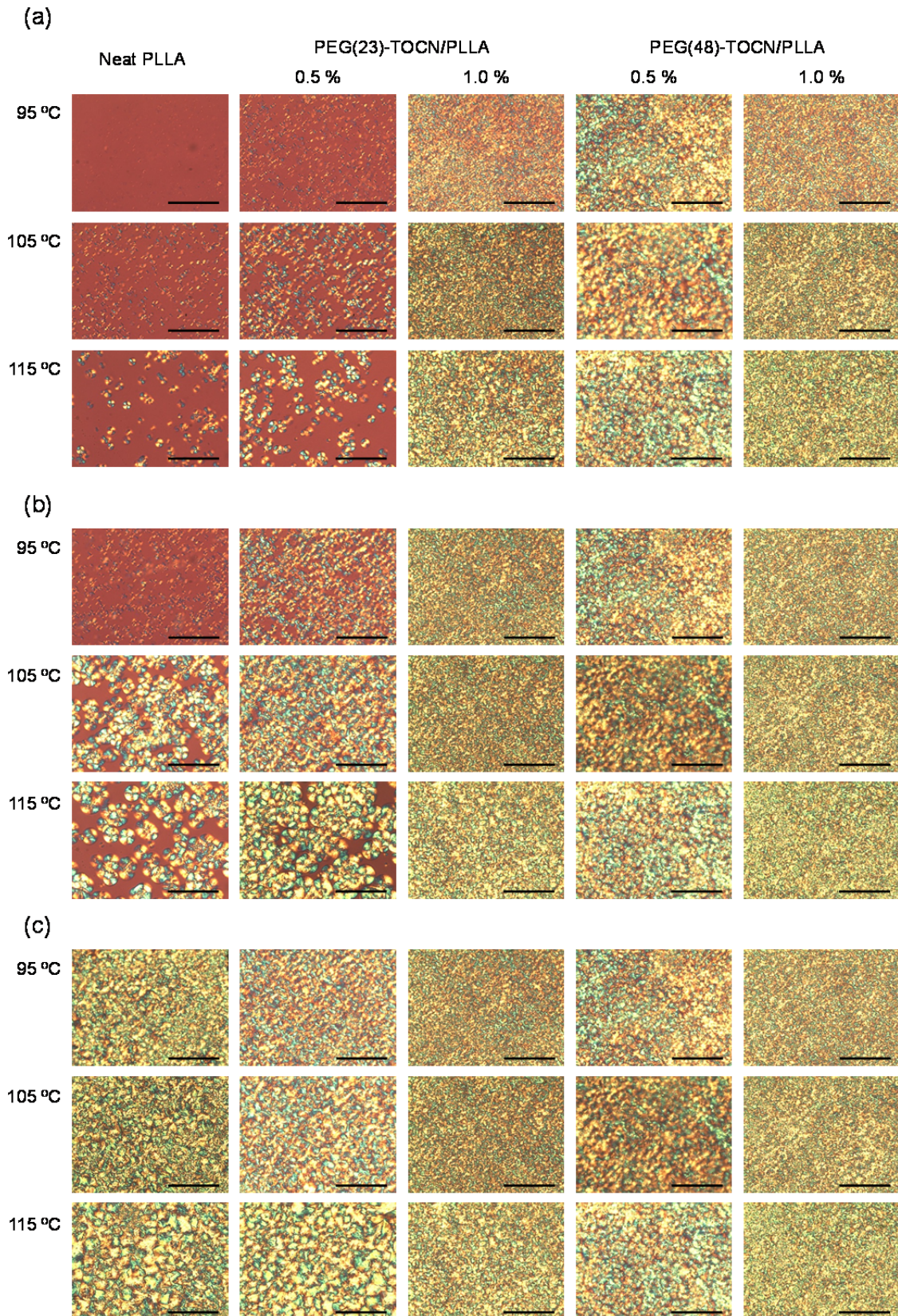


Figure 5.4. Optical micrographs of neat PLLA and PEG-TOCN composites observed between crossed polarizers after isothermal crystallization for (a) 5 min, (b) 10 min, and (c) 60 min at various crystallization temperatures. The scale bar represents 100 μm .

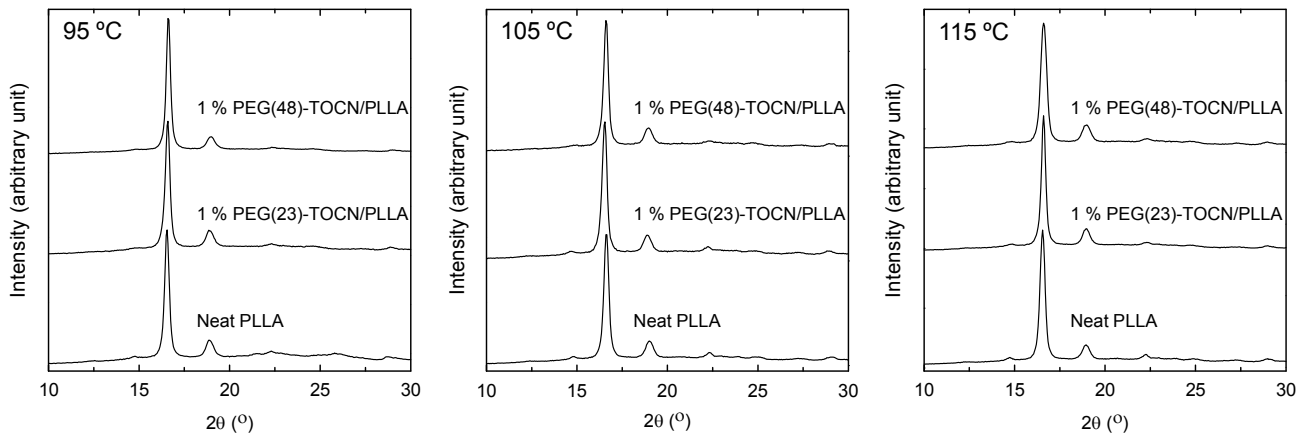


Figure 5.5. Wide-angle X-ray diffraction patterns for neat PLLA and PEG-TOCN/PLLA nanocomposites crystallized at 95, 105, and 115°C for 60 min. The films were composed of both α' and α phases.⁵⁴⁻⁵⁵

The thermal dimensional stability of the films after isothermal crystallization at 95, 105, and 115°C for 5 min was evaluated using thermomechanical analysis. The composites exhibited better thermal stability than neat PLLA, due to the increased crystallinity (Fig. 5.6a). The thermal expansion of the neat PLLA film increased above the T_g of ~60°C. In contrast, the thermal expansion values of the composite films were smaller than 4% in

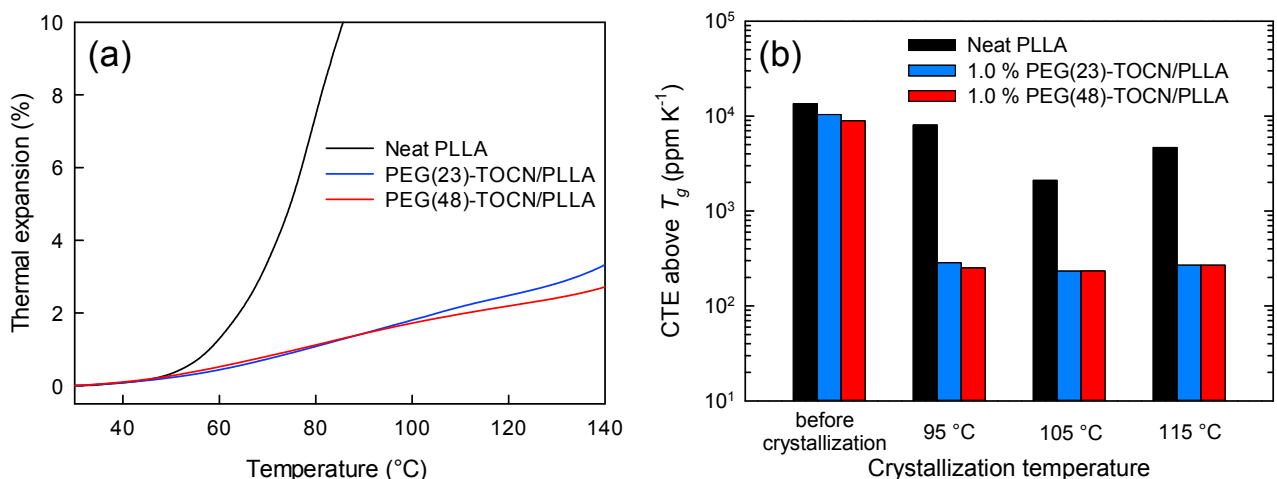
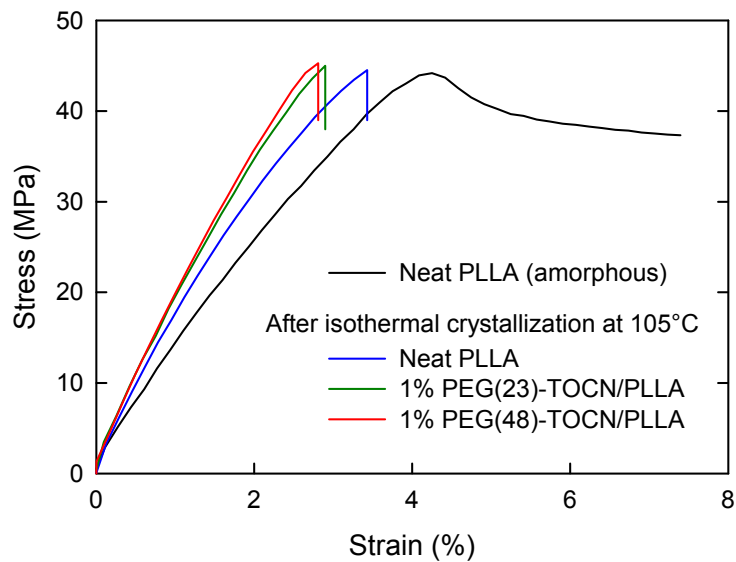


Figure 5.6. (a) Thermal expansion behaviour of neat PLLA and 1.0% PEG-TOCN/PLLA composites after isothermal crystallization at 105°C for 5 min, and (b) the linear thermal expansion coefficient (CTE) of the films above the glass transition temperatures (T_g) of the samples before and after isothermal crystallization at 95, 105, and 115°C for 5 min.

Table 5.4. Tensile properties of neat PLLA and PEG-TOCN films after isothermal crystallization for 5 min.

	T_c (°C)	Young's modulus (GPa)	ultimate tensile strength (MPa)	elongation at break (%)	X_c (%)
Neat PLLA	–	1.29 ± 0.12	40.1 ± 2.0	6.1 ± 0.45	0
	95	1.42 ± 0.29	40.8 ± 6.0	4.1 ± 0.42	2.9
	105	1.44 ± 0.15	41.9 ± 2.1	3.5 ± 0.36	4.6
	115	1.41 ± 0.22	42.3 ± 5.8	3.8 ± 0.43	3.0
1.0 % PEG(23)-TOCN/PLLA	95	1.61 ± 0.20	45.0 ± 4.6	4.0 ± 0.70	15.3
	105	1.61 ± 0.10	43.0 ± 2.9	3.0 ± 0.21	21.2
	115	1.56 ± 0.18	41.0 ± 4.1	3.7 ± 0.38	7.0
1.0 % PEG(48)-TOCN/PLLA	95	1.66 ± 0.28	50.0 ± 4.7	3.0 ± 0.48	18.6
	105	1.66 ± 0.13	45.1 ± 4.4	3.1 ± 0.23	24.9
	115	1.54 ± 0.10	43.4 ± 3.4	4.0 ± 0.74	8.8

**Figure 5.7.** Stress-strain curves for neat PLLA and PEG-TOCN/PLLA nanocomposite films after isothermal crystallization at 105°C for 5 min.

this temperature range. The CTE values of the composites decreased significantly (by approximately one order of magnitude) after the isothermal crystallization, whereas the neat PLLA showed a modest decrease in its CTE (Fig. 5.6b). The CTE value of the PEG-TOCN/PLLA nanocomposites was $\sim 230 \text{ ppm K}^{-1}$ after the crystallization, which is comparable that of xylan ester/PLLA blend (215 ppm K^{-1})¹⁹. This was primarily due to the increased degree of crystallinity of the PLLA in the composites. The Young's moduli of the samples increased as the degree of crystallinity increased (Fig. 5.7 and Table 5.4). However, the crystallization resulted in brittle failure as has been reported previously.^{22, 56-57}

5.5 Conclusions

In this study, we demonstrated the potential of PEG-TOCNs as a bio-based nucleating agent for PLLA. Because the PEG chains were densely immobilized on the surface of the TOCNs, which had high specific surface areas, the nucleation rate of PLLA was effectively increased on the surfaces. Because of the sustainability and biocompatibility of cellulose nanofibrils, this technique is applicable in many fields, and in, for example, medical and packaging applications. Moreover, this is a simple but efficient process. We expect that it will be possible to tune the nucleating properties by changing the grafting agents..

5.6 References

1. R. G. Sinclair, "The Case for Polylactic Acid as a Commodity Packaging Plastic." *J. Macromol. Sci. Pure.* 1996, **A33**, 585–597.
2. R. Auras, B. Harte and S. Selke, "An Overview of Poly lactides as Packaging Materials." *Macromol. Biosci.* 2004, **4**, 835–864.
3. L. T. Lim, R. Auras and M. Rubino, "Processing Technologies for Poly(Lactic Acid)." *Prog. Polym. Sci.* 2008, **33**, 820–852.
4. D. Garlotta, "A Literature Review of Poly(Lactic Acid)." *J. Polym. Environ.* 2001, **9**, 63–84.
5. Y. Ikada and H. Tsuji, "Biodegradable Polyesters for Medical and Ecological Applications." *Macromol. Rapid Commun.* 2000, **21**, 117–132.
6. K. Kim, M. Yu, X. H. Zong, J. Chiu, D. F. Fang, Y. S. Seo, B. S. Hsiao, B. Chu and M. Hadjiargyrou, "Control of Degradation Rate and Hydrophilicity in Electrospun Non-Woven Poly(D,L-lactide)

- Nanofiber Scaffolds for Biomedical Applications.” *Biomaterials* 2003, **24**, 4977–4985.
7. J. J. Kolstad, “Crystallization Kinetics of Poly(L-lactide-Co-Meso-Lactide).” *J. Appl. Polym. Sci.* 1996, **62**, 1079–1091.
 8. D. Battagazzore, S. Bocchini and A. Frache, “Crystallization Kinetics of Poly(Lactic Acid)-Talc Composites.” *Express. Polym. Lett.* 2011, **5**, 849–858.
 9. T. Y. Ke and X. Z. Sun, “Melting Behavior and Crystallization Kinetics of Starch and Poly(Lactic Acid) Composites.” *J. Appl. Polym. Sci.* 2003, **89**, 1203–1210.
 10. M. Pluta, A. Galeski, M. Alexandre, M. A. Paul and P. Dubois, “Polylactide/Montmorillonite Nanocomposites and Microcomposites Prepared by Melt Blending: Structure and Some Physical Properties.” *J. Appl. Polym. Sci.* 2002, **86**, 1497–1506.
 11. X. X. Li, J. B. Yin, Z. Y. Yu, S. F. Yan, X. C. Lu, Y. J. Wang, B. Cao and X. S. Chen, “Isothermal Crystallization Behavior of Poly(L-lactic Acid)/Organo-Montmorillonite Nanocomposites.” *Polym. Compos.* 2009, **30**, 1338–1344.
 12. Y. T. Shieh, G. L. Liu, Y. K. Twu, T. L. Wang and C. H. Yang, “Effects of Carbon Nanotubes on Dynamic Mechanical Property, Thermal Property, and Crystal Structure of Poly(L-lactic Acid).” *J. Polym. Sci., Part B: Polym. Phys.* 2010, **48**, 145–152.
 13. X. Hu, H. N. An, Z. M. Li, Y. Geng, L. B. Li and C. L. Yang, “Origin of Carbon Nanotubes Induced Poly(L-Lactide) Crystallization: Surface Induced Conformational Order.” *Macromolecules* 2009, **42**, 3215–3218.
 14. D. F. Wu, L. A. Wu, W. D. Zhou, M. Zhang and T. Yang, “Crystallization and Biodegradation of Polylactide/Carbon Nanotube Composites.” *Polym. Eng. Sci.* 2010, **50**, 1721–1733.
 15. J. Z. Xu, T. Chen, C. L. Yang, Z. M. Li, Y. M. Mao, B. Q. Zeng and B. S. Hsiao, “Isothermal Crystallization of Poly(L-lactide) Induced by Graphene Nanosheets and Carbon Nanotubes: A Comparative Study.” *Macromolecules* 2010, **43**, 5000–5008.
 16. H. S. Wang and Z. B. Qiu, “Crystallization Kinetics and Morphology of Biodegradable Poly(L-lactic Acid)/Graphene Oxide Nanocomposites: Influences of Graphene Oxide Loading and Crystallization Temperature.” *Thermochim. Acta* 2012, **527**, 40–46.
 17. H. S. Wang and Z. B. Qiu, “Crystallization Behaviors of Biodegradable Poly(L-lactic Acid)/Graphene Oxide Nanocomposites from the Amorphous State.” *Thermochim. Acta* 2011, **526**, 229–236.
 18. H. Nakajima, M. Takahashi and Y. Kimura, “Induced Crystallization of PLLA in the Presence of 1,3,5-Benzenetricarboxylamide Derivatives as Nucleators: Preparation of Haze-Free Crystalline PLLA Materials.” *Macromol. Mater. Eng.* 2010, **295**, 460–468.
 19. N. G. V. Fundador, Y. Enomoto-Rogers, A. Takemura and T. Iwata, “Xylan Esters as Bio-Based Nucleating Agents for Poly(L-lactic Acid).” *Polym. Degrad. Stab.* 2013, **98**, 1064–1071.
 20. O. Martin and L. Averous, “Poly(Lactic Acid): Plasticization and Properties of Biodegradable Multiphase Systems.” *Polymer* 2001, **42**, 6209–6219.
 21. M. Sheth, R. A. Kumar, V. Dave, R. A. Gross and S. P. McCarthy, “Biodegradable Polymer Blends of Poly(Lactic Acid) and Poly(Ethylene Glycol).” *J. Appl. Polym. Sci.* 1997, **66**, 1495–1505.

22. M. Baiardo, G. Frisoni, M. Scandola, M. Rimelen, D. Lips, K. Ruffieux and E. Wintermantel, "Thermal and Mechanical Properties of Plasticized Poly(L-lactic Acid)." *J. Appl. Polym. Sci.* 2003, **90**, 1731–1738.
23. H. B. Li and M. A. Huneault, "Effect of Nucleation and Plasticization on the Crystallization of Poly(Lactic Acid)." *Polymer* 2007, **48**, 6855–6866.
24. W. C. Lai, W. B. Liao and T. T. Lin, "The Effect of End Groups of PEG on the Crystallization Behaviors of Binary Crystalline Polymer Blends PEG/PLLA." *Polymer* 2004, **45**, 3073–3080.
25. Y. Nishiyama, "Structure and Properties of the Cellulose Microfibril." *J. Wood. Sci.* 2009, **55**, 241–249.
26. I. Sakurada, Y. Nukushina and T. Ito, "Experimental Determination of the Elastic Modulus of Crystalline Regions in Oriented Polymers." *J. Polym. Sci.* 1962, **57**, 651–660.
27. A. Sturcova, G. R. Davies and S. J. Eichhorn, "Elastic Modulus and Stress-Transfer Properties of Tunicate Cellulose Whiskers." *Biomacromolecules* 2005, **6**, 1055–1061.
28. S. Iwamoto, W. Kai, A. Isogai and T. Iwata, "Elastic Modulus of Single Cellulose Microfibrils from Tunicate Measured by Atomic Force Microscopy." *Biomacromolecules* 2009, **10**, 2571–2576.
29. R. Kose and T. Kondo, "Size Effects of Cellulose Nanofibers for Enhancing the Crystallization of Poly(Lactic Acid)." *J. Appl. Polym. Sci.* 2013, **128**, 1200–1205.
30. A. Pei, Q. Zhou and L. A. Berglund, "Functionalized Cellulose Nanocrystals as Biobased Nucleation Agents in Poly(L-lactide) (PLLA) – Crystallization and Mechanical Property Effects." *Compos. Sci. Technol.* 2010, **70**, 815–821.
31. L. Suryanegara, A. N. Nakagaito and H. Yano, "The Effect of Crystallization of PLA on the Thermal and Mechanical Properties of Microfibrillated Cellulose-Reinforced PLA Composites." *Compos. Sci. Technol.* 2009, **69**, 1187–1192.
32. D. T. Quillin, D. F. Caulfield and J. A. Koutsky, "Crystallinity in the Polypropylene/Cellulose System .1. Nucleation and Crystalline Morphology." *J. Appl. Polym. Sci.* 1993, **50**, 1187–1194.
33. A. Amash and P. Zugenmaier, "Study on Cellulose and Xylan Filled Polypropylene Composites." *Polym. Bull.* 1998, **40**, 251–258.
34. S. J. Son, Y. M. Lee and S. S. Im, "Transcrystalline Morphology and Mechanical Properties in Polypropylene Composites Containing Cellulose Treated with Sodium Hydroxide and Cellulase." *J. Mater. Sci.* 2000, **35**, 5767–5778.
35. D. G. Gray, "Transcrystallization of Polypropylene at Cellulose Nanocrystal Surfaces." *Cellulose* 2007, **15**, 297–301.
36. E. Ten, J. Turtle, D. Bahr, L. Jiang and M. Wolcott, "Thermal and Mechanical Properties of Poly(3-Hydroxybutyrate-Co-3-Hydroxyvalerate)/Cellulose Nanowhiskers Composites." *Polymer* 2010, **51**, 2652–2660.
37. S. Fujisawa, T. Saito, S. Kimura, T. Iwata and A. Isogai, "Surface Engineering of Ultrafine Cellulose Nanofibrils toward Polymer Nanocomposite Materials." *Biomacromolecules* 2013, **14**, 1541–1546.
38. T. Saito, Y. Nishiyama, J. L. Putaux, M. Vignon and A. Isogai, "Homogeneous Suspensions of

- Individualized Microfibrils from TEMPO-Catalyzed Oxidation of Native Cellulose.” *Biomacromolecules* 2006, **7**, 1687–1691.
39. A. Isogai, T. Saito and H. Fukuzumi, “TEMPO-Oxidized Cellulose Nanofibers.” *Nanoscale* 2011, **3**, 71–85.
 40. J. Araki, M. Wada and S. Kuga, “Steric Stabilization of a Cellulose Microcrystal Suspension by Poly(Ethylene Glycol) Grafting.” *Langmuir* 2001, **17**, 21–27.
 41. E. Lasseguette, “Grafting onto Microfibrils of Native Cellulose.” *Cellulose* 2008, **15**, 571–580.
 42. F. Azzam, L. Heux, J. L. Putaux and B. Jean, “Preparation by Grafting onto, Characterization, and Properties of Thermally Responsive Polymer-Decorated Cellulose Nanocrystals.” *Biomacromolecules* 2010, **11**, 3652–3659.
 43. R. K. Johnson, A. Zink-Sharp and W. G. Glasser, “Preparation and Characterization of Hydrophobic Derivatives of TEMPO-Oxidized Nanocelluloses.” *Cellulose* 2011, **18**, 1599–1609.
 44. M. Salajková, L. A. Berglund and Q. Zhou, “Hydrophobic Cellulose Nanocrystals Modified with Quaternary Ammonium Salts.” *J. Mater. Chem.* 2012, **22**, 19798–19805.
 45. S. Fujisawa, T. Saito and A. Isogai, “Nano-Dispersion of TEMPO-Oxidized Cellulose/Aliphatic Amine Salts in Isopropyl Alcohol.” *Cellulose* 2012, **19**, 459–466.
 46. S. Fujisawa, Y. Okita, T. Saito, E. Togawa and A. Isogai, “Formation of N-Acylureas on the Surface of TEMPO-Oxidized Cellulose Nanofibril with Carbodiimide in DMF.” *Cellulose* 2011, **18**, 1191–1199.
 47. J. Y. Nam, S. S. Ray and M. Okamoto, “Crystallization Behavior and Morphology of Biodegradable Polylactide/Layered Silicate Nanocomposite.” *Macromolecules* 2003, **36**, 7126–7131.
 48. M. Avrami, “Kinetics of Phase Change I - General Theory.” *J. Chem. Phys.* 1939, **7**, 1103–1112.
 49. M. Avrami, “Kinetics of Phase Change. II Transformation-Time Relations for Random Distribution of Nuclei.” *J. Chem. Phys.* 1940, **8**, 212–224.
 50. M. Avrami, “Granulation, Phase Change, and Microstructure - Kinetics of Phase Change. III.” *J. Chem. Phys.* 1941, **9**, 177–184.
 51. T. Miyata and T. Masuko, “Crystallization Behaviour of Poly(L-lactide).” *Polymer* 1998, **39**, 5515–5521.
 52. S. Fujisawa, T. Ikeuchi, M. Takeuchi, T. Saito and A. Isogai, “Superior Reinforcement Effect of TEMPO-Oxidized Cellulose Nanofibrils in Polystyrene Matrix: Optical, Thermal, and Mechanical Studies.” *Biomacromolecules* 2012, **13**, 2188–2194.
 53. A. P. Mathew, K. Oksman and M. Sain, “The Effect of Morphology and Chemical Characteristics of Cellulose Reinforcements on the Crystallinity of Polylactic Acid.” *J. Appl. Polym. Sci.* 2006, **101**, 300–310.
 54. J. Zhang, K. Tashiro, H. Tsuji and A. J. Domb, “Disorder-to-Order Phase Transition and Multiple Melting Behavior of Poly(L-lactide) Investigated by Simultaneous Measurements of Waxd and DSC.” *Macromolecules* 2008, **41**, 1352–1357.
 55. H. Marubayashi, S. Akaishi, S. Akasaka, S. Asai and M. Sumita, “Crystalline Structure and Morphology of Poly(L-lactide) Formed under High-Pressure CO₂.” *Macromolecules* 2008, **41**, 9192–

9203.

56. G. Perego, G. D. Cella and C. Bastioli, "Effect of Molecular Weight and Crystallinity on Poly(Lactic Acid) Mechanical Properties." *J. Appl. Polym. Sci.* 1996, **59**, 37–43.
57. A. C. Renouf-Glauser, J. Rose, D. F. Farrar and R. E. Cameron, "The Effect of Crystallinity on the Deformation Mechanism and Bulk Mechanical Properties of PLLA." *Biomaterials* 2005, **26**, 5771–5782.

Chapter 6

Summary

Surface modification of ultrafine cellulose nanofibrils with a width of ~3 nm has been developed, by using the carboxyl groups on TOCN surfaces as selective anchoring sites. The surface carboxyl groups can be selectively modified at high conversion ratios, by means of either covalent or non-covalent approaches. When TOCNs are reacted with either DIC or DCC, diisopropyl or dicyclohexyl groups are selectively introduced on the carboxyl groups via *N*-acylurea structures, respectively. By this reaction, hydrophobicity of TOCN films efficiently increases due to introduction of two isopropyl or cyclohexyl moieties to one carboxyl group of TOCN. When alkyl or PEG amines are used, they are introduced onto most of (>95%) carboxyl groups on the TOCN surfaces via ionic bondings. Solvent dispersibility of TOCNs can be controlled by the surface modification. When long PEG amines with a degree of polymerization of 48 are introduced to carboxyl groups via simple ionic bondings, the PEG-TOCNs are stably dispersed not only in water and polar organic solvents but also in nonpolar organic solvents such as chloroform and toluene, despite original TOCNs are dispersible only in water or polar organic solvents. These processes are highly surface-selective, and have great versatility to the design of good interaction with various matrices in hybrid nanomaterials.

Bio-based PEG-TOCN/PLLA nanocomposites can be prepared by using PEG-TOCNs as nanofillers. With the aid of the surface modification, PEG-TOCNs are individually dispersed and strongly interact with surrounding PLLA matrix, so that the resultant nanocomposites shows higher stiffness, strength, and toughness, compared with neat polymers. Young's modulus of the nanocomposites increases with TOCN addition following theoretically predicted values, which means that the reinforcing potential of cellulose microfibrils is fully realized. Since TOCN surfaces can be more finely modified than SWCNT surfaces, the PEG-TOCN/PLLA nanocomposites show superior properties to PEG-SWCNT/PLLA nanocomposites in terms of optical transparency, strength, and toughness. Moreover, the PEG-TOCNs show nucleating ability for PLLA; the TOCNs effectively enhance crystallization of PLLA matrix due to their extraordinary high specific surface areas, and therefore improve thermal dimensional stability of the nanocomposites.

In summary, we have demonstrated the potential of cellulose microfibrils as a reinforcing nanofiller in polymer composite materials, through surface modification of TOCNs. This surface engineering technique, i.e. dense and selective grafting onto cellulose nanofibril surfaces using TOCNs, is simple but effective, and properties of the nanocomposites can be finely tuned by changing the grafting agents. Because of the sustainability and biocompatibility of cellulose nanofibrils, we expect that this technique paves the way to design novel green nanocomposite materials with superior functional properties.

Appendix

Determination of average distance between two adjacent grafting points on TEMPO-oxidized cellulose nanofibril surfaces

The average density of carboxyl groups on the TEMPO-oxidized cellulose nanofibril surfaces (Γ_{COOH}) was determined by following equation (A1):

$$\Gamma_{\text{COOH}} = \Gamma_{\text{CH}_2\text{OH}} \times \frac{C_{\text{COOH}}}{C_{\text{CH}_2\text{OH}}} \quad (\text{A1})$$

where $\Gamma_{\text{CH}_2\text{OH}}$ is the average density of C6 primary hydroxyl groups exposed on the original cellulose microfibril surface, and $C_{\text{CH}_2\text{OH}}$ and C_{COOH} are the contents of C6 primary hydroxyl group exposed on the original cellulose crystalline surface and C6 carboxyl groups of the TEMPO-oxidized cellulose, respectively, expressed as mol per mol of monomer unit (mol mol^{-1} of monomer unit). The parameters $\Gamma_{\text{CH}_2\text{OH}}$, $C_{\text{CH}_2\text{OH}}$, and C_{COOH} were expressed as follows. Because the length of the repeating cellobiose unit in cellulose chains is 1.04 nm, $\Gamma_{\text{CH}_2\text{OH}}$ was described as:^{S1}

$$\Gamma_{\text{CH}_2\text{OH}} = \frac{\frac{1}{(1.04 \times d_1)} + \frac{1}{(1.04 \times d_2)}}{2} \quad (\text{A2})$$

where d_1 is a d -spacing of 0.60 nm, which corresponds to the (1 -1 0) plane of cellulose I $_{\beta}$, and d_2 is 0.54 nm, which corresponds to the (1 1 0) plane of cellulose I $_{\beta}$.^{S2} In this study, cellulose microfibrils were assumed to have square cross sections with sides of the same length.^{S3} From equation (A2), $\Gamma_{\text{CH}_2\text{OH}}$ was calculated to be 1.7 nm^{-2} . Following a previous paper, $C_{\text{CH}_2\text{OH}}$ was expressed by the following equation (A3):

$$C_{\text{CH}_2\text{OH}} = \frac{\left(\frac{C_1}{d_1} + \frac{C_2}{d_2} \right)}{\left[\left(\frac{C_1}{d_1} + 1 \right) \times \left(\frac{C_2}{d_2} + 1 \right) \right]} \quad (\text{A3})$$

where C_1 and C_2 are crystal sizes of 3 nm, and $C_{\text{CH}_2\text{OH}}$ was determined to be $0.23 \text{ mol mol}^{-1}$ of the monomer unit. Because the molecular weights of glucuronosyl acid Na salt and glucosyl units are 198 and 162,

respectively, $C_{\text{CH}_2\text{OH}}$ is expressed as:^{S1}

$$C_{\text{COOH}} = \frac{B}{(1000 - 36 \times B)/162} \quad (\text{A4})$$

where B is the carboxylate content of TEMPO-oxidized cellulose (mmol g^{-1}), which was determined by the conductivity titration method to be 1.3 mmol g^{-1} . From equation (A4), C_{COOH} was calculated to be $0.22 \text{ mol mol}^{-1}$ of the monomer unit.

From equation (A1)–(A4), Γ_{COOH} was determined to be $1.41 \text{ (nm}^{-2}\text{)}$

The average distance between two adjacent carboxyl groups on the TEMPO-oxidized cellulose nanofibril surfaces (D) was presented as:

$$D = \left[\Gamma_{\text{CH}_2\text{OH}} \times \frac{(C_{\text{COOH}} \times A)}{C_{\text{CH}_2\text{OH}}} \right]^{-1/2} \quad (\text{A5})$$

A is the conversion ratio from free carboxyl groups to amine salt formation calculated by elemental analysis to be 1. From equation (A5), D was determined to be 0.71 nm .

The thickness of the polymer brush layer on cellulose nanofibril surfaces

For polymer chains in a good solvent, the chain size is defined by the Flory radius (R_F):^{S4–S6}

$$R_F = aN^{3/5} \quad (\text{A6})$$

where a and N are the size of the monomer units and the degree of polymerization of the grafted chains, respectively. For PEG chains, a is 0.35 nm , and in this study, N was 48. The R_F calculated by equation (A6) is 3.6 nm while average distance between two adjacent grafting points (D) is 0.71 nm ; the grafting points are so close to each other that grafted PEG chains are forced to stretch away from the surface to avoid overlapping. When $D < R_F$, the thickness of grafted chain layer (L) in a good solvent was estimated as:^{S4,S5}

$$L = aN(a/D)^{2/3} \quad (D < R_F) \quad (\text{A7})$$

From equation (A7), the thickness of PEG layer was estimated to be ~11 nm.

Thermal properties of PEG-grafted cellulose nanofibrils/PLLA nanocomposite

The degree of crystallinity (X_c) of the PLLA matrix was estimated from DSC thermograms of the composites using the following equation (A8):^{S7}

$$X_c = \frac{\Delta H_m - \Delta H_c}{\Delta H_c^\infty} \times 100(\%) \quad (\text{A8})$$

where ΔH_m is the melting enthalpy and ΔH_c is the crystallization enthalpy of the PLLA component of the composites. ΔH_c^∞ is the theoretical melting enthalpy of 100% crystalline PLLA (93.0 J/g).^{S7}

Theoretical Approach for Predicting Young's Modulus of the Composites

The following four different models were used to predict the Young's modulus of each PEG-grafted cellulose nanofibril/PLLA nanocomposite, assuming that the nanofibrils were randomly laminated in the matrix, and the results were compared with experimental values.

1. Halpin-Tsai model^{S8, S9}

$$E_{\text{HT}} = \left[\frac{3}{8} \times \frac{1 + 2(l_f / d_f)\eta_L V_f}{1 - \eta_L V_f} + \frac{5}{8} \times \frac{1 + 2\eta_T V_f}{1 - \eta_T V_f} \right] E_m$$

$$\eta_L = \frac{(E_f / E_m) - 1}{(E_f / E_m) + 2(l_f / d_f)}$$

$$\eta_T = \frac{(E_f / E_m) - 1}{(E_f / E_m) + 2}$$

where E_f and E_m are the moduli of a single cellulose nanofibril and the PLLA matrix, respectively, and l_f , d_f , and V_f are the length, width, and volume fraction of cellulose nanofibrils in the composite, respectively. V_f was calculated assuming that the densities of cellulose nanofibril and PLLA were 1.6 and 1.26 g cm⁻³, respectively.^{S10}

2. Voigt-Reuss model^{S11}

$$E_{\text{VR}} = \frac{3}{8} (V_f E_f + (1 - V_f) E_m) + \frac{5}{8} \left(\frac{E_f E_m}{E_f (1 - V_f) + E_m V_f} \right)$$

3. Modified mixture law^{S11,S12}

$$E_{MML} = \frac{1}{5}V_f E_f + (1 - V_f)E_m$$

4. Cox model^{S11-S13}

$$E_{Cox} = \eta_0 \eta_L E_f V_f + (1 - V_f)E_m$$

$$\eta_0 = \frac{1}{5} \quad \eta_L = \left[1 - \frac{\tanh(\beta s)}{\beta s} \right] \quad s = \frac{2l_f}{r_f} \quad \beta^2 = \frac{2\pi E_m}{E_f(1 + \nu_m)\ln(1/V_f)}$$

References

- (S1) Okita, Y.; Saito, T.; Isogai, A. *Biomacromolecules* **2010**, *11*, 1969–1700.
- (S2) Wada, M.; Okano, T.; Sugiyama, J. *Cellulose* **1997**, *4*, 221–232.
- (S3) Revol, J.-F. *Carbohydr. Polym.* **1982**, *2*, 123–134.
- (S4) Israelachvili, J. N. *Intermolecular and Surface Forces*, 2nd ed.; Academic Press: London, 1991; pp 277–287.
- (S5) de Gennes, P. G. *Macromolecules* **1980**, *13*, 1069–1075.
- (S6) Zhao, B.; Brittain, W. J. *Prog. Polym. Sci.* **2000**, *25*, 677–710.
- (S7) Nam, J. Y.; Ray, S. S.; Okamoto, M. *Macromolecules* **2003**, *36*, 7126–7131.
- (S8) Zhang, X.; Liu, T.; Sreekumar, T. V.; Kumar, S.; Moore, V. C.; Hauge, R. H.; Smalley, R. E.; *Nano Lett.* **2003**, *3*, 1285–1288.
- (S9) Halpin, J. C.; Kardos, J. L.; *Polym. Eng. Sci.* **1976**, *16*, 344–352.
- (S10) Nishiyama, Y.; Langan, P.; Chanzy, H. *J. Am. Chem. Soc.* **2002**, *124*, 9074–9082.
- (S11) Guzmán de Villoria, R.; Miravete, A. *Acta Mater.* **2007**, *55*, 3025–3031.
- (S12) Laborde-Lahoz, P.; Maser, W.; Martinez, T.; Bonito, A.; Seeger, T.; Cano, P.; Guzmán de Villoria, R.; Miravete, A. *Mech. Adv. Mater. Struct.* **2003**, *59*, 385–392.
- (S13) Cox, H. L. *Br. J. Appl. Phys.* **1952**, *3*, 72–79.

Publications

Peer-reviewed journal articles

1. **Fujisawa, S.**, Isogai, T., Isogai, A., “Temperature and pH Stability of Cellouronic Acid”, *Cellulose*, Springer, **17**(3):607–615 (2010).
2. **Fujisawa, S.**, Okita, Y., Fukuzumi, H., Saito, T., Isogai, A., “Preparation and Characterization of TEMPO-Oxidized Cellulose Nanofibril Films with Free Carboxyl Groups”, *Carbohydrate Polymers*, Elsevier, **84**(1):579–583 (2011).
3. **Fujisawa, S.**, Okita, Y., Saito, T., Togawa, E., Isogai, A., “Formation of *N*-Acylureas on the Surface of TEMPO-Oxidized Cellulose Nanofibril with Carbodiimide in DMF”, *Cellulose*, Springer, **18**(5):1191–1199 (2011).
4. **Fujisawa, S.**, Saito, T., Isogai, A., “Nano-Dispersion of TEMPO-Oxidized Cellulose/Aliphatic Amine Salts in Isopropyl Alcohol”, *Cellulose*, Springer, **19**(2):459–466 (2012).
5. **Fujisawa, S.**, Ikeuchi, T., Takeuchi, M., Saito, T., Isogai, A., “Superior Reinforcement Effect of TEMPO-Oxidized Cellulose Nanofibrils in Polystyrene Matrix: Optical, Thermal, and Mechanical Studies”, *Biomacromolecules*, American Chemical Society, **13**(7):2188–2194 (2012).
6. **Fujisawa, S.**, Saito, T., Kimura, S., Iwata, T., Isogai, A., “Surface Engineering of Ultrafine Cellulose Nanofibrils toward Polymer Nanocomposite Materials”, *Biomacromolecules*, American Chemical Society, **14**(5):1541–1546 (2013).
7. **Fujisawa, S.**, Saito, T., Kimura, S., Iwata, T., Isogai, A., “Comparison of mechanical reinforcement effects of surface-modified cellulose nanofibrils and carbon nanotubes in PLLA composites”, *Composites science and technology*, Elsevier, **90**:96–101 (2014).
8. Okita, Y., **Fujisawa, S.**, Saito, T., Isogai, A., “TEMPO-Oxidized Cellulose Nanofibrils Dispersed in Organic Solvents”, *Biomacromolecules*, American Chemical Society, **12**(2):518–522 (2011).
9. Yang, Q., **Fujisawa, S.**, Saito, T., Isogai, A., “Improvement of Mechanical and Oxygen Barrier Properties of Cellulose Films by Controlling Drying Conditions of Regenerated Cellulose Hydrogels”, *Cellulose*, Springer, **19**(3):695–703 (2012).
10. Wu, C. N., Saito, T., **Fujisawa, S.**, Fukuzumi, H., Isogai, A., “Ultrastrong and High Gas-Barrier Nanocellulose/Clay-Layered Composites”, *Biomacromolecules*, American Chemical Society, **13**(6):1927–1932 (2012).
11. Puangsin, B., **Fujisawa, S.**, Kuramae, R., Saito, T., Isogai, A., “TEMPO-Mediated Oxidation of Hemp Bast Holocellulose to Prepare Cellulose Nanofibrils Dispersed in Water”, *Journal of Polymers and the Environment*, Springer, **21**(2):555–563 (2013).
12. Fukuzumi, H., **Fujisawa, S.**, Saito, T., Isogai, A., “Selective Permeation of Hydrogen Gas Using Cellulose Nanofibril Film”, *Biomacromolecules*, American Chemical Society, **14**(5):1705–1709 (2013).
13. Watanabe, E., Tamura, N., **Fujisawa, S.**, Saito, T., Habu, N., Isogai, A., “Stability of (1→3)- β -polyglucuronic acid under various pH and temperature conditions”, *Carbohydrate Polymers*, Elsevier, **97**(2):413–420 (2013).

International conference

Oral presentation

1. ○**Fujisawa, S.**, Okita, Y., Saito, T., Isogai, A. “Modification of sodium carboxylate groups on TEMPO-oxidized cellulose nanofibril surfaces” 243rd *American Chemical Society National Meeting & Exposition*, CELL 206, San Diego, March, 2012
2. ○**Fujisawa, S.**, Ikeuchi, T., Okita, Y., Takeuchi, M., Saito, T., Isogai, A. “Selective modification of carboxyl groups on TEMPO-oxidized cellulose nanofibril surfaces” 4th *International Conference of Pulping, Papermaking and Biotechnology*, O-1-1-004, Nanjing, November, 2012
3. ○**Fujisawa, S.**, Saito, T., Isogai, A. “Preparation and characterization of TEMPO-oxidized cellulose nanofibrils/poly(L-lactide) composites” 17th *International Symposium on Wood, Fibre and Pulping Chemistry*, Vouvouber, June, 2013
4. ○**Fujisawa, S.**, Saito, T., Isogai, A. “Thermal and mechanical properties of surface-modified TEMPO-oxidized cellulose nanofibrils/poly(L-lactide) composites” 247rd *American Chemical Society National Meeting & Exposition*, Texas, Dallas, 2014

Poster presentation

5. ○**Fujisawa, S.**, Fukuzumi, H., Okita, Y., Saito, T., Isogai, A. “Preparation and characterization of TEMPO-oxidized cellulose nanofibers with different counter ions” 241st *American Chemical Society National Meeting & Exposition*, CELL 72, Anaheim, March, 2011
6. ○**Fujisawa, S.**, Ikeuchi, T., Takeuchi, M., Saito, T., Isogai, A. “Nano-reinforcement of polystyrene with TEMPO-oxidized cellulose nanofibrils” 3rd *International Cellulose Conference*, PC-03, Sapporo, October, 2012

Domestic conference

Oral presentation

1. ○**藤澤秀次**、廣田真之、齋藤継之、磯貝 明 “セロウロン酸の pH 安定性と低分子化機構” 繊維学会年次大会 1C06 東京 2009 年 6 月
2. ○**藤澤秀次**、沖田祐介、齋藤継之、磯貝 明 “TEMPO 触媒酸化セルロースナノファイバーの表面化学改質” 繊維学会年次大会 2B13 東京 2010 年 6 月
3. ○**藤澤秀次**、池内智康、沖田祐介、竹内美由紀、齋藤継之、磯貝明 “TEMPO 酸化セルロースナノファイバー/ポリマー複合材料の調製とその特性解析” 第 19 回セルロース学会 K11 愛知 2012 年 7 月
4. ○**藤澤秀次**、池内智康、竹内美由紀、齋藤継之、磯貝明 “TEMPO 酸化セルロースナノファイバー/ポリスチレンナノコンポジットの調製と物性評価” 第 61 回高分子討論会 2Y09 愛知 2012 年 9 月

Poster presentation

5. ○**藤澤秀次**、金野尚武、齋藤継之、磯貝 明 “セロウロン酸の各 pH 下での安定性” 第 59 回日本木材学会 PK017 長野 2009 年 3 月
6. ○**藤澤秀次**、沖田祐介、齋藤継之、磯貝 明 “TEMPO 触媒酸化セルロースの表面改質” 第 17 回セルロース学会 香川 2010 年 7 月

Publications

7. ○藤澤秀次、沖田祐介、齋藤継之、磯貝 明 “TEMPO 触媒酸化セルロースナノファイバー表面カルボキシル基の化学修飾” ナノファイバー学会 P-13 東京 2010年6月
8. ○藤澤秀次、沖田祐介、齋藤継之、磯貝明、戸川英二 “有機溶媒中での TEMPO 酸化セルロースナノファイバー表面改質” 日本木材学会 K19-P-AM20 京都 2011年3月
9. ○藤澤秀次、齋藤継之、磯貝 明 “TEMPO 触媒酸化セルロースナノファイバー表面の界面活性剤修飾” 第18回セルロース学会 P034 長野 2011年7月
10. ○藤澤秀次、齋藤継之、磯貝 明 “TOCN/アミン塩の調製とその特性解析” 第61回日本木材学会 K15-P-PM14 北海道 2012年3月
11. ○藤澤秀次、齋藤継之、磯貝 明 “表面修飾 TEMPO 酸化セルロースナノファイバーを用いたポリマーナノコンポジットの調製” 第20回セルロース学会 京都 2013年7月

Patents

1. 磯貝 明、齋藤継之、藤澤秀次 “セルロースナノファイバー分散液の製造方法、セルロースナノファイバー分散液、セルロースナノファイバー成形体、及びセルロースナノファイバー複合体” 特開 2012-21081, 公開中, (2012)
2. 藤澤秀次、齋藤継之、磯貝 明 “セルロースナノファイバー分散液とその製造方法、セルロースナノファイバー修飾体、セルロースナノファイバー複合体” 特願 2011-254945
3. 磯貝 明、福住早花、藤澤秀次 “ガス分離膜とその製造方法” 特願 2012-155073

Acknowledgement

本論文は、筆者が東京大学大学院 農学生命科学研究科 生物材料科学専攻 製紙科学研究室において行った研究を博士論文として編纂したものです。本研究を進めるにあたり、多くの方々からご指導、ご鞭撻、ご協力を賜りました。この場をかりて厚く御礼申し上げます。

本研究において、指導教員として多くのご指導、ご鞭撻をいただいた磯貝明教授に心より感謝申し上げます。木村実特任教授には、研究および生活態度について、日々あたたかい叱咤激励をいただきました。齋藤継之准教授には、研究室に在籍した 6 年間、公私共に大変お世話になりました。心より感謝申し上げます。また、論文審査において多くのご助言、ご意見をいただきました岩田忠久教授、西野孝教授、横山朝哉准教授に心より感謝申し上げます。

研究室で出会ったすべての方々に感謝申し上げます。特に、研究生活の基礎を教えていただいた吉田穰博士、金野尚武博士、森陽太博士を中心とする先輩の皆様には厚く御礼申し上げます。また、生物材料科学専攻同期の皆様には在学中大変お世話になりました。ありがとうございました。

フィンランド留学中に研究を指導していただいた Aalto 大学 Olli Ikkala 教授をはじめとする Molecular Materials の皆様、滞在中に生活全般でお世話になった Tuomas Hänninen 博士、VTT の皆様に感謝申し上げます。

TOCN 表面改質物についての固体 ^{13}C -NMR スペクトルの測定を行っていただいた戸川英二様に、厚く御礼申し上げます。さらに、フィルムの透過型電子顕微鏡観察を行っていただいた木村聡助教に感謝いたします。

最後になりましたが、あたたかく見守ってくださった家族のみなさんありがとうございました。やっと卒業しました。

2014 年 3 月 24 日 藤澤秀次